Edvard Grimsmo Hofstad

Analysis of small-signal dynamics in a hybrid ship power system with a Virtual Synchronous Machine

Masteroppgave

NTNU
Kunnskap for en bedre verden

Edvard Grimsmo Hofstad

Analysis of small-signal dynamics in a hybrid ship power system with a Virtual Synchronous Machine

NTNU

Kunnskap for en bedre verden

Prephase

This Master thesis is the final result of my master's degree in the two-year study program Industrial Cybernetics at the Norwegian University of Science and Technology. The topic of this thesis is the implementation of Virtual Synchronous Machines based control of power converters in a marine power grid. The work documented here have been conducted in the spring of 2019 from January to June and is a continuation of the specialization project resulting from the subject TTK4551 form the autumn of 2018. In this specialization project a Simulink model of the VSM connected to a grid equivalent was tested. This model has been slightly altered in order for it to adapt to the system presented. All results presented in this master thesis have been developed in order to be presented here. This applies to simulations and calculations conducted on the material presented, as well as the nonlinear state space models and the small signal models presented, along with the analysis done on these models. The tools used for producing the results have been Matlab and Simulink with the Simpower systems toolbox. In addition, Maple have been used for simplifying algebraic operations.

I would like to thank my supervisor, Jon Are Suul, for taking his time and being inspirational in talks about the project. I would also like to thank my fellow students for the companionship and being able to talk discuss matters relating to this thesis as well as any other.

Edvard Grimsmo Hofstad
Trondheim, June 2019

Abstract

An increasing focus on the environmental impacts from marine power systems utilizing fossil fuel have resulted in implementation of Emission Controlled Areas, and an increasing demand for levels of pollution forces changes in the marine power systems. A solution for accommodating these demands and lowering the total use of fossil fuel for energy production is the implementation of energy storage systems. An implementation of such a system is a battery energy system. If this is used in a ship power system with AC-distribution the most common interface is for three phase transformation is three-phase voltage source converters.

This thesis studies a VSM implementation in a marine power grid. The design of the VSM is done such that the frequency of the virtual rotor is produced internally, removing the need for a Phase Locked Loop. This also gives room for the possibility of islanded operation of the power grid with only the VSM connected, using the same control topology for the VSM. The power grid studied is designed as a traditional marine power grid with a SM, a VSM connected to a battery energy system and a load model. A nonlinear state space model of these components has been developed and small signal models have been made for each. Small signal models have been made for the VSM with grid connection and connected to the load model, SM with grid connection and connected to the load model and a full model containing all three components. This has given the possibility to study the dynamics of the system and gain insight in the stability.

The small signal model developed have given the possibility to use linear analysis tools to evaluate stability and system response. The validation process gave room for validating the correctness of the small signal models and opened the possibility for assessing the system response of the disturbance. An eigenvalue analysis of the different small signal models has been done to determine critical modes and which states is influenced by these. This analysis has given further insight in the system response and the way that it is coupled. The eigenvalue analysis has also been tested for operational area of the power grid giving insight in how the system dynamics of the base case studied change as the total power flow is altered.

The analysis shows that the system is stable and have a good dynamic response for transients. The eigenvalue analysis shows that the system has a good stability margin, meaning that the system is not in danger of becoming unstable. The system is able to function with all components (SM, VSM,load) connected. The VSM have shown the ability to adapt to the frequency in the grid by synchronizing to the other frequency setting component in the grid. This shows the possibility of a grid being operated by an inverter without the need for a change in control system.

Sammendrag

Et økende fokus på miljøpåvirkningen fra marine kraftsystemer som benytter seg av fossilt brensel har resultert i implementeringen av Utlippskontrollerte soner og et økende krav til nivåer av utslipp av forurensede gasser fra marine kraftinstallasjoner. En løsning for å imøtekomme disse kravene og redusere det totale forbruket av fossilt brensel for energiproduksjon er implementeringen av Energy Storage systems. Et eksempel på dette er et batterisystem. Hvis dette benyttes i et kraftsystem med AC-distribusjon er det mest vanlige grensesnittet for trefase transformasjon en trefase spenningskilde-konverter.

Denne oppgaven undersøker en VSM implementasjon i et marint kraftsysem. Designet på VSMen er utført slik at frekvensen til den virtuelle rotoren blir produsert internt. Dette gjør at behovet for en PLL forsvinner. Dette gir rom for muligheten til at VSMen kan operere kraftsystemet alene, uten et behov for at andre komponenter skal styre frekvensen uten å bytte styresystem for VSMen. Kraftsystemet undersøkt er et tradisjonelt marint kraftsystem system bestående av en SM, en VSM og en lastmodell. En ulineær tilstandsrommodell har blitt laget for hver komponent. Disse har blitt linearisert til småsignalmodeller. Modellene består av VSM koblet til et nett, SM koblet til nett, VSM og SM koblet sammen og VSM, SM og lastmodell koblet sammen.

Småsignal modellene utarbeidet har gjort det mulig å bruke lineære analyseverktøy for å analysere systemets stabilitet og system responsen. Småsignalmodellene ble validert ved å sammenligne responsen ved en forstyrrelse med tilsvarende modeller laget I Simulink. Dette ga muligheten for å validere modellene og vurdere responsen til systemet ved en forstyrrelse. En eigenverdianalyse ble utført på småsignalmodellene for å undersøke kritiske moder og vurdere stabilitetsmarginen.

Analysen viser at systemet er stabilt og har en god dynamisk respons for transienter. Eigenverdianalysen viser at systemet har en god stabilitetsmargin. Systemet fungerer for alle komponenter tilkoblet og VSMen viser evnen til å tilpasse seg nettet den er koblet til. VSMen er i stand til å fungere for alle systemene introdusert uten å måtte endres. Dette viser muligheten for at en inverter kan operere et nett uten behov for en endring i kontrollsystemet.

Contents

List of Figures

List of Tables

Nomenclature

ω_b Base angualr frequency

$\omega_{ad,VSM}$ Cut off frequency of filter in active damping of the VSM

$\omega_{qf,VSM}$ Cut off frequency for reactive power droop VSM

$c_{,VSM}f$ Filter capacitance VSM

$c_{g,SM}$ Grid capacitance SM

I_b Base current

$k_{ad,vsm}$ Active damping gain, VSM

$k_{d,SM}$ SM damping coefficient SM

$k_{d,vsm}$ Damping coefficient VSM

$k_{i,ex}$ Integral gain exiter

$k_{ic,VSM}$ Integral gain, current controller VSM

$k_{iv,VSM}$ Integral gain PI voltage control VSM

$k_{p,ex}$ Proportional gain exiter

$k_{pc,VSM}$ Propotional gain, current controller VSM

$k_{pv,VSM}$ Proportional gain PI voltage control VSM

$k_{q,vsm}$ Droop gain for reactive power VSM

l_l Armature leakage inductance

$l_{1,d}$ D-axis damper winding inductance

$l_{1,q}$ Q-axis damper winding inductance

$l_{11,d}$ Damper winding d-axis selv inductance

$l_{11,q}$ Damper winding q-axis selv inductance

l_{ad} Armature mutual inductance d-axis

l_{aq} Armature mutual inductance q-axis

$l_{f,VS}$ Filter inductance VSM

$l_{f1,d}$ Mutual inductance between field and d-axis damper winding

$l_{f1,d}$ Mutual inductance between the field circuit and d-axis damper winding

$l_{ff,d}$ Field circuit self inductance

$l_{g,SM}$ Grid indutcance SM

$l_{g,VSM}$ Grid inductance VSM

$l_{s,VSM}$ Stator inductance VSM

PLL Phase Locked Loop

r_a Armature resistance SM

r_f Filter resistance VSM

$r_{1,d}$ Restistance damper d-axis

$r_{1,q}$ Resistance damper q-axis

$r_{f,d}$ Resistance field circuit

$r_{g,SM}$ Grid resistance SM

$r_{g,VSM}$ Grid resistance VSM

$r_{s,VSM}$ Stator resistance VSM

S_b Base appearent power

SM Synchronous machine

$T_{a,vsm}$ Inertia time constant VSM

T_{ex} Time constant excitation system

T_{gt} Time constant governor diesel generator

T_{SM} Time constant rotor SM

V_b Base voltage

$VISMA$ Virtual synchronous machine

VSM Virtual synchronous machine

Z_b Base imedance

Chapter 1

Introduction

1.1   Motivation

An increasing focus on the environmental impacts from marine power systems utilizing fossil fuel have resulted in the implementation of Emission Controlled Areas, and an increasing demand for levels of pollution forces changes in the marine power systems. [1] A solution for accommodating these demands and lowering the total use of fossil fuel for energy production is the implementation of energy storage systems. These systems are in an increasing rate used in ship power systems in order to lower the fuel consumption. This also enables the opportunity of hybrid operation of the power grid. An implementation of energy storage is battery energy systems. If this is used in a ship power system with AC-distribution the most common interface is for three phase transformation is three-phase voltage source converters. [2][3] The traditional control of these converters is utilizing a Phase locked loop for synchronization to the voltage at the ac bus, meaning the inverter is dependent on something else to control the frequency of the grid.[4]

By utilizing the control concept Virtual Synchronous Machines, the power electronic converters can allow islanded operation of a single or multiple battery systems powering the AC-bus, or operating parallel with a synchronous machine without the need of changing the control system. This gives the opportunity for hybrid operation of the marine power grid, and the possibility for an all-electric operation.

By linearizing a ship power system and making a small signal model equivalent for the nonlinear system in an equilibrium point can give some idea of the influence the VSM have on the system. By performing a linear analysis on this small signal model, the stability and its ability to handle disturbances in forms of load changes and such.

1.2   Problem description

This project should study the dynamic performances of a power electronic converter controlled as a Virtual Synchronous Machine (VSM) when operated in a typical ac ship power system. Especially, the study should evaluate how a battery system

with VSM-based control can influence the stability and transient response of a hybrid ship power system in various operating conditions. A simplified system configuration containing a VSM, a traditional diesel generator with a synchronous generator and a load interfaced to the ac-bus by an active rectifier should be modelled for time-domain simulations in Simulink and a corresponding state-space model should be derived for analytic studies. The obtained state-space model should be linearized to obtain a small signal model of the system. The system model should be developed in steps, starting with models of power electronic converters interfaced to an ideal grid voltage, and the model should be expanded until all components are represented in the same framework. The small-signal models should be validated against the detailed time-domain simulation models by evaluating the time-response to small perturbations. Established tools for linear system analysis should be applied to the derived and validated models in order to analyze how the use of a VSM can influence the small signal dynamics of the ship power system under various system configurations and operating conditions.

1.3   Limitations

This work has tested an implementation of a VSM topology in a model for a marine power grid. This marine power grid is simplified to a traditional generation unit with a SM and an inverter symbolizing a load in the grid.

In order to model the inverters for the VSM and load model an Average model from the Simpower systems toolbox is used. This means that modulation frequency can be assumed to be high enough not to inflict the transformations and can be neglected, because the control signal sent to the inverter model is a three-phase signal. Both the VSM and load model inverters have an ideal dc-voltage source on the dc-side. This combined with the use of an average model means that the dc side can be neglected as the voltage will be constant no matter the power flow.

The windings of the SM are assumed to be distributed uniformly along the air gap. The magnetic hysteresis and mechanical vibrations have been neglected in this model. In addition, magnetic saturation has also been neglected and in that way all circuits is assumed to be linearly coupled. The control system of the SM consists of an AVR and a Governor, modelled with two first order delays in order to be more similar to a physical implementation. The damping of the rotor due to mechanical losses have also been neglected.

When simulating the results, the transient phase leading to steady state have not been studied. The models have only been used for steady state analysis.

The VSM model studied have been taken from [5]. The tuning of the virtual impedance has not been conducted in this thesis, and uses this model with some minor alterations. The SM model used is taken from [6]. Some alterations have been done here as well, but the inspirations for the fundamentals is taken from here.

1.4 Report outline

The report can be divided into three parts. The first part deals with some background laying the fundamentals of the report and explaining some methods used. The second part is modeling. This section goes through the modeling of the system and explains how the system is connected. It starts with the VSM model and goes through each main component and controllers used. Then the SM model is presented in the same manner, and finally the load model. The last part is simulation results. This part presents the results of different simulations and calculations. The report finishes with a summary of results, discussion, conclusion and suggestions for further work.

Chapter 2

Background

2.1 Marine power grids

The main difference between land-based power systems and marine power systems is that the power consumption is closer to the source. This means that the engineering problems related to transmission lines can be neglected. Because the installed power compared to the voltage level is high leads to different engineering challenges for these systems. Because of the size of the marine power grid, controls have the possibility of a much tighter implementation, compared to the traditional land based power system.[7]
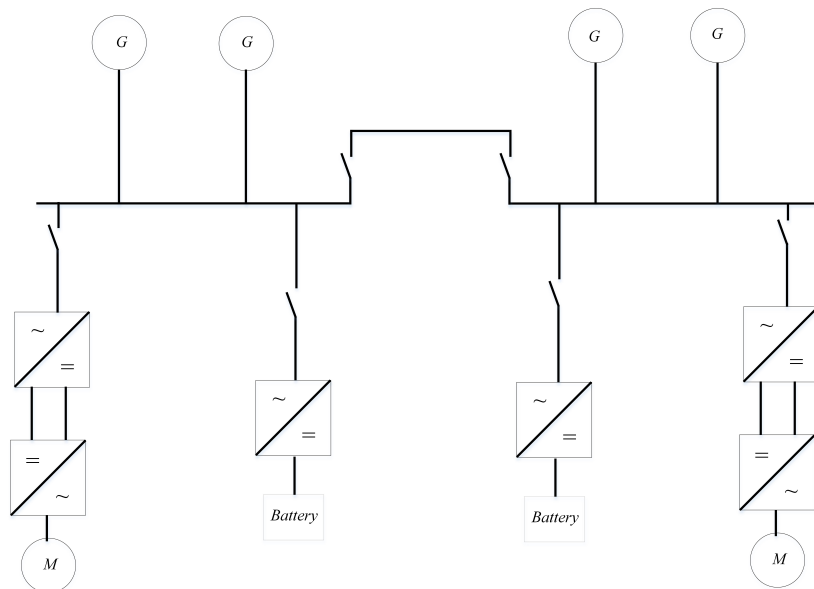
Figure 2.1: System figure showing the main components of the power grid.

A ship power system can be modeled as a small micro grid containing different sources of energy and different energy consumers. Using gas turbines or diesel engine driven electric propulsion gives room for various ways of implementing the electric grid on a marine vessel, including loads like electric propulsion to smaller

loads that may be needed for the marine vessel. There are also alternatives to diesel and gas like liquid natural gas, nuclear steam turbine plants, fuel cells and battery energy storage systems. This also opens for hybrid solutions giving the possibility to handle the peaks of energy need lowering the use of fossil fuel.[8] A simplified implementation of a marine power grid can be seen in figure 2.1. Here a battery energy storage system is implemented along with the diesel-powered generators.

The implementation of Emission Controlled Area at different locations along coastlines defines an acceptable emission level coming from diesel engines. This contributes to focus more on the consumption of the fossil fuel and pushes development towards more alternative solutions.[8] The International Marine Organization (IMO) continuously updates the limits pollution rates and updates emission free areas. As technology develops the requirements set by the IMO tightens, leading to a lower legal total amount of pollution and a higher requirement for pollution on newly built ships relative to its size.[1]

2.2   Virtual synchronous machine

As the use of renewable energy sources like photovoltaics and wind power plays a bigger role for delivering power to grids, relieving the generators formerly delivering power. The renewable sources rely on voltage source converters (VSC) in order to connect to power grids. This means that the power system will have less inertia coming from the synchronous machines, if the VSC works as replacements of for SM. Having a low inertia in the power grid can lead problems with stability, like the rate of change for the frequency changes when power system transients is applied. [9] A solution for this problem can be implementing additional inertia with the use of virtual inertia.

The concept of a virtual synchronous machine was first introduced in 2007 by Beck and Hesse and was introduced as VISMA. [10] Here they described a type of inverter control having inertia and electromechanical damping properties as a synchronous machine. As time has gone by several approaches have been documented and tested. Some of them can be found here: [11][12][13][14][15][16]. Varying in implementation and complexity different models can be used for implementing a mathematical SM model in the control system. The high order models can give accurate and precise results, but the tradeoff here is the complexity of the system. In [13] a classification of the different types of implementations for a VSM is introduced. This gives an insight in the different types of solutions for modeling the VSM.

By focusing on the control system and implementation of the swing equation [17] emulating the inertia, the VSM can be divided into four main groups: Synchronverter, Inertia-emulation, Voltage controlled VSM and Current controlled VSM. [18]. Presented here is a generalized model of these topologies. This means that there are other possibilities and variations of the models presented here.

The synchronverter was introduced by [19] and is the simplest VSM implementation compared to the ones mentioned here, in terms of topology and complexity. Some application of this control topology can be seen in [20] and[21]. This method can be generalized as a reactive power controller and a frequency droop combined with the swing equation. The main advantage of this control topology is the simplicity. But as a result, from this simplicity, the control has few degrees of freedom, leading to few control parameters giving a limitation to the possibility to adapt the control for a desired dynamic response. This method in general requires a PLL in order to unless alterations is done.

The topology of the inertia emulation is based on using the swing equation to calculate the power reference using the frequency. The current reference is then calculated using this power reference and a voltage measurement on the output of the inverter. [22] [14] The topology can be generalized as a current controller as inner control loop, with an outer loop consisting of a frequency droop controller. This method is as well not that complex as it uses few measurements and have few controllers. This generalized method as well requires a PLL in order to function but can be avoided by altering the controller.

The voltage controlled VSM is the most complex of the models presented here. The generalized control system consists of a swing equation model with a frequency droop for angle and power control. A reactive power controller feeds a virtual impedance a voltage reference. This impedance uses along with the voltage reference, measurements of the output current of the inverter to calculate a voltage reference. This reference is then sent to a voltage controller in in cascade with a current controller. A drawback with this control is the complexity. Having multiple cascaded controllers leads to a comprehensive strategy needed to tune the parameters of these controllers. This generalized model requires a PLL in order to synchronize to the frequency of the grid, but with some adjustments the need for a PLL can be avoided.[23], [24]

Current controlled VSM topology is somewhat simpler than the voltage controlled VSM. In the generalized model a frequency droop cascaded with the swing equation is used in order to find the phase angle and the frequency of the VSM. A reactive power controller is used in cascade with a virtual impedance, using a mathematical model of a SM, and a current controller. The advantage of the control topology is that there is no need for a PLL for synchronization. A filter is used on the output value of the swing equation replacing the need for a PLL. The mathematical model of the SM used in the virtual impedance must be designed with care, because of its influence on the system stability [5].

The method implemented in this thesis is the current controlled VSM and is chosen for various reasons. Being able to function without a Phase locked loop is a important trait. This makes it possible for the model to function without relying on measurements of the grid, producing its own frequency internally instead of measuring the phase angle for the grid. Being able to function independently of other sources or frequencies in the grid is important. Because of this the VSM is redun-

dant and can function if the SM is tripped and enable a hybrid power supply for a
marine power grid.

In [24] an implementation of several VSM have been investigated. A small signal
analysis shows the results of adding inertia to a grid consisting of several distributed
energy sources. The implementation used was without a PLL controlling the refer-
ence frame of the VSM. A benefit of using a mathematical model of a SM is that
the machine parameters can be changed unlike a SM where the parameters are con-
stants. This opens for tuning of the machine parameters in order to get a more
desired behavior of a SM.

2.3   Small signal modelling

In order to study power systems in steady state with small disturbances, a small
signal model of the system is made, meaning that the system is linearized around
the steady state values. The general linearization method is taking the first order
Taylor expansion of the nonlinear system.[25] By defining the perturbations $\Delta\mathbf{x}, \Delta\mathbf{u}$,
and $\Delta\mathbf{y}$ from the solutions

$$
\begin{aligned}
\mathbf{x}(t) &= \mathbf{x}_0(t) + \Delta\mathbf{x} \\
\mathbf{u}(t) &= \mathbf{u}_0(t) + \Delta\mathbf{u} \\
\mathbf{y}(t) &= \mathbf{h}[\mathbf{x}_0(t), \mathbf{u}_0(t), t] + \Delta\mathbf{y}
\end{aligned}
\tag{2.1}
$$

and taking the first order Taylor expansion around the solution $\mathbf{x}_0$ and $\mathbf{u}_0$ leads the
expression

$$
\begin{aligned}
\dot{\mathbf{x}} &= \left.\frac{\partial \mathbf{f}}{\partial \mathbf{x}}\right|_{x_0(t), u_0(t)} \Delta\mathbf{x} + \left.\frac{\partial \mathbf{f}}{\partial \mathbf{u}}\right|_{x_0(t), u_0(t)} \Delta\mathbf{u} \\
\mathbf{y} &= \left.\frac{\partial \mathbf{h}}{\partial \mathbf{x}}\right|_{x_0(t), u_0(t)} \Delta\mathbf{x} + \left.\frac{\partial \mathbf{h}}{\partial \mathbf{u}}\right|_{x_0(t), u_0(t)} \Delta\mathbf{u}
\end{aligned}
\tag{2.2}
$$

By modeling a power system and solving the set of equations with respect to the
first derivative equal to zero, implying that the system is in equilibrium, the desired
linearization points can be found, here defined as x_0 and u_0. Thus, the system
equations can be expressed as

$$
\begin{aligned}
\dot{\mathbf{x}} &= A(x_0, u_0)\mathbf{x} + B(x_0, u_0)\mathbf{u} \\
\mathbf{y} &= C\mathbf{x} + D\mathbf{u}
\end{aligned}
\tag{2.3}
$$

Here A, B, C and D represents the system matrices. As equation 2.3 shows, both
the A and B matrices are dependent on the linearization points, x_0 and u_0.

Using this model the stability of the system can be analyzed and evaluated in various
ways. This thesis has completed an eigenvalue analysis and evaluated the partici-
pation factors by using the system eigenvalues and eigenvectors. By analyzing the

eigenvalues, it is possible to understand how the components of the system behaves and how parameters influence the dynamic response of the system. The eigenvalues and eigenvectors for the system can be calculated from the matrix **A** in equation 2.3.

The article [26] have made classification on different types of stability. According to this power system stability can be divided into three main groups, rotor angle stability, frequency stability and voltage stability. Small signal rotor angle stability is focused around the power grids ability to be synchronized under small disturbances. These disturbances need to be small enough for the linearized model of the power system to still be valid for analysis. This means that the validity of the linearized model is limited to small disturbances when validating the model.

Small signal voltage stability specifies the power systems ability to keep a even voltage when exposed to small disturbances like changes in the load of the system. This stability can be impacted by controls and load characteristics. By making some assumptions a linearized model can be analyzed in order to study this stability. By studying the linearized model some information of the nonlinear system can also be deduced, such as if the linearized system is asymptotically stable the nonlinear system will also be asymptotically stable. [25]

2.3.1 Eigenvalues

The eigenvalues of a system defined as the solution of the characteristic equation [27]

$$det(\mathbf{A} - \lambda\mathbf{I}) = 0 \tag{2.4}$$

Here λ is the eigenvalue, **A** is the system matrix and **I** is the identity matrix. The eigenvalues also appear in the time domain solution for the general states space formulation seen in equation2.3. This solution is

$$\mathbf{x}(t) = e^{\mathbf{A}(t-t_0)}\mathbf{A}\mathbf{x}_0(t_0) + \int_{t_0}^{t} e^{\mathbf{A}(t-\tau)}\mathbf{B}(\tau)\tau \tag{2.5}$$

The eigenvalues can be real valued or complex conjugated. From equation 2.3 it can be seen that the dimension of the derivative is $\frac{1}{t}$ therefore the unit for the real part of the eigenvalue is $\frac{1}{s}$ while the imaginary part is $\frac{rad}{s}$. From this the time constant of the eigenvalue can be calculated from the real part, and is related to the damping. The damping ratio can be calculated as

$$\frac{real(\lambda)}{\sqrt{real(\lambda)^2 + imag(\lambda)^2)}} \tag{2.6}$$

for eigenvalues containing an imaginary part. The imaginary part describes the natural frequency of the eigenvalue. The frequency can be found in Hz by multiplying the imaginary part with 2π. This will be the oscillating frequency of the eigenvalue if there was no damping.

2.3.2   Participation factor

By evaluating the eigenvalues of the system, one can identify modes giving the system the characteristics like oscillations or damping. By calculating the participation factor a measure of relative participation can be calculated. This can be used to identify different states contributing to a mode. The participation factor matrix is defined as

$$\mathbf{P} = \begin{bmatrix} p_{11} & p_{12} & ... & p_{1n} \\ p_{21} & p_{22} & ... & p_{2n} \\ ... & ... & ... & ... \\ p_{n1} & p_{n2} & ... & p_{nn} \end{bmatrix} = \begin{bmatrix} \phi_{11}\psi_{11} & \phi_{12}\psi_{21} & ... & \phi_{1n}\psi_{n1} \\ \phi_{21}\psi_{12} & \phi_{22}\psi_{22} & ... & \phi_{2n}\psi_{n2} \\ ... & ... & ... & ... \\ \phi_{n1}\psi_{1n} & \phi_{n2}\psi_{2n} & ... & \phi_{nn}\psi_{nn} \end{bmatrix} \tag{2.7}$$

Here P is the participation matrix while ϕ and ψ is the right and left eigenvalue matrix respectively. Each participation factor is product of the kth element of the ith left and right eigenvector. This gives the sensitivity of the ith eigenvalue to the kth diagonal element of the state matrix. [17] [6] This can be expressed in a more general way as $p_{ki} = \phi_{ki}\psi_{ik}$ where p gives a relative participation of the state k in the mode i and the other way around. Because the participation factor is the product of two eigenvectors make p dimensionless, and therefore independent of the choice of units

2.4   Tuning methods for control loops

The methods Modulus optimum and Symmetric optimum is approaches for tuning PI controllers with systems that fulfill some special requirements. Modulus optimum is a method often used for low order systems, or high order simplified into a low order system, containing a dominant time constant and a smaller time constant. If the system fulfills the requirements of either Modulus optimum or Symmetric optimum the methods is applicable.

2.4.1   Modulus optimum

Modulus optimum is a method for tuning low order systems with a dominant time constant and a smaller time constant.[28] By inspecting the open loop transfer function the integrator gain should be set to cancel the dominant time constant. Take the transfer function

$$G(s)_{ol} = K_p \frac{1 + T_i s}{T_i s} \frac{1}{1 + T_{dom}s} \frac{1}{1 + T_{min}s}$$
$$G(s)_{ol} = K_p \frac{1}{T_{dom}s} \frac{1}{r_f} \frac{1}{1 + T_{min}s} \tag{2.8}$$

This is not a random choice for the transfer function. The inner loop control of a inverter have a similar transfer function as shown above. The Modulus tuning

criterion for this transfer function can be written as

$$T_i = T_{dom}$$
$$K_p = \frac{T_{dom}r}{2} \tag{2.9}$$

This results in the closed loop transfer function

$$G(s)_{cl} = \frac{1}{T_{min}s^2 + T_{min}s + 1} \tag{2.10}$$

This is a mass, spring damper system and the natural frequency and damping ratio equal to $\omega_n = \frac{1}{T_a\sqrt{2}}$ and $\zeta = \frac{1}{\sqrt{2}}$. [27] This method is based in pole cancellation removing a dominant time constant with the integral time and achieving the absolute value of the transfer function equal to one. This means that the natural frequency and damping ration will always be equal to the result shown above.

2.4.2   Symmetric optimum

Modulus optimum is a tuning method for systems similar to 2.8, but instead of having a minor first order delay a integrator part is present. Using the Symmetric optimum will lead to a pole with a real part equal to zero, leading to no guarantee for stability. The method maximizes phase margin such that the phase margin appears at the crossover frequency. Achieving the highest possible phase margin results in a system more robust against delays. This is important considering a control system for an inverter, where the switching and inner control loop can be considered as delays. The tuning criteria is obtained using the Nyquist criteria for stability:

$$|G_{ol}(j\omega)| = 1 \ and \ \angle G_{ol}(j\omega) = -180^o + \Phi_m \tag{2.11}$$

Here Φ_m is the phase margin. Taking the general open loop transfer function with a pole in origo 2.12

$$G(s)_{ol} = K_p \frac{1 + T_i s}{T_i s} \frac{1}{1 + T_{dom}s} \frac{1}{T_{min}s} \tag{2.12}$$

By differentiating the angle part of the Nyquist criteria with respect to ω, the criteria becomes

$$\omega_d = \frac{1}{\sqrt{T_i T_{dom}}} \tag{2.13}$$

This means that if the the integral time constant is set to $T_i = T_{dom}(\frac{1+sin(\phi)}{1-sin(\phi)})$ the resulting system will have a maximum phase margin at the crossover frequency ω_d. The crossover frequency will be symmetric about $\frac{1}{T_i}$ and $\frac{1}{T_{dom}}$.[28]

Both Modulus optimum and Symmetric optimum are efficient and accurate methods for achieving a stable and accurate controller. The downside of using these methods is the need for an approximation. When tuning the current controller, the switching and the filter is approximated by a first order delay. When tuning the outer control loop the current controller, switching delay and the filter time constant is approximated. These estimates can be inaccurate leading to a controller that may not have the most optimal response. In addition, the assumption of a stiff grid with voltage equal to 1 pu d-axis. When disconnecting the grid and connecting something with different traits the system dynamics may change. This is why using the eigenvalues and participation factors, and identifying the what modes belongs to what sate, the controller parameters can be changed after using these tuning methods in order to move the system modes to a more desired place in the left half plane.

Chapter 3

System description

The system this thesis has worked with consists of three main parts, the VSM, the SM and the load model. The VSM and the SM are the sources in this marine power grid, and an inverter along with a resistive and capacitive load is implemented a as power consumers. Having a SM in a power grid is very common and relevant for modeling a marine power grid. The inverter modeled as a load is meant to symbolize a relatively big load for the system and is thought of as a motor operating the propulsion system. The load is thought to have a DC-bus between the AC-grid and the motor. The resistive and capacitive loads implemented is to add a small load in the grid in addition to the inverter feeding a DC-bus. In figure 3.1 the one line schematic of the system can be seen.
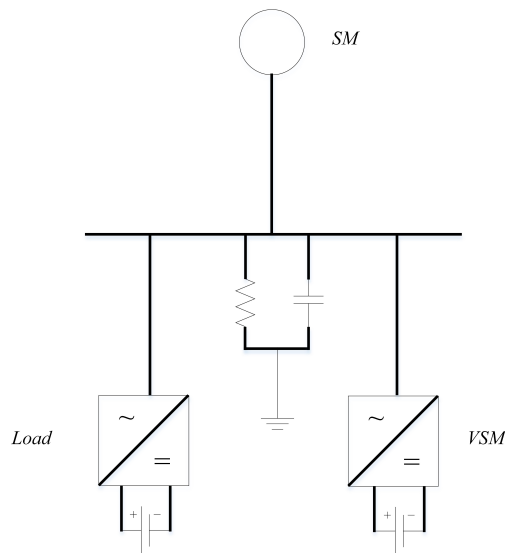
Figure 3.1: System figure showing the main components of the power grid.

Comparing 3.1 to the one line schematic for a general ship power system it can be seen that this represent one side of the of the 2-split distribution system. This is why the system in figure 3.1 can be representative for a simplified marine power system.

17

3.1   Modeling conventions

The per unit system chosen is based on a chosen phase peak voltage and a chosen apparent power rating. All parameters discussed is in per unit unless other is specified. The transformation between three phase variables and dq variables is done with the amplitude invariant park transformation. The axis alignment chosen is the a-phase of the three-phase aligned with the d-vector of the dq-reference frame. The notation used for dq variables in this thesis is as complex space vectors and can be written as

$$\mathbf{x} = x_d + jx_q \tag{3.1}$$

3.2   Per unit system

The per unit system chosen for the system for the AC side is as follows

$$
\begin{aligned}
V_b &= Nominal\ peak\ phase\ voltage \\
S_b &= Nominal\ power \\
I_b &= Nominal\ peak\ phase\ current \\
Z_b &= Base\ AC\ impedance \\
\omega_b &= Base\ frequency
\end{aligned}
\tag{3.2}
$$

3.3   Reference frame orientation

When designing the state space model for the investigated system, a reference for the synchronously rotating reference frames needs to be chosen, since this is a closed system with two sources. Because of the choice of VSM model, the necessity for a PLL disappears as the frequency of the VSM is produced internally. Because the influence of the VSM on the system is the highest interest of analyzing in this system, the deviation of phase angles is chosen to be referenced to the VSM. The load, VSM and the SM all have different phase shifts in the frequency. By expressing the phase angles as a deviation to this reference, a state space model can be made. The figure 3.2 shows how the different reference frames may look like.
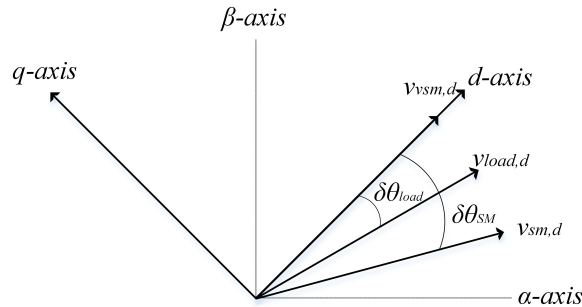
Figure 3.2: Vector diagram showing the reference frame.

By defining the deviation between the rotating frames of the SM and load as

$$\delta\theta = \theta - \theta_{VSM} \tag{3.3}$$

The derivative of the angle deviation and expressing this in angular velocity it can be rewritten as

$$\frac{d}{dt}\delta\theta = \omega - \omega_{VSM} \tag{3.4}$$

Here the ω without subscript is either ω_{SM} or ω_{pll}.

The reason this state is important is because when coupling the systems together, the states having a phase shift need to be in phase with the rest of the states in the equation. By looking at the phasor diagram 3.2 the rotation of the synchronously rotating reference frames can be done by

$$\mathbf{x}^{ref} = \mathbf{x}e^{-j\delta\theta}$$
$$\mathbf{x}^{ref} = \mathbf{x}(cos(\delta\theta) - jsin(\delta\theta)) \tag{3.5}$$

This equation can be expressed in matrix form as:

$$\begin{bmatrix} d \\ q \end{bmatrix} = \begin{bmatrix} cos(\delta\theta) & sin(\delta\theta) \\ -sin(\delta\theta) & cos(\delta\theta) \end{bmatrix} \begin{bmatrix} d' \\ q' \end{bmatrix} \tag{3.6}$$

This rotation matrix is used multiple times to connect systems together. The systems are first modeled connected to a grid and the connected. The coupling will be explained in detail in chapter 8, after the relevant equations is presented. The states taking an effect from this coupling will be the states modeling the outgoing currents or voltages from the different component with defined phase shifts.

3.4 Investigated models

This thesis will take a look on different systems containing the VSM, SM and load model. Firstly, the VSM and SM will be analyzed separately connected to an ideal voltage source in order to test and validate the responses and see how the systems influence each other when connected. Then a model of the VSM and SM connected is analyzed. This model is done with a capacitive and resistive load at the AC-bus. Finally, the VSM and SM are set together with the load model and the system is complete.

Chapter 4

Virtual synchronous machine model

This chapter will go through the VSM model and present the equations used in the state space model. The control topology will also be presented and explained. The model introduced is connected to a grid.
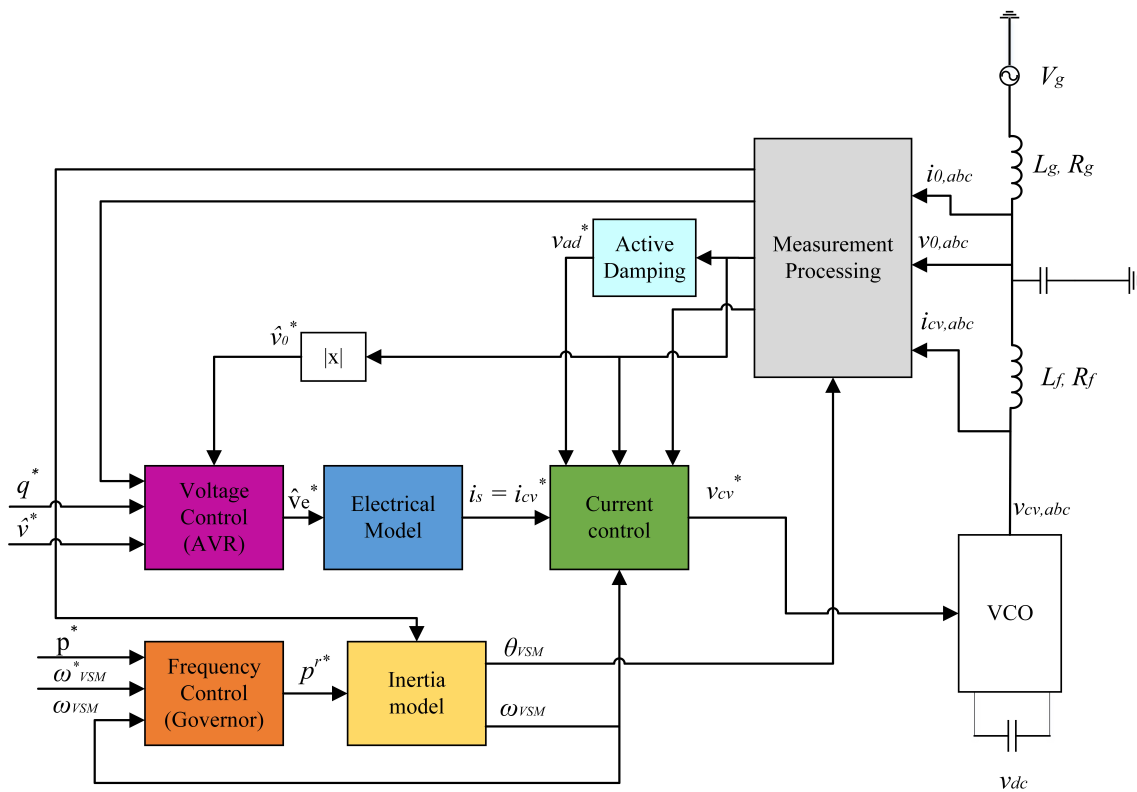
Figure 4.1: Figure showing the VSM control topology. The Voltage Control block, Electrical Model, Frequency control and Inertia Model blocks make up the virtual SM.

4.1   VSM model

The design chosen for the VSM is based on the dynamic synchronous machine model from [5]. In figure 4.1 the system model of the investigated VSM can be seen. A VSC is connected to a LCL-filter and the filter is then connected to a grid equivalent representing the rest of the system. In the measurement processing block an amplitude invariant park transformation is done to the three phase signals, resulting in three DC signals. Here the phase angle θ_{vsm} is used as transformation angle, with the d-axis aligned with the a-phase in the three-phase side. When modeling the VSM the DC side of the VSC have not been considered and it is assumed that the source connected have the sufficient power. The voltage level on the DC side of the inverter is $2V_b$. For modeling the VSC, an average model has been implemented, resulting in no need for a modulation index. This means that any delay due to the PWM implementation can be neglected. Furthermore, the assumption that the input voltage reference signal for the VSC can be assumed to be approximately equal to the output voltage as seen in equation 4.1.

$$\mathbf{m} = \frac{\mathbf{v}^*_{cv}}{v_{dc}}, \mathbf{v}_{cv} = \mathbf{m}v_{dc}, \implies v_{cv} \approx v^*_{cv} \tag{4.1}$$

There are several ways to implement a mathematical model of a SM in the control design for an inverter. Here the tradeoff considering the level of detail the SM model contains needs to be evaluated. A high order or full order model would result in an unnecessary complex model. This is studied in [13].

4.1.1   Inertia emulation

For emulating inertia with the same characteristics as a SM, the swing equation is used, giving a similar damping and inertia behavior as a SM. [17] [6] This equation is central, among others, for the power system stability analysis describing the behavior of the SM when there is unbalance in the electromagnetic and mechanical torque. The general equation is given as 4.2, expressed as the first derivative of the speed. Here T_{el} represents the electromagnetic torque, T_0 is the mechanical torque, ω the rotating speed of the machine, ω_g is the angular frequency of the grid, J is the inertia of the rotor and D is a coefficient that represents the damping torque associated with the damper windings during transient responses. Since the changes done in the frequency is small perturbations D is assumed constant in the case studied, giving the equation limited but sufficient operating range.

$$T_a = T_m - T_e \tag{4.2}$$

Here T_a describes the accelerating torque, T_m the mechanical torque and T_e the electromagnetic torque all with unit Nm.

$$T_{el} - T_0 = D(\omega - \omega_g) + J\frac{d\omega}{dt} \tag{4.3}$$

The grid frequency, ω_g, either needs to be measured or estimated. The measurement would be done by a PLL, making the VSM frequency synchronize with the grid. In

this thesis ω_g in equation 4.3 is produced internally using a high pass filter. The high pass filter is implemented by using a low pass filtered negative feed forward, avoiding derivative action. By removing the stationary part of the signal, the resulting effect will be similar to a subtraction of the grid frequency in pu. Using the fact that $P = T\omega$ and introducing the mechanical time constant $T_a = 2H$, the equation can be rewritten as 4.4.

$$\frac{d}{dt}\omega_{vsm} = \frac{p^{r*}}{T_a} - \frac{p_0}{T_a} - \frac{k_d}{T_a}(\omega_{vsm} - \kappa)) \tag{4.4}$$

$$\frac{d}{dt}\kappa = \omega_d * \omega_{VSM} - \omega_b * \kappa \tag{4.5}$$

$$\frac{d}{dt}\theta_{VSM} = \omega_{VSM} * \omega_b \tag{4.6}$$

p^{r*} represents the virtual power driving the inertia and is described further in section Frequency control further down in this chapter. p_0 is the power measured after the LC-filter. The constants k_d is a damping factor used to scale the feedback signal and ω_d is the high pass filter coefficient. θ_{vsm} is used for the park transformation in the VSM model. The integrator seen in 4.2 is a wrapped state integrator or VCO, creating a sawtooth signal going from 0 to 2π.

The figure 4.2 shows the block chart of the implementation of the emulated inertia,
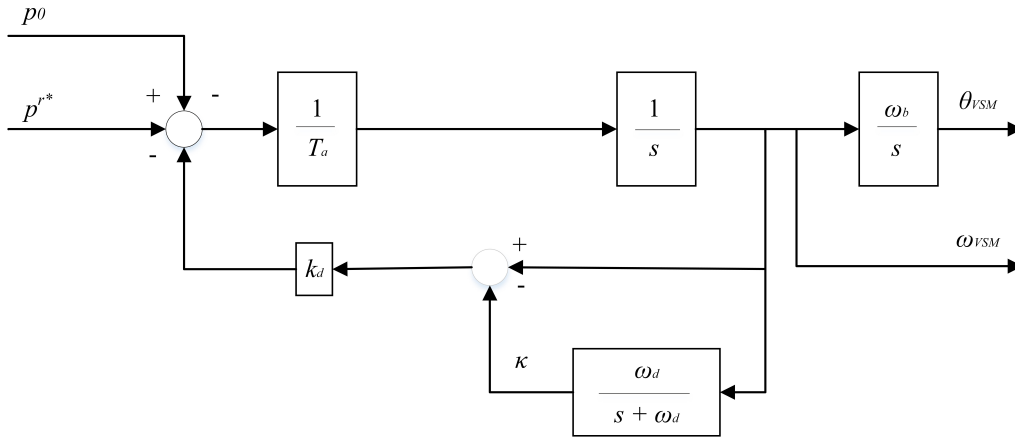
Figure 4.2: Implemetation of the swing equation.

and is represented as the block "Voltage Control" in the system figure 4.1.

By observing the phasors seen in the phasorplot 3.2 from the previous chapter, the state $\delta\theta$ is introduced. With the state space modeling in mind, it is desired to achieve a steady state value used for linearizing. θ_{VSM} is the angle used for SRRF transformations. Form the phasor plot the expression

$$\delta\theta = \theta_{VSM} - \theta_g \tag{4.7}$$

This is because the VSM is chosen for reference when modeling and linearizing. By inserting equation 4.7 in equation 4.8, results in the following expression

$$\frac{d}{dt}\delta\theta_{VSM} = \omega_{VSM}\omega_b - \omega_g\omega_b \tag{4.8}$$

4.1.2 Electrical model of the VSM

In order to be able to control the amplitude of the voltage at the capacitance in the LCL-filter for the VSM, a virtual impedance is used. This is done such that the voltage signal can be transformed to a current signal used as reference for the current controller. Defining the output of the voltage controller as v_e, symbolizing the internally induced voltage of an SM in series with a RL impedance which representing the virtual stator windings. By using Kirchhoff's law of voltage, the internally induced voltage should be equal to the sum of the voltage across the virtual impedance and the voltage measured at the capacitance of the LC filter. This leads to the states given in complex vector form

$$\frac{d}{dt}\mathbf{i}_s = \frac{\omega_b}{l_s}v_e - \frac{\omega_b}{l_s}\mathbf{v}_0 - \left(\frac{r_s\omega_b}{l_s} + j\omega_{VSM}\omega_b\right)\mathbf{i}_s \tag{4.9}$$

Here r_s and l_s is the stator resistance and inductance respectively. As mentioned, r_s and l_s is here tunable, unlike a real SM where these parameters are constant.

4.1.3 Electrical model of the filter inductances

The voltage at the capacitor is calculated in a similar manner as the stator current described above. Kirchhoff's law for current describes that the current $\mathbf{i}_{cv}$, coming out of the inverter is equal to the sum of the current going down in the capacitor at the filter and the current delivered to the grid.

$$\frac{d}{dt}\mathbf{v}_0 = \frac{\omega_b}{c_f}\mathbf{i}_{cv} - \frac{\omega_b}{l_s}\mathbf{i}_0 + j\omega_{VSM}\omega_b \tag{4.10}$$

The current delivered to the grid, i_0, and the current from the inverter, i_{cv}, is modeled in the same way as the stator current, using the sum of voltage.

$$\frac{d}{dt}\mathbf{i}_0 = \frac{\omega_b}{l_g}\mathbf{v}_0 - \frac{\omega_b}{l_g}\mathbf{v}_g - \left(\frac{r_g\omega_b}{l_g} + j\omega_{SM}\omega_b\right)\mathbf{i}_0 \tag{4.11}$$

$$\frac{d}{dt}\mathbf{i}_{cv} = \frac{\omega_b}{l_f}\mathbf{v}_{cv} - \frac{\omega_b}{l_f}\mathbf{v}_0 - \left(\frac{r_f\omega_b}{l_f} + j\omega_{VSM}\omega_b\right)\mathbf{i}_{cv} \tag{4.12}$$

Since the VSM is a virtual machine the parameters that is normally constant be altered in order to achieve a better functioning system. The stator inductance and resistance are two parameters inflicting the poles coming from the state representing the stator current and can be tuned in order to get a more desirable system.

4.2 Control design

The control design of the inverter is a conventional design with an inner loop controlling the current i_{cv} out from the inverter, and an outer loop controlling the amplitude of the voltage at the capacitor in the LC-filter. For active and reactive power control, droop controllers are utilized.

4.2.1 SRRF current controller, inner loop

The synchronous reference frame current controller uses PI-controllers for achieving desired control. The block chart can be seen in figure 4.3. k_{pc} and k_{ic} are the control parameters, and in order to achieve state space form the state γ is introduced, representing the integral of the PI-controller. This controller is based on the expression from 4.12. Reformulating this equation, the equations for the filter inductor is derived as

$$\mathbf{v}_{cv} = \mathbf{v}_f + r_f \mathbf{i}_{cv} + \frac{l_f}{\omega_b}\frac{d}{dt}\mathbf{i}_{cv} + j\omega_b l_f \mathbf{i}_{cv} \tag{4.13}$$

The current through the inductor l_f can be controlled by manipulating $\mathbf{v}_{cv}$. The converter voltage reference can be derived with PI-controllers and decoupling terms. By implementing decoupling terms this system goes from being a MIMO system to a SISO system.

$$
\begin{aligned}
v_{cv,d}^* = v_{d,PI} + v_{f,d}\omega_b l_f i_{cv,q} = v_{0,d} + r_f i_{cv,d}\frac{l_f}{\omega_b}\frac{d}{dt}i_{cv,d} - \omega_b l_f i_{cv,q} \\
v_{cv,q}^* = v_{q,PI} + v_{f,q}\omega_b l_f i_{cv,d} = v_{0,q} + r_f i_{cv,q}\frac{l_f}{\omega_b}\frac{d}{dt}i_{cv,q} - \omega_b l_f i_{cv,d}
\end{aligned}
\tag{4.14}
$$

This leads to the block chart seen in 4.3.
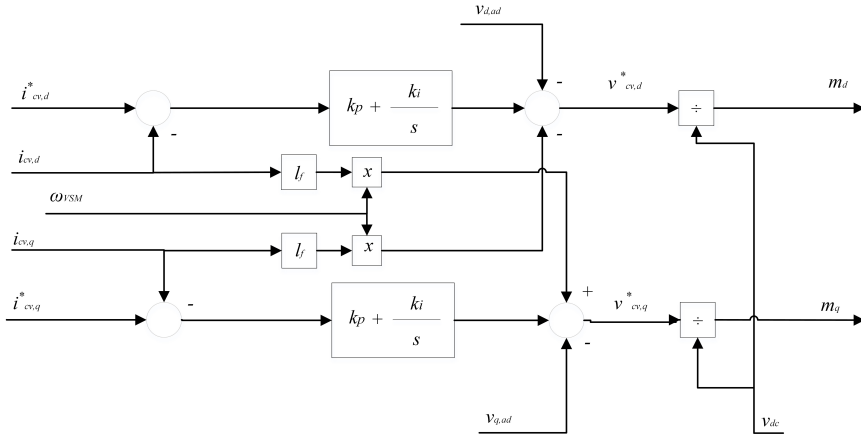
Figure 4.3: Synchronously rotation reference frame controller.

The current and voltage controller have been tuned using modulus optimum and symmetric optimum respectively. The switching and the filter on the AC-side of the
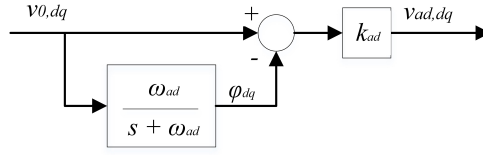
Figure 4.4: Active damping for oscillations on the voltage of the LC-filter capacitor.

inverter can be modeled as a first order delay. This leads to an open loop transfer function as described in section Modulus optimum and Symmetric optimum2.4.

$$\mathbf{v}^*_{cv} = k_{pc}(\mathbf{i}^*_{cv} - \mathbf{i}_{cv}) + k_{ic} * \boldsymbol{\gamma} + jl_1\omega_{SM}\mathbf{i}_{cv} + k_{ffv}\mathbf{v}_0 - \mathbf{v}^*_{AD} \tag{4.15}$$

$$\frac{d}{dt}\boldsymbol{\gamma} = \mathbf{i}^*_{cv} - \mathbf{i}_{cv} \tag{4.16}$$

In equation 4.15 there is also included a term called v_{ad}. This term is for active damping of LC oscillations in the filter. This is designed as a negative feed forward of the, v_0, with a gain called k_{ad} and is high pass filtered. The high pass filter is implemented as a low pass filter with negative gain added to a positive feed forward of the system with a cut off frequency ω_{ad}. This can be seen in the block chart 4.4. Here the state ϕ is introduced, which is the low pass filtered signal of the voltage v_0. The resulting state space equation can be seen in equation 4.18.

$$\mathbf{v}^*_{ad,vsm} = k_{ad,vsm}(\mathbf{v}_{0,vsm} - \boldsymbol{\phi}_{vsm}) \tag{4.17}$$

$$\frac{d}{dt}\boldsymbol{\phi}_{vsm} = \omega_{ad}(\mathbf{v}_{0,vsm} - \omega_{ad}\boldsymbol{\phi}_{vsm}) \tag{4.18}$$

4.2.2   AVR, outer loop

The automatic voltage regulator is modeled as the outer control loop, such that the output from this controller becomes the set point for the current controller. The control variable for this is the internally induced voltage, $\hat{v}_e$. With this the magnitude of the voltage at the capacitor in the filter $\mathbf{v}_0$ is controlled. The controller contains a PI-controller and includes a droop function for low pass filtered reactive power, q_m. As in the current controller, there is introduced a state representing the integral part of the controller, namely ζ. The low pass filter in the droop function introduces a state resulting from the low pass filter. The block chart can be seen in figure 4.5, and the output of the controller is given by

$$\hat{v}_e = k_{pv}(\hat{v}^* - \hat{v}_0) + k_{pv}(q^* - q_m) + k_{iv}\zeta \tag{4.19}$$

The state equations describing the low pass filtered reactive power, q_m, and the integrator part of the PI-controller, ζ, is given by

$$\frac{d}{dt}\zeta = \hat{v}^* - \hat{v}_0 + k_q(q^* - q_m) \tag{4.20}$$
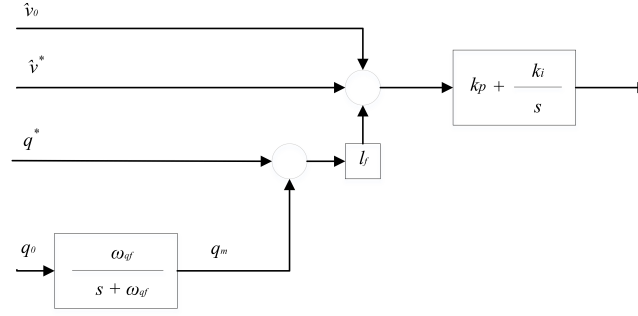
Figure 4.5: Voltage control as outer loop for VSM.

$$\frac{d}{dt}q_m = \omega_{qf}q - \omega_{qf}q_m \tag{4.21}$$

4.2.3 Frequency control

The frequency control block seen in 4.1 is simply a frequency droop function. The output of this droop controller symbolizes the virtual mechanical input power of the VSM. This can be expressed as

$$p^{r*} = p^* - k_\omega(\omega_{VSM} - \omega^*) \tag{4.22}$$

Here p^* is the set point of the active power made by the VSM, k_ω is the active power frequency droop gain and ω^* is the set point for the frequency of the VSM.

4.3 State space model

The equations presented in this chapter forms the states space model with the states seen in 4.23.

$$
\begin{aligned}
\mathbf{x}_{vsm} = \big[& v_{0,d,vsm} \; v_{0q,vsm} \; i_{cv,d,vsm} \; i_{cv,q,vsm} \; \gamma_{d,vsm} \; \gamma_{q,vsm} \; i_{0d,vsm} \; i_{0q,vsm} \\
& \phi_{d,vsm} \; \phi_{q,vsm} \; \zeta_{vsm} \; is_{d,vsm} \; is_{q,vsm} \; q_{m,vsm} \; \omega_{vsm} \; \delta\theta_{vsm} \; \kappa_{vsm} \big] \\
& \mathbf{u}_{vsm} = \big[p^*_{vsm} \; q^*_{vsm} \; v_{g,d} \; v_{g,q} \; \hat{v}^* \; \omega^*_{vsm} \big]
\end{aligned} \tag{4.23}
$$

A summary of the equations for each states can be found in the Appendix 11.1.1.

Chapter 5

Synchronous machine model

This chapter will go through the state space modeling of a SM connected to a grid. The basis of this modeling is taken from [6] with some modifications. This modification is the exclusion of the second damping winding in the q-axis. A similar state space model for the SM can be seen in [29]. The presented model for the synchronous machine based on per unit inductance. When modeling the SM, the assumption of no saturation is made. Hence this is not taken in consideration when modeling the SM. This chapter will first go through the equations for the SM and then present the state space equations with control design.

5.1   The synchronous machine

The In figure 5.1 a overview of the control system of the SM can be seen.
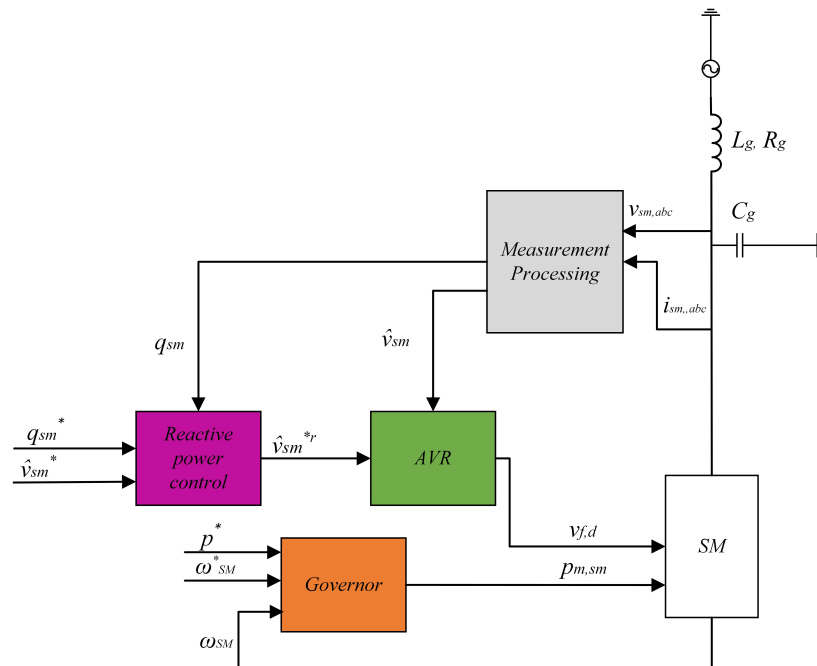
Figure 5.1: System model of the controllers of the SM.

5.2   The SM system equations

This section will present electrical equations of the SM. These equations describe the model of the SM and lays the foundation of the state space model.

5.2.1   Voltage equations

The equivalent circuit of the SM can be seen in figure 5.2 and 5.3 [6]. Here $\phi_d(t)$ and $\phi_q(t)$ are the flux linkages, $v_{SM,d}$ and $v_{SM,q}$ is the armature voltage, $i_{sm,d}$ and $i_{sm,q}$ is the armature current. $i_{1,d}$ and $i_{1,q}$ is the currents in the damper windings. The figure shows that the SM is modeled with a generator convention with currents with defined direction out of the machine, while the direction of the field current and the current in the dampers have been assumed to be flowing in to the machine.
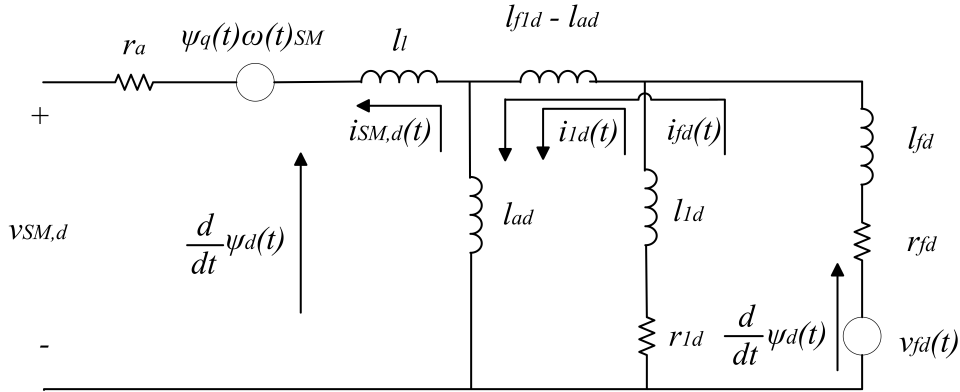
Figure 5.2: Equivalent of the SM for the d-axis.
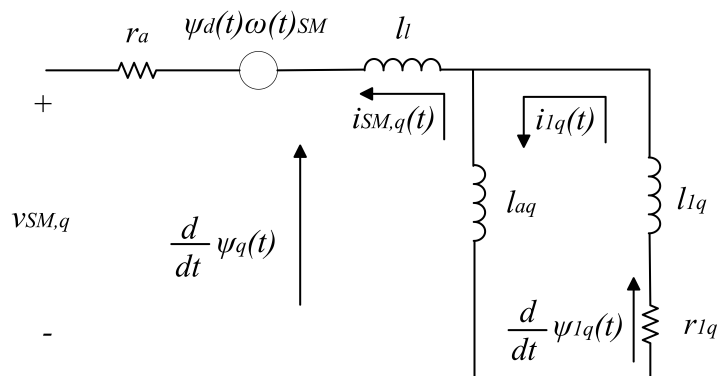
Figure 5.3: Equivalent of the SM for the q-axis.

From the equivalent circuit it can be seen that the voltages $v_{SM,d}$ and $v_{SM,q}$ can be written as

$$v_{SM,d}(t) = \frac{1}{\omega_b}\frac{d}{dt}\psi_d(t) - r_a i_{SM,d}(t) - \psi_q(t)\omega_{SM}(t) \tag{5.1}$$

$$v_{SM,q}(t) = \frac{1}{\omega_b}\frac{d}{dt}\psi_q(t) - r_a i_{SM,q}(t) - \psi_d(t)\omega_{SM}(t) \tag{5.2}$$

Here r_a is the stator resistance, i_{SM} is the armature current and ψ_d and ψ_q are the armature flux linkages. The voltage equations for the rotor can be seen in equations 5.3-5.5. From the equivalent circuit the following context can be interpreted. These equations describe the rotor voltages, flux linkages and currents.

$$v_{fd}(t) = \frac{1}{\omega_b}\frac{d}{dt}\psi_{fd}(t) - r_{fd}i_{fd}(t) \tag{5.3}$$

$$0 = \frac{1}{\omega_b}\frac{d}{dt}\psi_{1d}(t) - r_{1d}i_{1d}(t) \tag{5.4}$$

$$0 = \frac{1}{\omega_b}\frac{d}{dt}\psi_{1q}(t) - r_{1q}i_{1q}(t) \tag{5.5}$$

5.2.2 Flux linkage equations

Writing the stator flux linkage equations results in 5.6 and 5.7. Here l_{ad} and l_{aq} are the armature mutual inductance and l_l is the armature leakage inductance.

$$\psi_d = -(l_{ad} + l_l)i_{SM,d}(t) + l_{ad}i_{fd}(t) + l_{ad}i_{1d}(t) \tag{5.6}$$
$$\psi_q = -(l_{aq} + l_l)i_{SM,q}(t) + l_{aq}i_{1q}(t) \tag{5.7}$$

The rotor flux linkage equations can be written as equation 5.11 - 5.13. Here l_{ffd}, l_{11d}, l_{11q} are the self-inductance of the d-axis and q-axis damping circuit, l_{fd}, l_{1d}, l_{1q} are the leakage inductances and l_{f1d} is the mutual inductance between the d-axis damping circuit and the field.

$$l_{ffd} = l_{f1d} + i_{fd} \tag{5.8}$$
$$l_{11d} = l_{f1d} + i_{1d} \tag{5.9}$$
$$l_{11q} = l_{aq} + i_{1q} \tag{5.10}$$

$$\psi_{fd} = l_{ffd}i_{fd}(t) + l_{f1d}i_{1d}(t) - l_{ad}i_{SM,d}(t) \tag{5.11}$$
$$\psi_{1d} = l_{f1d}i_{fd}(t) + l_{11d}i_{1d}(t) - l_{ad}i_{SM,d}(t) \tag{5.12}$$
$$\psi_{1q} = l_{11q}i_{1q}(t) - l_{ad}i_{SM,d}(t) \tag{5.13}$$

5.3 State space model and control design

The equations resulting from the state space model of the SM can be seen in the appendix 11.1.2. By using the equations from the previous chapter the system can be written in compact form and can be represented in the following manner

$$\mathbf{v} = \frac{1}{\omega_b}\mathbf{l}\frac{d}{dt}\boldsymbol{i}(t) - \mathbf{r}\boldsymbol{i}(t) - \mathbf{J}\boldsymbol{\psi}\omega_{SM}(t) \tag{5.14}$$

In order to write this in sate space form the equation is transformed to

$$\frac{d}{dt}\boldsymbol{i}(t) = \mathbf{l}^{-1}\omega_b(\mathbf{v} + \mathbf{r}\mathbf{i}(t) + \mathbf{J}\boldsymbol{\psi}\omega_{SM}(t)) \qquad (5.15)$$

In order to find these equation and implement them in Matlab, Maple have been used. The $\mathbf{i}$ matrix is $(i_{d,sm}\ i_{q,sm}\ i_{f,sm}\ i_{1d,sm}\ i_{1q,sm})^T$

5.3.1   SM equations of motion

In order to model the dynamics of the SM the swing equation is used. This is done in a similar manner as the implementation in the VSM chapter. As in the VSM the swing equation is modeled as the first derivative of the rotational speed equal to the difference of the mechanical and the electromagnetic torque.

$$T_{SM}\frac{d}{dt}\omega(t) = T_m(t) - T_e(t) \qquad (5.16)$$

T_m and T_e are given by

$$T_m = \frac{p_{m,SM}(t)}{\omega_{SM}(t)} \qquad (5.17)$$

$$T_e = \psi_d(t)i_{SM,q}(t) - \psi_q(t)i_{SM,d}(t) \qquad (5.18)$$

In order to define the phase shift of the grid voltage and the SM voltage the state $\delta\theta_{SM}$ is defined. This is in order to model the SM in the SRRF and can be expressed as

$$\delta\theta_{sm} = \theta_{sm} - \theta_g \qquad (5.19)$$

Here θ_{sm} describes the angle of the reference frame of the SM, while θ_g is the angle of the grid voltage. In order to achieve state space form the first derivative of the expression 5.19 leading to the right hand side of the expresssion to be angular velocities as

$$\frac{d}{dt}\delta\theta_{sm} = \omega_{sm} - \omega_g \qquad (5.20)$$

5.3.2   Reactive power control

The reactive power control is implemented as a droop function. A low pass filter on the measured value of the reactive power produced by the SM is subtracted to a reference then multiplied with a droop gain, here $k_{q,sm}$, and finally subtracted to the voltage amplitude reference. The low pass filter filtering the reactive power leads to the state variable $q_{m,sm}$. The block chart of the implementation can be seem in figure 5.4. This leads to the expression

$$\frac{d}{dt}q_{m_sm}(t) = -\omega_{f,sm}q_{m,sm}(t) + \omega_{f,sm}q_{sm} \qquad (5.21)$$

$$(5.22)$$

where the reactive power is defined as

$$q_{sm}(t) = -v_{sm,d}(t)i_{sm,q}(t) + v_{sm,q}(t)i_{sm,d}(t) \qquad (5.23)$$

The reactive power control sends its signal to the exiter and AVR. This signal can be expressed as

$$\hat{v}_{sm}^{r*}(t) = \hat{v}_{sm}^{*}(t) + k_{q,sm}(t) - q_{m,sm} \qquad (5.24)$$
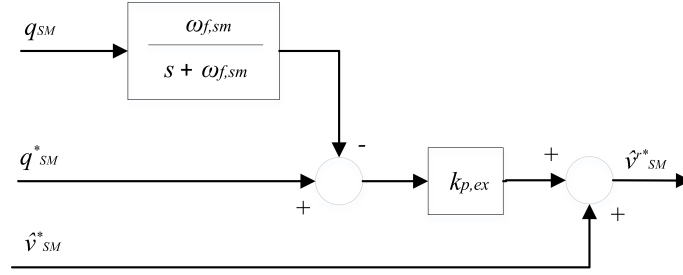
Figure 5.4: Droop function for reactive power.

5.3.3   Exiter with AVR

The exitation system is modeled as a first order delay. It takes in the reference value of the voltage $\hat{v}_{sm}^{r*}$ and controls the field voltage directly. The control objective of the AVR is to control the terminal voltage by using the adjusting the field voltage. It is controlled using a PI with a voltage reference along with a droop function for the reactive power as seen in figure 5.5. Because of the integration part of the PI-controller, the state ζ is introduced. Using the first order delay the field voltage v_{fd} can be modeled as

$$\frac{d}{dt}v_{fd}(t) = \frac{v_{fd}^{*}(t)}{T_{ex}} - \frac{v_{fd}(t)}{T_{ex}} \qquad (5.25)$$

T_{ex} is the filter time constant, and from figure 5.4 and 5.5 it can be seen that

$$v_{fd}^{*}(t) = k_{p,ex}(\hat{v}_{sm}^{r*}(t) - \hat{v}_{sm}(t)) + k_{i,ex}\zeta(t)) \qquad (5.26)$$

$$\frac{d}{dt}\zeta(t) = \hat{v}_{sm}^{r*}(t) - \hat{v}_{sm}(t) \qquad (5.27)$$
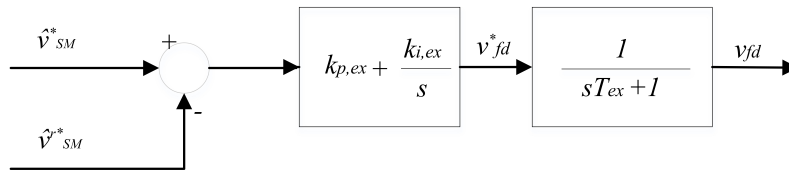
Figure 5.5: Frequency droop with a first order delay.

5.3.4   Governor

For controlling the frequency, active power and the diesel generator the topology in figure 5.6, have been implemented. The frequency is controlled with a droop function, added to a power reference which then goes through a first order delay. The output of the controller is p_m, and symbolizes the mechanical power reference sent to the diesel generator which then deliverers mechanical power to the SM. ω^*_{vsm} and ω_{sm} and p^*_{sm} symbolizes the frequency set point, the actual frequency and the SM active effect set point respectively.

$$p^*_{m,sm}(t) = p^*_{sm}(t) - k_{\omega,sm}(\omega_{sm}(t) - \omega^*_{sm}(t)) \tag{5.28}$$

Because of the first order delay, the mechanical power can be expressed as

$$\frac{d}{dt}p_{m,sm} = \frac{p^*_{m,sm}}{T_{gt}} - \frac{p_m}{T_{gt}} \tag{5.29}$$
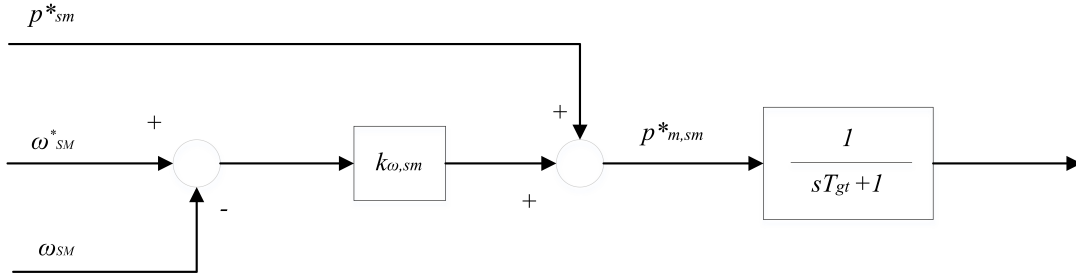
Figure 5.6: Frequency droop with a first order delay.

5.4   Small signal model

The states represented in the small signal model can be seen in equation 5.30.

$$\mathbf{x} = [v_{d,sm}\ v_{q,sm}\ i_{0,d,sm}\ i_{0,q,sm}\ i_{d,sm}\ i_{q,sm}\ i_{fd,sm}\ i_{1d,sm}\ i_{1q,sm}\ \omega_{sm}\ \delta\theta_{sm}\ p_{m,sm}\ ...$$
$$q_{m,sm}\ \zeta_{sm}\ v_{fd,sm}] \tag{5.30}$$
$$\mathbf{u} = [\hat{v}_{g,d}\ \hat{v}_{g,q}\ \omega_g\ p^*_{sm}\ q^*_{sm}\ \hat{v}^*\ \omega^*_{sm}]$$

The equations for each state can be seen in the Appendix 11.1.2.

Chapter 6

Load model

A load model is included in order to make the system more similar to a marine power grid. This load is modeled as a inverter feeding a DC-bus and draws continuously draws power form the grid. As done in the modeling of the VSM, an average model is used to represent the inverter. The DC side of this inverter is modeled as a ideal DC voltage source, with a voltage level set to two times the peak phase voltage of the AC side.

6.1 Control design

The control structure is somewhat similar to the VSM. There is a current controller as an inner control loop controlling the AC-current of the inverter. This controller is designed like the current controller implemented in the VSM. A filter for active damping for oscillations similar to the VSM implementation have also her been implemented in order damp oscillations. A Phase locked loop is used to synchronize the frequency to the grid. A similar implementation of the PLL can be seen in [30].

Because of the filter used in the active damping and the LCL-filter the following states can be deduced respectively

$$\frac{d}{dt}\phi_l = \omega_{ad,l}\mathbf{v}_{0,l} - \omega_{ad,l}\phi_l \tag{6.1}$$

$$\frac{d}{dt}\mathbf{i}_{cv} = \frac{\omega_b}{l_f}\mathbf{v}_{cv} - \frac{\omega_b}{l_f}\mathbf{v}_0 - (\frac{r_f\omega_b}{l_f} + j\omega_{vsm}\omega_b) \tag{6.2}$$

$$\frac{d}{dt}\mathbf{v}_0 = \frac{\omega_b}{c_f}\mathbf{i}_{cv} - \frac{\omega_b}{c_f}\mathbf{i}_0 - j\omega_b\omega_{vsm}\mathbf{v}_0 \tag{6.3}$$

$$\frac{d}{dt}\mathbf{i}_0 = \frac{\omega_b}{l_g}\mathbf{v}_0 - \frac{\omega_b}{l_g}\mathbf{v}_g - (\frac{r_g\omega_b}{l_g} + j\omega_{vsm}\omega_b) \tag{6.4}$$

$$\tag{6.5}$$

Notice that the currents i_{cv} and i_0 have defined direction leaving the inverter. This requires the set point of the active power to be negative. This also must be taken in consideration when modeling the grid voltage.

The the integral part of the PI-controller in the current current controller is expressed by

$$\boldsymbol{\gamma}_{load} = \mathbf{i}_{cv}^{*} - \mathbf{i}_{cv} \qquad (6.6)$$

6.1.1   Phase locked loop

The PLL is used to calculate the position of the synchronous rotating reference frame by measurements. This is done by measuring the voltage at the capacitor in the LCL-filter and calculating the phase angle. First the signal is transformed in to dq signals and low pass filtered. This results in the states $\mathbf{v}_{PLL}$

$$\frac{d}{dt}\mathbf{v}_{PLL}(t) = \omega_{PLL}\mathbf{v}_{0}(t) - \omega_{PLL}\mathbf{v}_{PLL}(t) \qquad (6.7)$$

The phase angle error is then found by using the inverse tangent function. The error between the phase angle is then sent to a PI-controller for minimizing the angle between the two reference frames. Because of the integrator of the PI-controller the state ϵ_{PLL} is introduced as

$$\frac{d}{dt}\epsilon = tan^{-1}(\frac{v_{pll,q}(t)}{v_{pll,d}(t)}) \qquad (6.8)$$

Since the modeling of reference frame of the state space model is done with respect to the SM in the system the state $\delta\theta_{PLL}$ describing the deviation of the rotating reference frames, the state results in

$$\frac{d}{dt}\delta\theta_{pll}(t) = \omega_{b}(\omega_{pll}(t) - \omega_{g}(t)) \qquad (6.9)$$

The implementation of the PLL can be seen in figure 6.1. The incoming voltage signals have been low pass filtered. Then the angle deviation θ is calculated by using the inverse tangent. The desired deviation between the reference frames is zero, and the deviation goes to the PI-controller. The normalized frequency is added. The transformation of the frequency to an angle is an integrator. The integrator is in wrapped state, oscillating from 0 to 2π, creating a sawtooth signal used for the park-transformations.

6.2   State space model

The equations presented in this chapter forms the states space model with the states seen in 6.10.

$$\begin{aligned} \mathbf{x}_{load} = [&v_{0,d,load} \; v_{0q,load} \; i_{cv,d,load} \; i_{cv,q,load} \; \gamma_{d,load} \; \gamma_{q,load} \; i_{0d,load} \; i_{0q,load} \\ &\phi_{d,load} \; \phi_{q,load} \; \zeta_{load} \; is_{d,load} \; is_{q,load} \; q_{m,load} \; \omega_{load} \; \delta\theta_{load} \; \kappa_{load}] \\ &\mathbf{u}_{load} = [i_{cv,d}^{*} \; i_{cv,q}^{*}] \end{aligned} \qquad (6.10)$$

A summary of the equations for each states can be found in the Appendix 11.1.1.
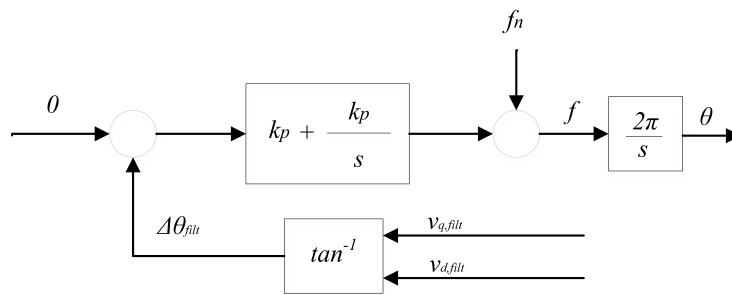
Figure 6.1: Phase locked loop. The incoming voltage signals have been low pass filtered.

Chapter 7

Small signal model

The full model for the SM and VSM results in a equation system of 47 states and 10 inputs as seen in 7.1. The equations for most of the states is derived in previous chapters. Models for the VSM, SM and load, each connected to a grid, have been presented. In addition to this a model with only the VSM and SM, and only the VSM and load have been analyzed and the whole system together.

$$\begin{aligned}
\mathbf{x}_{vsm} = [&v_{0,d,vsm}\ v_{0q,vsm}\ i_{cv,d,vsm}\ i_{cv,q,vsm}\ \gamma_{d,vsm}\ \gamma_{q,vsm}\ i_{0d,vsm}\ i_{0q,vsm} \\
&\phi_{d,vsm}\ \phi_{q,vsm}\ \zeta_{vsm}\ is_{d,vsm}\ is_{q,vsm}\ q_{m,vsm}\ \omega_{vsm}\ \kappa_{vsm}] \\
\mathbf{x}_{sm} = [&v_{d,sm}\ v_{q,sm}\ i_{0,d,sm}\ i_{0,q,sm}\ i_{d,sm}\ i_{q,sm}\ i_{fd,sm}\ i_{1d,sm} \\
&i_{1q,sm}\ \omega_{sm}\ \delta\theta_{sm}\ p_{m,sm}\ q_{m,sm}\ \zeta_{sm}\ v_{fd,sm}\ ] \\
\mathbf{x}_{load} = [&v_{0d,l}\ v_{cvq,l}\ i_{cvd,l}\ \gamma_{d,l}\ \gamma_{q,l}\ i_{0d,l}\ i_{0d,l}\ \phi_{d,l} \\
&\phi_{q,l}\ v_{pll,d,l}\ v_{pll,d,l}\ \delta\theta_{pll,l}\ v_{g,d,l}\ v_{g,d,l}] \\
\mathbf{u}_{vsm} = [&p_{vsm}^*\ q_{vsm}^*\ \hat{v}_{vsm}^*\ \omega_{vsm}^*] \\
\mathbf{u}_{sm} = [&p_{sm}^*\ q_{sm}^*\ \hat{v}_{sm}^*\ \omega_{sm}^*] \\
\mathbf{u}_{load} = [&i_{cv,d,load}^*\ i_{cv,q,load}^*]
\end{aligned} \tag{7.1}$$

In order to implement the different variations of the models, some equations have been changed. This mainly relates to the states that appears in the coupling equations tying the system together. This is the output currents $\mathbf{i}_0$ and the grid voltage $\mathbf{v}_g$. The state $\delta\theta_{VSM}$ is removed from the model containing both SM and VSM. This is because of the modeling choice of using the VSM as reference for the SRRF. The state $\delta\theta_{SM}$ and $\delta\theta_{pll}$ is for the full system model referenced to the frequency of the virtual rotor of the VSM. For the grid connected models the state $\mathbf{v}_g$ have been replaced by the input values $\hat{\mathbf{v}}_g$ and is represented in the u-matrix. When putting the full system model together a few alterations have to be done to the equations in order to tie the different components together. As the grid equivalent is removed, states for the grid voltage must be introduced. These can be derived as the current summation in a node.

$$\mathbf{I}_{0,vsm} + \mathbf{I}_{0,sm} = \mathbf{I}_{0,load} + \frac{\mathbf{V}_g}{R_l} + c_l \frac{d}{dt} \mathbf{V}_g \tag{7.2}$$

Here the left-hand side is the sum of currents going in to the AC-bus, namely the currents from the VSM and SM, and the right-hand side is the sum of outgoing currents which is the current going to the load model and the resistor and capacitance on the AC-bus. This equation is not in per unit. The problem with this equation is that the currents is phase shifted and is not in phase as this equation may assume. Since the reference is the VSM-angle the currents $i_{0,sm}$ and $i_{0,load}$ needs to be rotated such that the phase angel shift is taken in consideration. As shown in chapter 2, section 3.3 this could be done with the states $\delta\theta_{sm}$ and $\delta\theta_{load}$ representing the phase shift from the VSM for the SM and load model.

Using the rotation matrix derived in chapter two the equation for the first derivative of the grid voltage can be rewritten as

$$
\begin{aligned}
\frac{d}{dt}v_{g,d} &= \omega_b\omega_{vsm}v_{g,q} - \omega_b\frac{v_{g,d}}{c_l r_l} + \omega_b\frac{i_{0,vsm,d}}{c_l} + \omega_b i_{0,load,d}cos(\delta\theta_{load}) \\
&\quad -\omega_b i_{0,load,q}sin(\delta\theta_{laod}) + \omega_b i_{0,d,sm}cos(\delta\theta_{sm}) - \omega_b i_{0,q}sin(\delta\theta_{sm}) \\
\frac{d}{dt}v_{g,q} &= -\omega_b\omega_{vsm}v_{g,d} - \omega_b\frac{v_{g,q}}{c_l r_l} + \omega_b\frac{i_{0,vsm,q}}{c_l} + \omega_b i_{0,load,q}sin(\delta\theta_{load}) \\
&\quad +\omega_b i_{0,load,q}cos(\delta\theta_{laod}) + \omega_b i_{0,d,sm}sin(\delta\theta_{sm}) + \omega_b i_{0,q}cos(\delta\theta_{sm})
\end{aligned}
\tag{7.3}
$$

Here the equation is on per unit form and the phase shift is taken in consideration.

Since the reference angle of the phase shift, the state $\delta\theta_{vsm}$ have no function and is therefore removed. The expressions for the states $\mathbf{i}_{0,sm}$ and $\mathbf{i}_{0,load}$ also needs to be altered in order to take the phase shift in consideration. The equation altered for the states belong to the load model is

$$
\begin{aligned}
\frac{d}{dt}i_{0,d,load} &= \omega_b\frac{v_{0,d,load}}{l_{g,SM}} - \omega_b\frac{i_{0,d,load}r_g}{l_{g,load}} + \omega_b\omega_{vsm}i_{0,q,load} - \frac{\omega_b v_{g,d}cos(\delta\theta)}{l_{g,load}} - \frac{\omega_b v_{g,q}sin(\delta\theta)}{l_{g,load}} \\
\frac{d}{dt}i_{0,q,load} &= \omega_b\frac{v_{0,d,load}}{l_{g,load}} - \omega_b\frac{i_{0,q,load}r_g}{l_{g,load}} - \omega_b\omega_{vsm}i_{0,d,load} + \frac{\omega_b v_{g,d}sin(\delta\theta)}{l_{g,load}} - \frac{\omega_b v_{g,q}cos(\delta\theta)}{l_{g,load}}
\end{aligned}
$$

and the change in the equations of the SM is

$$
\begin{aligned}
\frac{d}{dt}i_{0,d,SM} &= \omega_b\frac{v_{0,d,SM}}{l_{g,SM}} - \omega_b\frac{i_{0,d,SM}r_{mg}}{l_{g,sm}} + \omega_b\omega_{vsm}i_{0,q,SM} - \frac{\omega_b v_{g,d}cos(\delta\theta)}{l_{g,SM}} - \frac{\omega_b v_{g,q}sin(\delta\theta)}{l_{g,SM}} \\
\frac{d}{dt}i_{0,q,SM} &= \omega_b\frac{v_{0,d,SM}}{l_{g,SM}} - \omega_b\frac{i_{0,q,SM}r_{mg}}{l_{g,sm}} - \omega_b\omega_{vsm}i_{0,d,SM} + \frac{\omega_b v_{g,d}sin(\delta\theta)}{l_{g,SM}} - \frac{\omega_b v_{g,q}cos(\delta\theta)}{l_{SM}}
\end{aligned}
$$

Parameter	Value	Parameter	Value	Inputs	Value
S_b	$2.75 \cdot 10^6 MVA$	T_{sm}	$4s$	p^*_{sm}	0.5
V_b	$690V_{LL,RMS}$	$k_{d,sm}$	40	$q^*_{m,sm}$	0
ω_b	$2\pi \cdot 50Hz$	$T_{gt,sm}$	$0.5s$	ω^*_{sm}	1
$T_{a,vsm}$	$4s$	$T_{ex,sm}$	$0.1s$	$\hat{v}^*_{sm}$	1
$k_{d,vsm}$	40	$k_{p,ex}$	13.2	p^*_{vsm}	0.5
$\omega_{d,vsm}$	$5\frac{rad}{s}$	$k_{i,ex}$	38.5	q^*_{vsm}	0.2
$l_{s,vsm}$	$0.25pu$	$k_{\omega,sm}$	20	$\hat{v}^*_{vsm}$	1
$r_{s,vsm}$	$0.1pu$	$\omega_{f,sm}$	$1000\frac{rad}{s}$	ω^*_{vsm}	1
$k_{pc,vsm}$	1.27	$k_{q,sm}$	0.2	$i^*_{cv,dload}$	-1
$k_{ic,vsm}$	15	$c_{g,sm}$	$1.5 \cdot 10^{-5}pu$	$i^*_{cv,q,load}$	0
$k_{ad,vsm}$	1.5	$l_{g,sm}$	$0.2pu$		
$\omega_{ad,vsm}$	$50\frac{rad}{s}$	$r_{g,sm}$	$0.01pu$		
$k_{\omega,vsm}$	20	c_l	$1 \cdot 10^{-2}pu$		
$k_{pv,vsm}$	0.29	r_l	$0.2pu$		
$k_{iv,vsm}$	92	$k_{p,pll}$	0.084		
$\omega_{qf,vsm}$	$200\frac{rad}{s}$	$k_{i,pll}$	4.7		
$k_{q,vsm}$	$0.1pu$	$k_{p,p}$	0.81		
$r_{f,vsm}$	$0.003pu$	$k_{i,p}$	167		
$l_{f,vsm}$	$0.08pu$	$k_{p,c}$	1.27		
$r_{g,vsm}$	0.005	$k_{i,c}$	11.8		
$l_{g,vsm}$	0.074	k_{ad}	1.5		

Table 7.1: Parameters used for the the full system model.

The small signal model for the full system contain the states seen in 7.4. The equations used for this model can be seen in the Appendix 11.1.3

$$
\begin{aligned}
\mathbf{x} = [&v_{0,d,vsm} \; v_{0q,vsm} \; i_{cv,d,vsm} \; i_{cv,q,vsm} \; \gamma_{d,vsm} \; \gamma_{q,vsm} \; i_{0d,vsm} \; i_{0q,vsm} \cdots \\
&\phi_{d,vsm} \; \phi_{q,vsm} \; \zeta_{vsm} \; is_{d,vsm} \; is_{q,vsm} \; q_{m,vsm} \; \omega_{vsm} \; \kappa_{vsm} v_{d,sm} \; v_{q,sm} \cdots \\
&i_{0,d,sm} \; i_{0,q,sm} \; i_{d,sm} \; i_{q,sm} \; i_{fd,sm} \; i_{1d,sm} \; i_{1q,sm} \; \omega_{sm} \; \delta\theta_{sm} \; p_{m,sm} \cdots \\
&q_{m,sm} \; \zeta_{sm} \; v_{fd,sm} v_{0d,l} \; v_{cvq,l} \; i_{cvd,l} \; \gamma_{d,l} \; \gamma_{q,l} i_{0d,l} \; i_{0d,l} \; \phi_{d,l} \cdots \\
&\phi_{q,l} \; v_{pll,d,l} \; v_{pll,d,l} \; \delta\theta_{pll,l} \; v_{g,d,l} \; v_{g,d,l} \; \rho_l \; v_{dc,l}]
\end{aligned}
\tag{7.4}
$$

$$
\mathbf{u} = [p^*_{vsm} \; q^*_{vsm} \; \hat{v}^* \; \omega^*_{vsm} \; p^*_{sm} \; q^*_{sm} \; \hat{v}^* \; \omega^*_{sm} \; i^*_{cv,d} \; i^*_{cv,q}]
$$

The table 7.1 describes the base values for the model containing the VSM, SM and the load model. Some parameters may have been changed when modeling and simulating the different variations of the system.

Chapter 8

Simulation results

In order to analyze the stability of the system, a small signal model was developed, and the stability of the linear system was investigated. As mentioned, the equation system was solved in Matlab with respect to the derivative equal to zero. This gave the stationary values used as linearization points for the respective variable. The linearized model has been compared to a Simulink simulation to ensure the linearization is correct. All relevant plots and information are in steady state. The transient phase leading to the steady state for the VSM, SM and load is not a topic discussed in this thesis.

8.1 Model verification

The linearized model and a model created in Simulink have been compared in order to validate the linearized model. The system is exposed to perturbations in variables defined as inputs seen in the **u**-matrix. The dynamical response should be similar to some extent. Because linearization is an approximation method valid around the linearization point, and that the system is not linear, leaving the linearized area can give some offsets between the small signal model and the simulated model. Although this is true, the linearization model is still valid for the system in steady sate and with small disturbances. The offset mentioned will disappear if the perturbations is set to the value used for linearization. The dynamics of the two systems should be similar if the perturbation is not far from the linearization point. When testing this the model is in steady state and as a step is done in the input value the two systems is observed until steady state is achieved with new stationary values.

In order to validate and analyze the model containing the VSM, SM and load, the three was first tested separately connected to a grid. Then divided in systems, the VSM connected to the SM and the VSM connected to the load was tested and a final model of the system containing all three models. This is to validate not only the small signal model but also the control parameters for the SM and the VSM.

8.1.1 VSM connected to grid

The inputs used for linearization can be seen in table 7.1. A perturbation on the system is done by using as step in the active power reference delivered from the inverter. This step is from 0.5 to 0.55 and back from 0.55 to 0.5. Even though the VSM model can handle a greater step in active power reference, it is chosen to be limited to a change of 0.05 because it is desired to compare the response of the VSM and SM from the next chapter. Because of limitations in the small signal model of the SM the disturbance is limited to 0.05. As seen in figure 8.1, both the linearized model and the model simulated in Simulink have a similar dynamic and the offset in the models is low even despite leaving the linearized area.

The figure 8.1 shows the frequency and the current out of the LCL-filter of the VSM in addition to the active power delivered from the VSM. As the step in the input value is done, the speed of the virtual rotor starts to increase, and the currents start to change leading to a change in the active power. The system stabilizes at $p^*_{vsm} = 0.55$ for a moment before the reference value is reset. The transient response is well damped and reaches steady state almost within a second. The system is well damped and reaches steady state after a reasonable time.
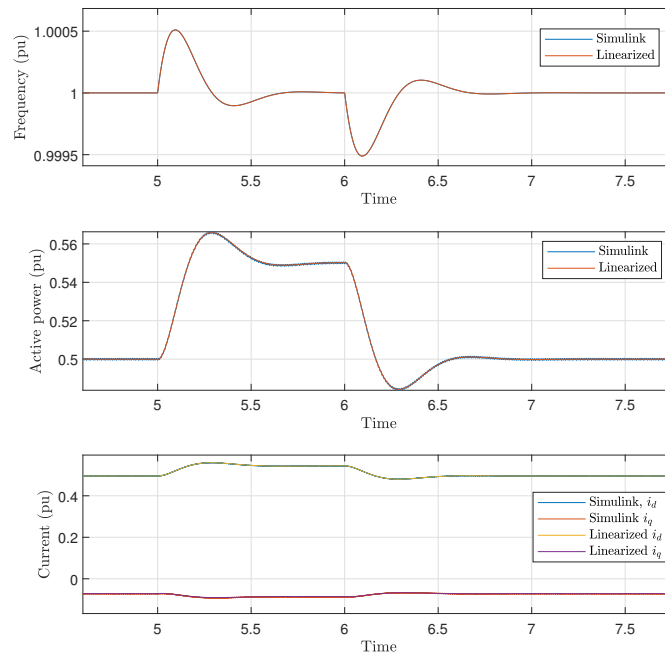
Figure 8.1: This figure show some of the states to VSM connected to the grid. Here the frequency, active power delivered and current from the VSM of the linearized model and the model simulated in Simulink of the VSM connected to a grid is compared. A step change in the delivered active power reference is done, from 0.5 to 0.55

8.1.2   SM connected to grid

As the VSM, the SM was validated for a perturbation in the active power reference. The comparison of the dynamical response of the linearized model and the model made in Simulink can be seen in 8.2. As the plot shows, the linearized model is a good fit for the simulated model in Simulink. Making a bigger step than 0.05 gives an offset in the states influenced by the perturbation. This may be due to the mathematical modeling of the SM; the linearized system is less accurate when leaving the linearization point due to nonlinearities around the linearized are. Because of this a smaller perturbation is done on the VSM in order to compare the two.

The response of the SM and VSM is similar. As the step is done the frequency starts rising together with the current coming out of the LCL-filter and the active power. The difference is the oscillatory behavior of the SM. For the SM, all states shown in the figure is oscillating more than the VSM but reaches steady state after a few seconds. Here the advantage of tuning the virtual impedance is displayed. The damping factor, $k_{d,vsm}$ can be altered in order to achieve a more damped performance for the VSM, while the machine parameters of the SM is constants that cannot be changed. The oscillations for the SM can also be seen in the current and the active power but cease after little time and the model reaches steady state.
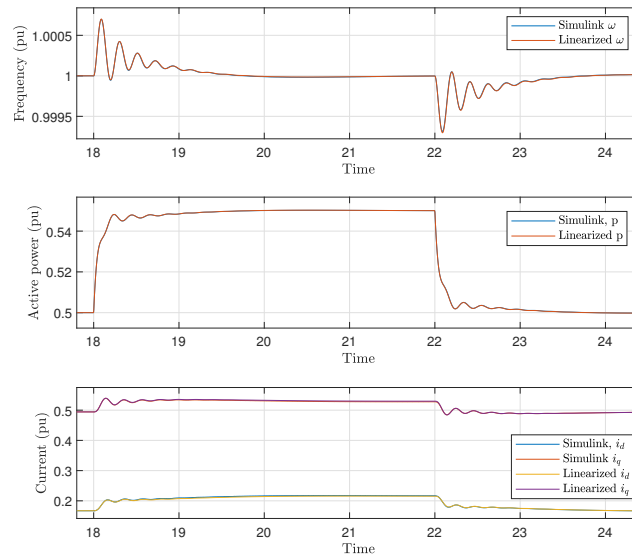
Figure 8.2: This figure show some of the states to SM connected to the grid. Here the frequency, active power delivered and current from the inverter of the linearized model and the model simulated in Simulink of the VSM connected to a grid is compared. A step change in the delivered active power reference is done, from 0.5 to 0.55

8.1.3   VSM and load

The system containing the VSM and load model have been linearized and validated against a grid model, and the system response can be seen in figure 8.3. Here a step in the in the active power reference in the load model, $i_{cv,d}$ is done from -1.2 to -1.21. Some offset in the plot for frequency can be seen in the figure. As mentioned some dynamic characteristics may be lost in the linearization, and a thing to have in mind is that the state perturbed consists of nonlinear terms. Altering this state can lead to some difference in the linearized model and the model simulated in Simulink. Also, the noise in the currents may contribute to the offset. Still the models have similar dynamics and reaches the same steady state values when in the linearization point.

The response resulting from the step in the current reference is damped. The frequency shows a transient phase lasting over a second before settling. No oscillations can be observed in the frequency and the q-axis current, but a small oscillation can be seen in the d-axis current.
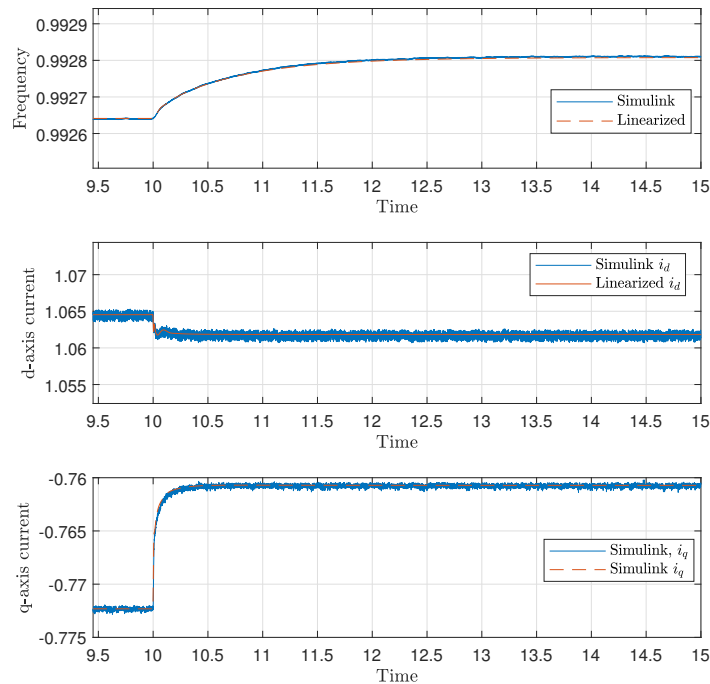
Figure 8.3: This figure shows the response of the VSM and load model when a step in the current reference in the load model is done. The step is from 1.2 pu to 1.21 in the d-axis current.

8.1.4 SM and load

The response of the SM connected to a load model can be seen in figure 8.4. The signals plotted is the frequency of the SM and the currents out of the filter of the SM. The change in inputs is identical to the VSM in the previous section, a step is done in the d-axis current reference in the load model from 1.2 pu to 1.21 pu, but the response is not similar. As the figure shows, the response is oscillation for several seconds before settling. This goes for the frequency and the currents out of the SM. From this figure it can be seen that the SM could use some more damping on the rotor speed.

It can also in this plot be seen that there is some noise in the currents, but the frequency of the SM is a good fit. The figure 8.4 shows that the linearized model and the one simulated in Simulink is a good match.
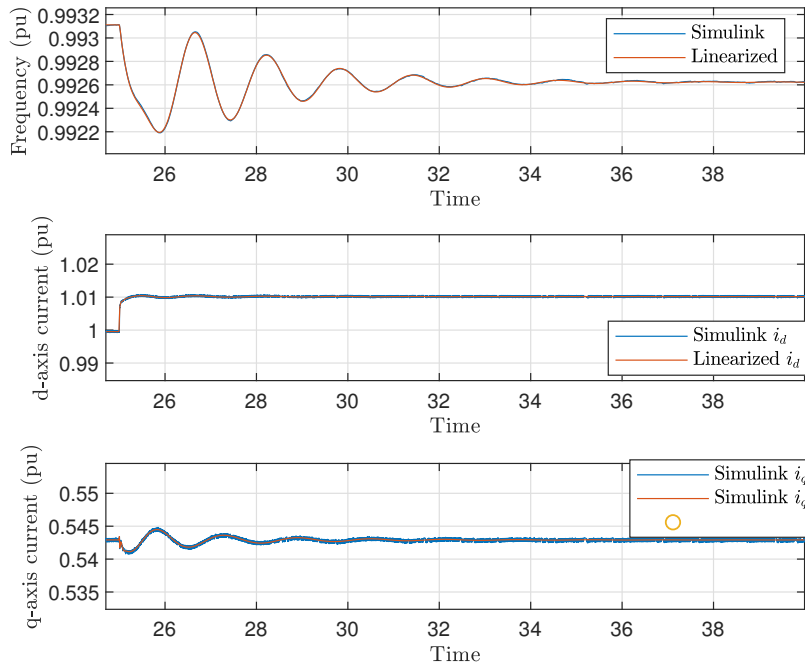
Figure 8.4: This figure shows the response of the SM and load model when a step in the current reference in the load model is done. The step is from 1.2 pu to 1.21 in the d-axis current.

8.1.5 VSM and SM

After validating the VSM and the SM with a grid connection and the load model, the two systems are coupled together forming its own grid. A resistive and a capacitive load is implemented at the bus connection after the LCL-filter for the VSM and inductor from the SM. The load model is not included in this simulation. The
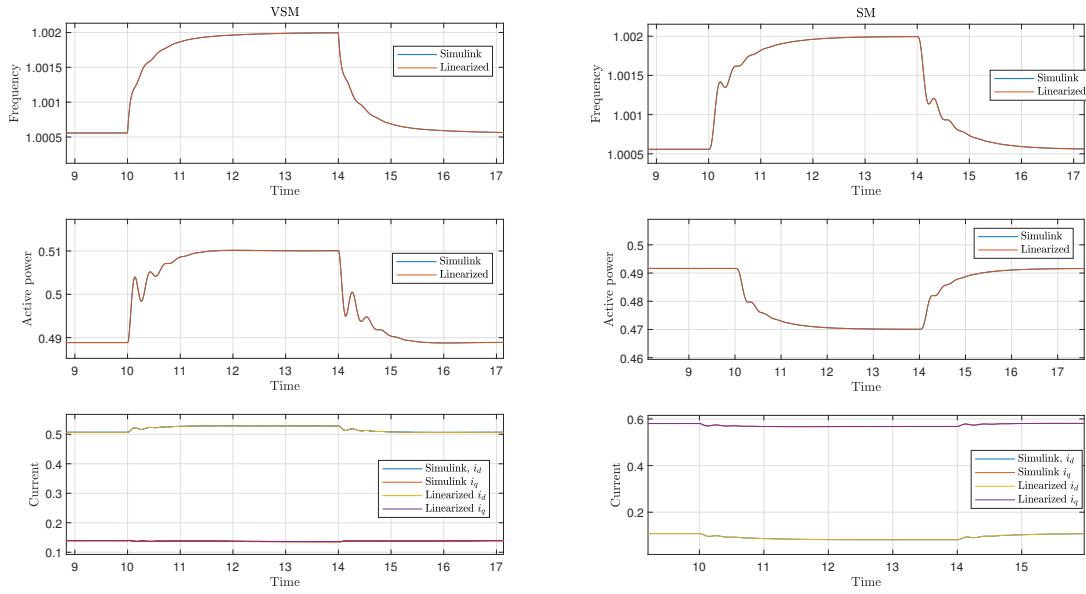
Figure 8.5: Figure showing some of the states of the SM and VSM changing because of a change in reference value in active power.

reisitive load is set to 0.2 pu, while the capacitance is 0.054 pu.

The input values for active power reference, p^*_{vsm} and p^*_{sm}, is set from 0.5 to 0.6 for both VSM and SM. A step from 0.6 to 0.65 and back after a few seconds is done for set point to the VSM. The dynamic response of states belonging to the VSM and SM can be seen in figure 8.5. In these figures it is shown how the active power from the VSM rises while the active power from the SM decreases. As the step is back to its original position, the power delivered goes back to its steady state. While the response of the frequency for the VSM is somewhat similar to the grid connected case, the current is oscillating more. This may be due to the lack of damping in the SM. The reason the active power out of both VSM and SM does not go to the reference value is that the load is not 1.2 pu, and because of the droop controllers the load is shared.

8.1.6   Full system model

The dynamical response of the model including the VSM, SM and load model can be seen in figure 8.6. The figure is showing the frequency of the VSM and the SM in the two top plots, d-axis current for the VSM and SM in the second row and the q-axis current for the VSM and SM at the bottom. As this figure shows, the linearized model of the system and the Simulink model is a good match. A small offset in the transient of the current can be observed. This may be due to some loss of characteristic caused by the linearization. The system goes to the same steady state value. Although the currents have some disturbance the linearized model lies

on an appropriate level within the noise.

Comparing the responses of the VSM connected to the load model and the SM connected to the load model to the full system put together it can be seen that the responses is merged together combining the damped response of the VSM and the undamped response of the SM. The oscillations for the rotor speed of the SM can be recognized from the grid connected model. Even though the frequency of the SM is oscillating, the response of the currents of the SM shows a response that is dominated by a damped response.
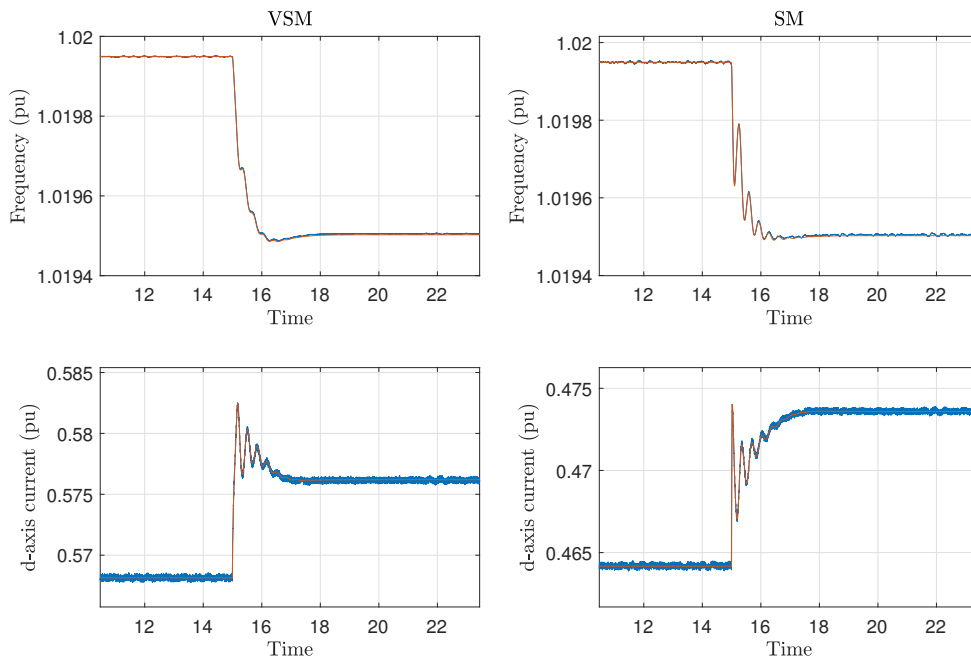
Figure 8.6: This figure is showing the response of the full system after a step change in the active power reference from -0.5 to -0.55.

Chapter 9

Eigenvalue analysis

In addition to evaluate the system response to a perturbation in the defined inputs, the eigenvalues of the small signal model have been used for a system analysis. The eigenvalues are calculated from the system matrix $\mathbf{A}$ in the steady state equilibrium points, and with chosen inputs for the system, using Matlab. By defining the input values when linearizing and changing these in small steps while linearizing each time, the system eigenvalues can be observed as the input values change. This shows the stability margin for different inputs of the system and can descirbe how the system response is with different inputs. The stability of the linearization can be analyzed using the eigenvalues. If the eigenvalues change relatively much when moving the linearization points of the inputs, it can be because the system is nonlinear around these points.

Using the linearized models presented in the previous chapter and calculating the eigenvalues of each system the participation factors have been calculated. These can be used to tie each mode to a state and decide what states influence each other. The participation factors are presented as the main participating factor, meaning the states with the highest influence of the respective mode is shown. After calculating the participation factors the values have been normalized using the sum of the absolute value of each state to the different modes. In addition, the factors have been sorted from highest to lowest, meaning the first factor have the most influence of the pole. Values under 10% have been neglected in order to most efficiently present the results. This means that some information could get lost because some states are more dominant than the others. The participation factors can be seen in the tables describing the modes and the main participating factors. If a eigenvalue is a complex conjugated pair the it will be presented as $\lambda_{n,m}$. The participation factors for these modes is the same.

9.1   VSM to grid

As mentioned, the VSM was modeled connected to a grid with 1 pu voltage as shown in figure 4.1. After calculating the stationary values for the system equilibrium and linearizing around these operation points the eigenvalues of the system matrix $\mathbf{A}$

was calculated and can be found in table 9.1.

Mode	Value	Participation factor
$\lambda_{1,2}$	-1693.8+6520.4i	$v_{0,d,VSM}\ v_{0,q,VSM}\ i_{cv,d,VSM}\ i_{cv,q,VSM}$
$\lambda_{3,4}$	-1860+6161.2i	$i_{cv,q,VSM}\ i_{cv,d,VSM}\ v_{0,q,VSM}\ v_{0,d,VSM}$
$\lambda_{5,6}$	-1483.7+260.7i	$i_{0,q,VSM}\ i_{0,d,VSM}\ i_{cv,d,VSM}\ i_{cv,q,VSM}\ i_{s,d,VSM}\ i_{s,q}$
$\lambda_{7,8}$	-61.14+305.19i	$i_{s,d,VSM}\ i_{s,q,VSM}\ i_{0,d,VSM}\ i_{0,q,VSM}$
λ_{9}	-191.77	$q_{m,VSM}\ \zeta_{VSM}$
$\lambda_{10,11}$	-57.01+17.78i	$\zeta_{VSM}\ \phi_{d,VSM}\ \phi_{q,VSM}$
λ_{12}	-37.97	$\phi_{q,VSM}\ \phi_{d,VSM}\ \zeta_{VSM}$
$\lambda_{13,14}$	-6.23+9.03i	$\delta\theta_{VSM}\ \omega_{VSM}\ \kappa_{VSM}$
$\lambda_{15,16}$	-9.36+0.19i	$\kappa_{vsm}\ \delta\theta\ \gamma_{q,VSM}\ \omega_{VSM}\ \phi_{d,VSM}\ \gamma_{d,VSM}\ \phi_{q,VSM}$
λ_{17}	-12.05	$\gamma_{d,VSM}\ \gamma_{q,VSM}$

Table 9.1: VSM eigenvalues together with participation factors

The first thing to notice is that the real part of each eigenvalue is negative. If a real part of the any of the eigenvalues was positive it would imply that the system is unstable [27]. By looking at table 9.1 it can be observed that the poles are well damped and sufficient fast. The lowest damping ratio results from the modes $\lambda_{7,8}$ and is equal to $-\sigma_{7,8}/\sqrt{\sigma_{7,8}^2 + \omega_{7,8}^2} \approx 0.19$ where σ is the real part and ω is the imaginary part. All of the eigenvalues that have a complex part seem to have a sufficient real part leading to damped response. The eigenvalue closest to origo is the complex conjugated pair $\lambda_{13,14}$, but their real value is not of any concern because despite being the highest it is still far from the right half plane. The complex conjugated pairs $\lambda_{1,2}$ and $\lambda_{3,4}$ have a high oscillation frequency but is well damped. The states participating in these modes is the voltage over the filter capacitor and the current from the inverter. Looking at the participation factors it can be noticed that some states are more often represented as a major participant for different modes. In this case the currents of the VSM shows that many states are coupled with other and is a participant in many modes.

The figure 9.1 shows how the eigenvalues of the VSM model connected to a grid changes as the set point for delivered power for the linearized model is changed. By changing the input values used for linearization the eigenvalues change. The plot is divided into three parts, zoomed in on the groups of eigenvalues. The plot shows how the eigenvalues change as the set point is changed with small steps from -2 to 2 pu and is zoomed in on different locations in the left half plane. The interval testes describes power flow in both directions, meaning if a battery energy storage system is utilized this would describe charging and discharging the battery. Even though the interval of change in setpoint is relatively big, the system modes is not much inflicted, the modes are relatively stationary. This means that the VSM model connected to a grid can operate within an operation range without having trouble with stability if the only thing changing is the load delivered or absorbed.
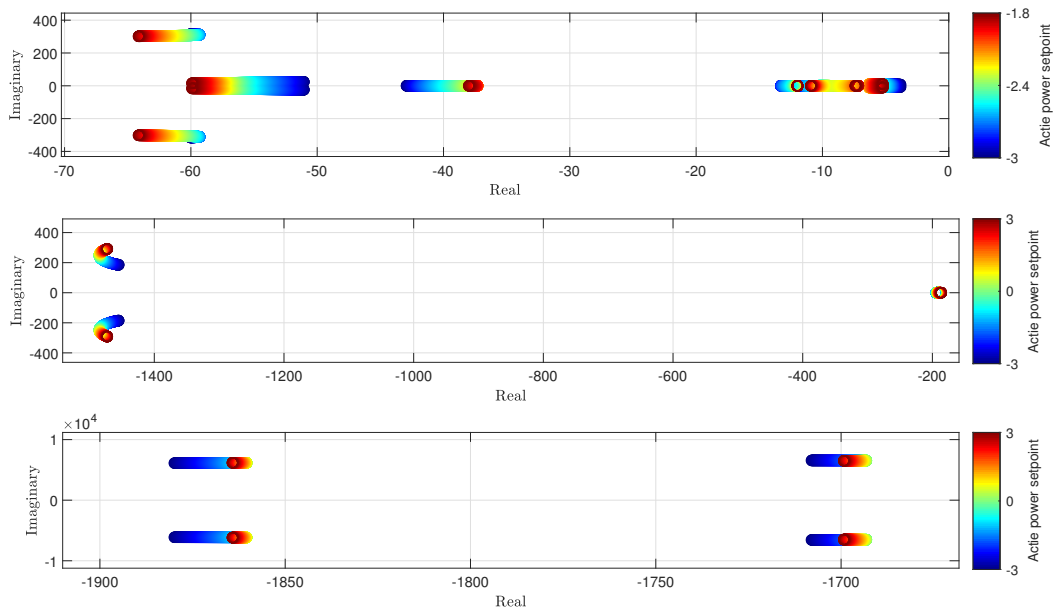
Figure 9.1: Plot showing how the VSM eigenvalues changes as the setpoint of delivered power is changed from -3 to 3 pu. Starting with the fastest eigenvalues on top and the slowest on the bottom.

9.2 SM to grid

The SM was first modeled connected to a grid, with the same assumptions for the grid voltage as in the VSM. The eigenvalues can be seen in the table 9.2. The eigenvalues for the SM contain some critical modes. There is two high frequency complex conjugated pairs λ_{1-4}. These are the modes belonging to the filter of the SM. Even though they have a high imaginary part, they have a real part damping some of the oscillations. The complex conjugated pair $\lambda_{13,14}$ is the modes closest to origo. As seen in the table of eigenvalues the participation factors for this mode is the currents $i_{sm,d}$, $i_{sm,q}$, i_f, $i_{1,d}$, $i_{1,q}$ and ζ. Even though this eigenvalue is slow with a fairly high time constant, its imaginary part is low enough to not give unwanted oscillations.

In figure 9.2 the eigenvalues for the system linearized around a set point changed from 0 to 3. Not all eigenvalues are included in this figure because they had no relevant change. By inspecting the modes in table 9.2, it can be deduced that the modes not included are the modes $\lambda_{1,2}$, $\lambda_{3,4}$ and λ_5. The main participating states for these modes are the output of the filter and the reactive power. Since the active power is changed and the voltage is controlled to be constant, it is reasonable for these states not to be influenced in a change in delivered active power. The complex conjugated pair $\lambda_{1,2}$, $\lambda_{3,4}$ is the modes resulting from the LCL-filter. This can be argued based on the participation factors. According to the participation factors, the mode λ_5 is the mode coming from the low pass filtered reactive power, q_m. This mode is around real 1000, which is about the same as the cut off frequency of the low pass filter, 1000 Hz.

Mode	Value	Participation factors
$\lambda_{1,2}$	-1482.2 + 32579.4i	$v_{sm,d}$ $i_{0,sm,d}$ $v_{sm,q}$ $i_{0,sm,d}$
$\lambda_{3,4}$	-1500.6 + 31842.5i	$v_{sm,q}$ $i_{0,sm,q}$ $v_{sm,d}$ $i_{0,sm,d}$
λ_5	-1000.5	$q_{m,sm}$
$\lambda_{6,7}$	-185.02 + 306.55i	$i_{sm,d}$ $i_{f,d}$ $i_{sm,q}$ i_{1d} $i_{1,q}$
λ_8	-46.49	i_{1d} $i_{f,d}$ $i_{sm,d}$
$\lambda_{9,10}$	-2.3522 +27.2682i	$\omega_{sm} i_{sm,d}$ $i_{f,d}$ $i_{sm,q}$
$\lambda_{11,12}$	-8.3228 + 5.0535i	$i_{f,d}$ $i_{sm,d}$ $i_{1,q}$ $i_{sm,q}$
$\lambda_{13,14}$	-1.2694 + 1.2866i	$i_{f,d}$ ζ_{sm} $i_{sm,d}$ $i_{1,q}$
λ_{15}	-4.3069	$p_{m,sm}$ $i_{f,d}$ $i_{sm,d}$

Table 9.2: Table of eigenvalues and the main participating factors for the model of the SM connected to a grid.
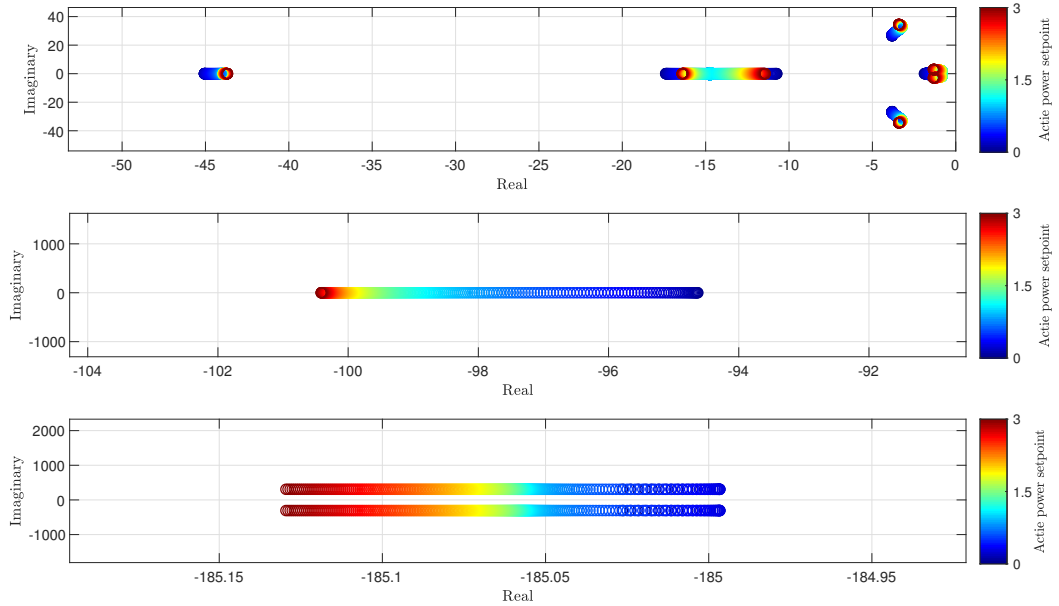
Figure 9.2: Plot of the eigenvalues of the SM as the reference point of the active power delivered i changed from 0 to 3. The first of these three shows the modes nearest origo, second the mode around -100 along the real axis and the second the complex conjugated pair around -180 real. Dark blue symbolizes the eigenvalues when the set point of active power is 0, and the color changes as the setpoint goes to 3

As the VSM, the SM eigenvalues can handle a reasonable operating area, with no relatively big changes in the eigenvalues, as the dynamic response in the last chapter describing the response of the linearized model. As seen in the figure 9.2 of the changing eigenvalues, the critical modes nearest origo moves nearer the right half plane and some gets a increased imaginary value. This means that the system will have less damping and be less robust against disturbances.

In figure 9.3 the response of the SM frequency after a step in the grid frequency of
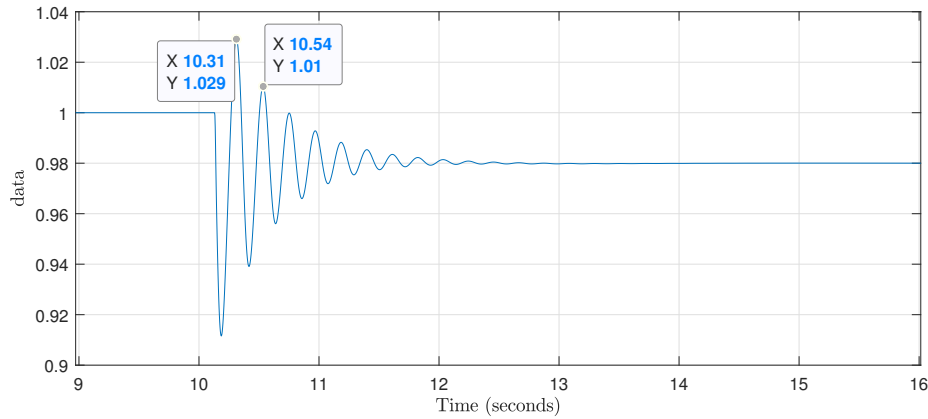
Figure 9.3: A step change on 0.2 pu in the grid frequency. The markings shows the peak time and value of the frequency, ω_{sm}, of the SM

the SM can be seen. The step is from 1 pu to 0.98 pu for ω_g. As seen in the figure the frequency oscillates for some time before stabilizing. In the figure the period is measured to approximately 0.23 seconds which corresponds to the frequency $4.34Hz$. By transforming the frequency from $\frac{1}{s}$ to $\frac{rad}{s}$ by multiplying with 2π the frequency is $27.3\frac{\omega}{s}$, the same as the unit for the imaginary part of the eigenvalue. By looking in table 9.2 the imaginary part of the complex conjugated mode $\lambda_{9,10}$ is approximately the same. This means that this pole is influenced by the grid frequency. From the participation factor it can be seen that both the angular velocity and the angle deviation is represented in this mode. Comparing the real part to the imaginary part of the eigenvalue, the damping factor can be found by $-\sigma_{9,10}/\sqrt{\sigma_{9,10}^2 + \omega_{9,10}^2}$ resulting in a damping factor of ≈ 0.0859. According to [17] a damping ratio greater than 0.05 for rotor oscillations is considered desirable in practice. The oscillation can also be seen in figure 8.5 of the frequency of the VSM after the perturbation in the grid frequency is done. This oscillating behaviour can also be seen in the system response of a step change in the active power reference. Comparing the VSM response with grid connection and the SM with grid connection, it can be seen that the VSM have significantly more damping. When connected to each other the oscillating is still there but is more damped.

9.3 VSM to load

The table 9.3 contains the eigenvalues and the main participating factor of the system consisting of the VSM and load model. As the table show there is many eigenvalues with high damping. The first eigenvalues can also here be recognized as modes resulting from the filter values and according to the main participant factor the states involved only appears in these modes. Since these modes are the least dominant of the system with a low time constant, they pose no concern regarding stability and reliability of the power grid. The response of a perturbation of these modes will be a high frequency transient with a low amplitude and low time constant

because of the time constant of the modes.

A thing to notice is that the system has many overdamped eigenvalues. Many of the complex conjugated eigenvalue pairs can be recognized from the main participation factor where both eigenvalues are on the real axis. The outcome of all this damping can be seen in the figure of with the system response of a step in the active power. The dynamics are slow and damped, and take some time reaching steady state. This results in a slow and stable system. The damping might be a bit excessive for this application. The VSM application have a damping coefficient, $k_{d,vsm}$, on 40. This causes the system to be very damped, and the response slow.

The figure 9.4 shows the trajectory of the eigenvalues of this system as the load models starts with a -2 pu current reference and goes to 0 pu. As seen in the figure, the eigenvalues seem volatile. As the input is changes and the system is linearized again, the placement of the modes is different, resulting in the behavior of the system to change. This may be because of the nonlinearity of the linearization area. If the system is nonlinear around the point of linearization the linearized model will change relatively big because of the nonlinear system dynamics. It seems as when the load goes up the eigenvalues $\lambda_{21,22}$ becomes less damped and the natural frequency goes up. This mode belongs to the PLL of the load. This means that the reference frame of the load model will become less damped and the synchronization will have more perturbations as the d-axis current is increasing.
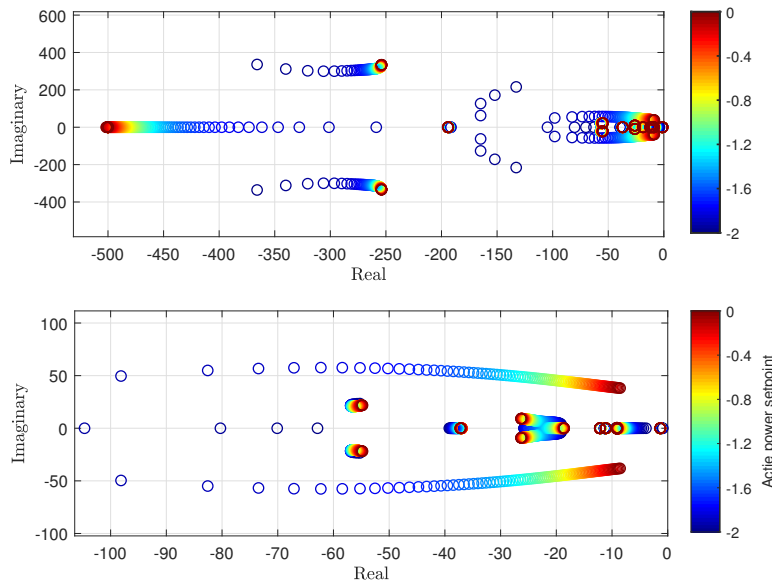
Figure 9.4: Plot of how the eigenvalues of the VSM connected to the load model change when the as the load draws more active power. The plot on top shows all eigenvalues, and the bottom is zoomed in.

Mode	Value	Main participation factor
$\lambda_{1,2}$	-76212+311.85i	$v_{g,d}v_{g,q}$
$\lambda_{3,4}$	-23466+311.27i	$v_{g,d}v_{g,q}i_{0,vsm,d}i_{0,vsm,q}i_{0,load,d}i_{0,load,q}$
$\lambda_{5,6}$	-1848.4+6493.4i	$i_{cv,d,vsm}i_{cv,q,vsm}v_{0,vsm,d}v_{0,vsm,q}$
$\lambda_{7,8}$	-1999.1+6141.7i	$i_{cv,d,vsm}i_{cv,q,vsm}v_{0,vsm,d}v_{0,vsm,q}$
$\lambda_{9,10}$	-2465.5+6234.5i	$v_{0,load,d}v_{0,load,q}i_{cv,d,load}i_{cv,q,load}$
$\lambda_{11,12}$	-2595.2+5929.6i	$v_{0,load,d}v_{0,load,q}i_{cv,d,load}i_{cv,q,load}$
$\lambda_{13,14}$	-1285.4+280.22i	$i_{s,d,vsm}i_{s,q,vsm}$
$\lambda_{15,16}$	-257.88+315.16i	$i_{sm,d}i_{sm,d}i_{0,d,vsm}i_{0,q,vsm}$
λ_{17}	-465.7+0i	$v_{pll,q}$
λ_{18}	-500+0i	$v_{pll,d}$
λ_{19}	-193.63+0i	$q_{m,vsm}$
$\lambda_{20,21}$	-25.528+48.507i	$\delta\theta_{load}\epsilon_{load}$
$\lambda_{22,23}$	-56.519+20.7i	$\zeta_{vsm}\phi_{d,vam}\phi_{q,vsm}$
λ_{24}	-37.345+0i	$\phi_{q,vsm}\zeta_{vsm}\phi_{d,vam}$
$\lambda_{25,26}$	-23.998+7.4087i	$\epsilon_{load}\phi_{d,load}\phi_{q,load}$
λ_{27}	-20.776+0i	$\omega_{vsm}\epsilon$
λ_{28}	-1.3293+0i	$\kappa_{vsm}\omega_{vsm}$
λ_{29}	-7.8615+0i	$\gamma_{d,load}\gamma_{q,load}$
λ_{30}	-9.1531+0i	$\gamma_{d,load}\gamma_{q,load}$
λ_{31}	-11.13+0i	$\gamma_{q,vsm}\gamma_{d,vsm}$
λ_{32}	-12.08+0i	$\gamma_{d,vsm}\gamma_{q,vsm}$

Table 9.3: Table showing the eigenvalues and main participating state in each mode for the VSM model connected to the load model

9.4   SM to load

The table 9.4 the eigenvalues and the main participating state of the respective mode of the model with SM model connected to the load model. Many of the modes are similar to the model of the VSM connected to grid. The exception is that the states from the load model is included.

As the dynamic response of a step in the d-axis current reference in the load model presented in the previous section shows, the model has some undamped modes. As the SM to grid, the mode resulting in oscillations can be seen in the table. This is the complex conjugated modes $\lambda_{25,26}$. These modes have a damping ratio of approximately 0.1 and a time constant of 2.4. This means that this mode is slow and have little damping and will dominate the system dynamics. This corresponds with the response of the step done in the previous chapter, where the frequency is oscillating and takes seconds to reach steady state, but also the currents is oscillating as the frequency does.

The figure 9.5 shows how the eigenvalues of the SM connected to load changes as the current reference is changed from -2 pu to 0. This plot is enhanced on order to show the eigenvalues closest to origo. This was done because the other modes showed to have little of the change in the current reference. It can be seen that the dynamics of the dominant modes, $\lambda_{25,26}$, gets an increased real part as the current reference changes, thus leading to a higher damping ratio.
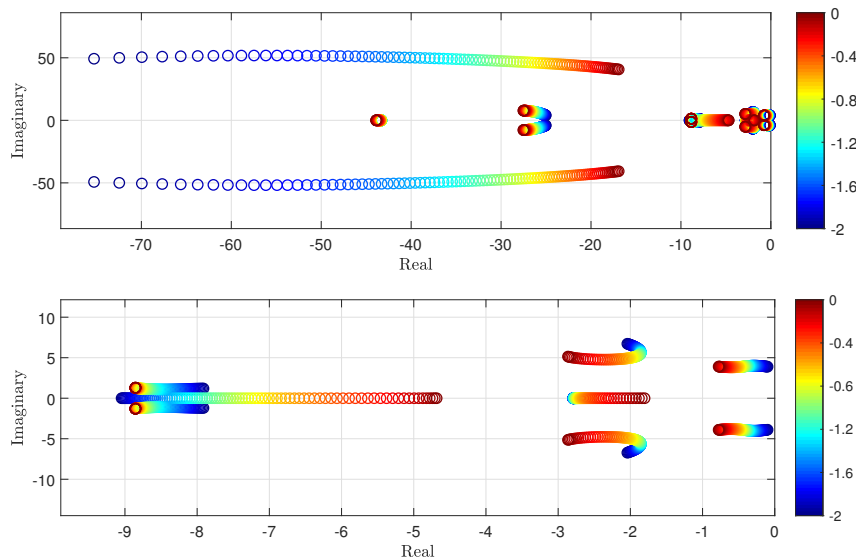
Figure 9.5: Plot of how the eigenvalues of the SM connected to the load model change when the as the load draws a higher d-axis current. The plot on top shows all eigenvalues, and the bottom is zoomed in.

Mode	Value	Main participation factor
$\lambda_{1,2}$	-49891+45684i	$v_{g,d}v_{g,q}i_{0,sm,d}i_{0,sm,q}$
$\lambda_{3,4}$	-49891+45060i	$v_{g,d}v_{g,q}i_{0,sm,d}i_{0,sm,q}$
$\lambda_{5,6}$	-2005.5+6461.1i	$i_{cv,d,vsm}i_{cv,q,vsm}v_{0,vsm,d}v_{0,vsm,q}$
$\lambda_{7,8}$	-2186.8+6106.8i	$i_{cv,d,vsm}i_{cv,q,vsm}v_{0,vsm,d}v_{0,vsm,q}$
$\lambda_{9.10}$	-651.6+4698.8i	$v_{sm,d}i_{sm,d}$
$\lambda_{11,12}$	-642.38+3834.4i	$v_{sm,q}i_{sm,q}$
λ_{13}	-1000+0i	$q_{m,sm}$
$\lambda_{14,15}$	-400.08+278.86i	$i_{sm,d}i_{sm,d}i_{f,d}i_{1,d}i_{1,q}$
λ_{16}	-500+0i	$v_{pll,d}$
λ_{17}	-484.47+0i	$v_{pll,q}i_{sm,d}$
$\lambda_{18,29}$	-30.419+47.595i	$i_{1,q}i_{sm,q}i_{sm,d}$
λ_{20}	-43.321+0i	$i_{1,d}i_{f,d}$
$\lambda_{21,22}$	-26.433+6.9638i	$i_{f,d}i_{sm,d}\epsilon_{pll}$
$\lambda_{23,24}$	-1.8935+5.2556i	$i_{sm,d}i_{f,d}(\omega_{sm})$
$\lambda_{25,26}$	-0.41804+3.9289i	$\omega_{sm}p_{m,sm}$
λ_{27}	-2.7571+0i	$p_{m,sm}$
$\lambda_{28,29}$	-8.6996+1.1522i	$\gamma_{d,vsm}\gamma_{q,vsm}$
λ_{30}	-7.6504+0i	$i_{sm,d}i_{f,d}v_{f,d}$

Table 9.4: Table showing the eigenvalues and main participating state in each mode for the SM model connected to the load model

9.5 SM and VSM

This section contains the VSM and SM connected. The eigenvalues of the system matrix $\mathbf{A}$ can be seen in table 9.5 along with the main participating factors.

The eigenvalues coming first in the table, λ_{1-8}, is the modes resulting from the LCL-filter. These eigenvalues stand out because of their high real and imaginary part. From the participation factors for these modes it can be seen that there appears only eight states, the same as there are modes, meaning there is also no apparent coupling between the states coming from the equations for the electrical model for the LCL-filter.

The modes λ_{15} and λ_{18} comes from the low pass filters filtering the states q_{sm} and $q_{m,vsm}$ respectively. These modes have a real part very close to the cut off frequency of the respective filter, and by looking at the participation factors it can be seen that there are no other states that influence this mode in any relevant way. The low pass filters filtering the mechanical power and the field voltage for the SM cannot be seen so easily as these filters. They have a cut off frequency of 0.5 and 0.25 respectively, but there are significant coupling between the two states $p_{m,sm}$ and $v_{f,d}$, and other.

The mode resulting in the oscillations when making a step in the grid frequency, $\lambda_{23,24}$, is still present with a high imaginary part compared to its real part. By comparing it to the SM grid connected model it can be seen that the damping ratio

Mode	Value	Main participation factor
$\lambda_{1,2}$	-1489.3+32846i	$i_{0,d,sm}i_{0,q,sm}v_{sm,d}v_{sm,q}$
$\lambda_{3,4}$	-1506.8+32110i	$i_{0,d,sm}i_{0,q,sm}v_{sm,d}v_{sm,q}$
$\lambda_{5,6}$	-1681.8+6529.3i	$i_{0,d,vsm}i_{0,q,vsm}v_{0,vsm,d}v_{0,vsm,q}$
$\lambda_{7,8}$	-1850.9+6166.3i	$i_{0,d,vsm}i_{0,q,vsm}v_{0,vsm,d}v_{0,vsm,q}$
$\lambda_{9,10}$	-411.88+1533.6i	$i_{sm,d}i_{sm,q}v_{g,d}v_{g,q}$
$\lambda_{11,12}$	-1312.8+279.5i	$i_{s,vsm,d}i_{s,vsm,d}$
$\lambda_{13,14}$	-422.42+894.4i	$i_{sm,d}i_{f,d}v_{g,d}v_{g,q}$
λ_{15}	-1000+0i	$q_{m,sm}$
$\lambda_{16,17}$	-98.874+307.92i	$i_{sm,d}i_{f,d}i_{sm,q}i_{i,d}i_{i_q}$
λ_{18}	-195.93+0i	$q_{m,vsm}$
$\lambda_{19,20}$	-52.099+22.949i	$\zeta_{vsm}\phi_{d,vsm}\phi_{q,vsm}$
λ_{21}	-42.883+0i	$i_{1,d}i_{f,d}$
λ_{22}	-37.617+0i	$\phi_{q,vsm}\phi_{d,vsm}\zeta_{vsm}$
$\lambda_{23,24}$	-2.6908+19.916i	$\omega_{sm}i_{sm,d}i_{f,d}$
λ_{25}	-15.476+0i	$\omega_{vsm}\kappa_{vsm}$
λ_{26}	-12.065+0i	$\gamma_{d,vsm}\gamma_{q,vsm}$
λ_{27}	-11.098+0i	$\gamma_{d,vsm}\gamma_{q,vsm}$
$\lambda_{28,29}$	-6.1207+3.2936i	$i_{sm,q}i_{1,q}v_{f,d}$
$\lambda_{30,31}$	-1.8427+0.88061i	$p_{m,sm}\kappa_{vsm}$
$\lambda_{32,33}$	-1.34+1.8609i	$\zeta_{sm}i_{sm,d}i_{sm,q}$

Table 9.5: Eigenvalues and main participating factor for the VSM and SM.

have increased from approximately 0.0859 to 0.13. This explains the difference in the dynamic response between the grid connected model and the model connected to the VSM. The natural frequency has for this mode have decreased, resulting in a less oscillating response.

A eigenvalue sweep have for this model can be seen in figure 9.6. A change in the reference value of the VSM is done. The interval of the change of the active power reference for the SM is from -1 to 1, while the active power reference of the SM was set to 1.2 for the whole sweep. This interval was chosen in order to test the grid for a realistic operating range, where the VSM can both absorb active power and deliver. The plots are zoomed in on different parts of the eigenvalue plot and not all are included because some modes are not influenced by the change in active power and remains on the same place through the change of the power reference.
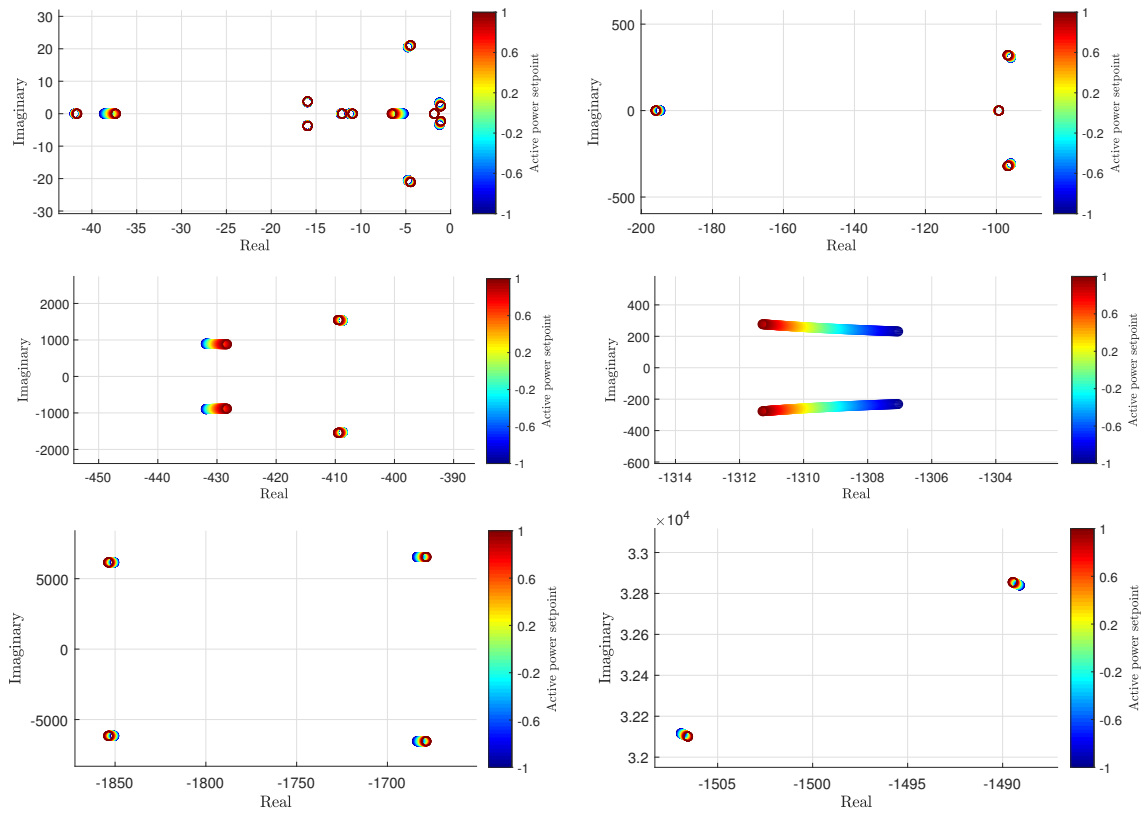
Figure 9.6: Plots showing how the eigenvalues changes when the reference value for delivered power is changed from -1 to 1. The plot starts with dark blue.

9.6 Full system model

The eigenvalues of the system matrix $\mathbf{A}$ belonging to the full system can be seen in table 9.6, along the main contributors for each mode.

As in the system where the VSM is connected to the SM, there is possible to recognize some of the modes from the grid connected models. The modes λ_{1-12} is the modes resulting from the filters of the outgoing signals from the VSM, SM and load models. Comparing these values to the other modes of the small signal models a complex conjugated pair is different. This is the modes $\lambda_{1,2}$ connected to the grid voltage states $\mathbf{v}_g$, and the high real part comes as a result of the values of the loads connected directly on the AC-bus, c_l and r_l. These have a significantly higher real and imaginary part than the rest of the modes. Keeping in mind that there are other minor participating states, it can be observed that the participation factors of these states does not appear as a major participant in any other mode.

The modes λ_{19}, λ_{22}, λ_{23} and λ_{26} comes from the low pass filters filtering the states q_{sm}, $v_{pll,q}$, $v_{pll,d}$ and $q_{m,vsm}$ respectively. The values of the real part of the modes are close to the cut off frequency of the filters, and these low pass filters have a cut off frequency close to the real part of the eigenvalue. There are some other low pass filters used in a similar way as the filters mentioned, but they have a relatively low

Mode	Value	Main participation factor
$\lambda_{1,2}$	-1.6744$\cdot 10^5$+320.43i	$v_{g,d} v_{g,q}$
$\lambda_{3,4}$	-31931+320.37i	$i_{0,sm,d} i_{0,sm,q}$
$\lambda_{5,6}$	-2001.2+6488.9i	$v_{0,load,d} v_{0,load,q} i_{cv,d,load} i_{cv,q,load}$
$\lambda_{7,8}$	-1588.2+6366.2i	$i_{cv,d,vsm} i_{cv,q,vsm} v_{0,vsm,d} v_{0,vsm,q}$
$\lambda_{9,10}$	-2181.4+6113.1i	$v_{0,load,d} v_{0,load,q} i_{cv,d,load} i_{cv,q,load}$
$\lambda_{11,12}$	-1833.4+6023.2i	$i_{cv,d,vsm} i_{cv,q,vsm} v_{0,vsm,d} v_{0,vsm,q}$
$\lambda_{13,14}$	-1000.7+5375.8i	$v_{sm,d} i_{sm,d}$
$\lambda_{15,16}$	-928.31+4495.8i	$v_{sm,q} i_{sm,q}$
$\lambda_{17,18}$	-1328.9+282.35i	$i_{s,d,vsm} i_{s,q,vsm}$
λ_{19}	-1000+0i	$q_{m,sm}$
$\lambda_{20,21}$	-443.47+303.01i	$i_{sm,d} i_{sm,q} i_{f,d} i_{1,d} i_{1,q}$
λ_{22}	-492.1+0i	$v_{pll,q}$
λ_{23}	-500+0i	$v_{pll,d}$
$\lambda_{24,25}$	-92.393+313.81i	$i_{sm,d} i_{sm,q} i_{f,d} i_{1,d} i_{1,q}$
λ_{26}	-193.84+0i	$q_{m,vsm}$
$\lambda_{27,28}$	-8.6945+41.621i	$\epsilon_{load} \delta\theta_{pll}$
$\lambda_{29,30}$	-54.189+20.111i	$\phi_{q,vsm} \phi_{d,vsm} \zeta_{vsm}$
λ_{31}	-44.025+0i	$i_{1,d} i_{f,d} i_{sm,d}$
$\lambda_{32,33}$	-35.514+13.673i	$\phi_{d,load} \phi_{q,load}$
λ_{34}	-37.676+0i	$\zeta_{vsm} \phi_{q,vsm} \phi_{d,vsm}$
$\lambda_{35,36}$	-2.3584+18.643i	$i_{sm,d} i_{f,d} \omega_{sm} \delta\theta_{sm}$
λ_{37}	-15.695+0i	$\omega_{vsm} \kappa_{vsm}$
λ_{38}	-12.069+0i	$\gamma_{d,vsm} \gamma_{q,vsm}$
λ_{39}	-11.204+0i	$\gamma_{q,vsm} \gamma_{d,vsm}$
λ_{40}	-9.0695+0i	$\gamma_{d,load} \gamma_{q,load}$
λ_{41}	-8.7828+0i	$\gamma_{q,load} \gamma_{d,load}$
$\lambda_{42,43}$	-5.6752+2.9923i	$v_{f,d} i_{f,d} i_{1,q}$
$\lambda_{44,45}$	-2.0434+2.4174i	$\zeta_{sm} i_{sm,d} i_{sm,q}$
$\lambda_{46,47}$	-1.8078+0.95617i	$p_{m,sm} \kappa_{vsm} i_{sm,d} i_{f,d}$

Table 9.6: Table showing the eigenvalues and the main participating state of each node.

cut off and is coupled with other states. The last pole, λ_{47}, comes partially from the filter symbolizing the delay of the diesel generator. This first order delay has a cut off frequency of 2 Hz. Despite having a relatively large filter time constant the states are coupled other states, leading to a more damped mode.

The complex conjugated pair $\lambda_{35,36}$ can be recognized from earlier. This was the eigenvalue associated with oscillations of the rotor when a change in the grid frequency occurred. The difference now is that the natural frequency is lower while the real part is about the same. This leads to a higher damping ratio for the oscillations concerning the oscillations in the speed of the SM rotor. Comparing it to the eigenvalue λ_{37}, which is according to the participation factors the eigenvalue linked to the speed of the virtual rotor of the VSM, it can be seen that the SM have a damping ratio of 0.13, while the VSM have a damping ratio of 1.

In figure 9.7 a plot of how the eigenvalues changed based on how much power is drawn from the load model. Here $i^*_{cv,d,load}$ changes from -2 to 0. Before simulation the set point of delivered power, p^*_{VSM} and p^*_{SM}, of both the SM and the VSM was set to 1, in accordance base case for the full system model. Comparing this sweep with the others done previously, it can be seen that there are not that much change. A important observation from this is the trajectory of the modes $\lambda_{27,28}$. This mode is changing fast towards the right half plane as the current increases. This plot shows that the models will work in the operating range -2 to 0, but the response will be better as the power of the inverter increases. The modes $\lambda_{27,28}$ become less dominant as the absolute value of the real part increases.

Observing the eigenvalue trajectory in figure 9.7 and focusing on the eigenvalues with the highest real value, it can be seen that the eigenvalues will cross if the load gets too high. This means that if the power consumption of the load model becomes to great the system will become unstable.

As mentioned in Chapter 2, section 2.2 Virtual synchronous machine, the VSM implementation is sensitive to changes in the virtual impedance. In figure 9.8 the parameter $r_{s,vsm}$ is changed from 0.001 to 1. Here it can be seen that the system goes from stable to having pole in the right half plane meaning instability. It can be seen that many of the poles is influenced by changing this parameter.
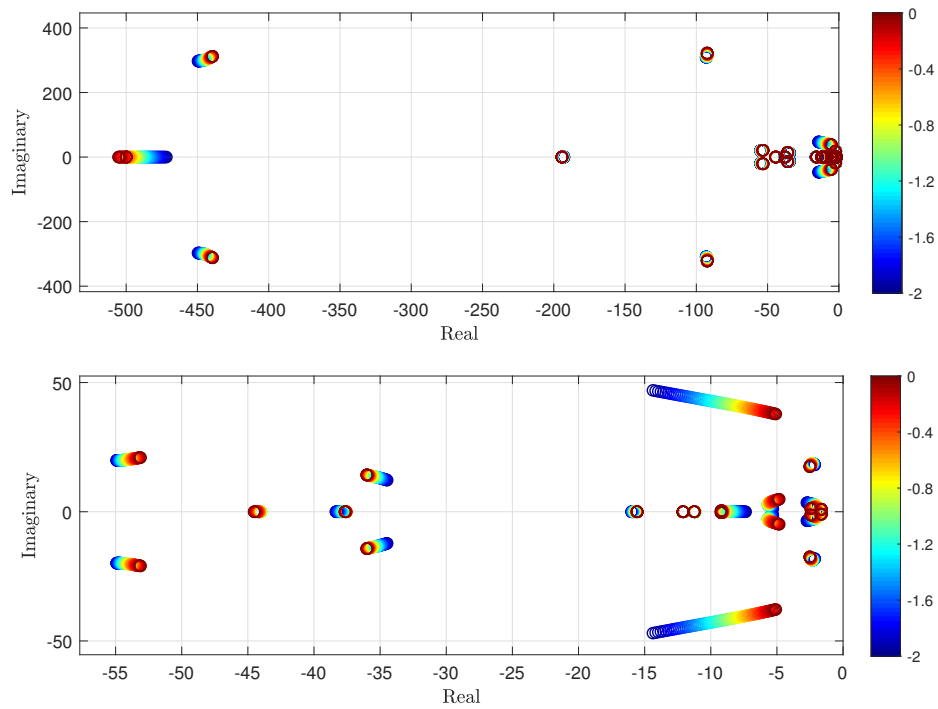
Figure 9.7: The plot on top is showing a zoomed plot of the eigenvalues, and the lowest plot is showing the eigenvalues closest to origo, as the power drawn from the load model goes from 0 to 2.
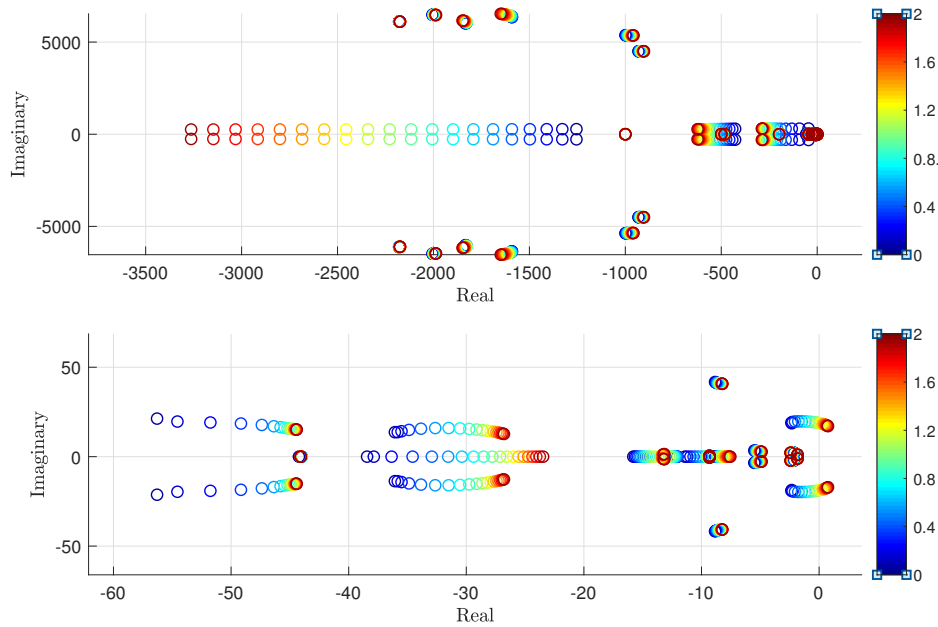
Figure 9.8

This figure shows that many of the dominant poles with the highest time constant is moving towards origo as the virtual stator resistance is increasing.

Chapter 10

Conclusion and future work

A VSM, SM and a load model have been modeled, linearized, validated and analyzed. The tools used for this task are Matlab, Simulink and Maple. All models have first been modeled with a grid connection and then models containing different the different components have been developed. When validating the small signal models, they have been compared against a corresponding model made in Simulink using the Simpower systems tool box.

The VSM is adapted from [5]. This type of implementation has been chosen because of the flexibility. It has no PLL included in the virtual inertia, which makes it possible to operate without having the need for a frequency to synchronize to. This is crucial if it is desired to maintain the grid only using the VSM, isolating the SM from the system. In order to model the SM the equations from [6], with some alterations, and the SM parameters was used to linearize the model. To help the algebraic process of inverting and modeling the SM equations, Maple have been used. Maple have been of great help when modeling the SM, simplifying this algebraic process. The load model is built as a simplification of the VSM, with no outer loop control, meaning the only control implemented in the load model is the current controller and the PLL. A similar model for the VSC can be found in [9].

The system modeled is symbolizing a marine power grid. The results presented shows that the different small signal models are stable and can operate under various linearization points. The system can function with all components (SM, VSM, load) connected. The VSM have shown the ability to adapt to the frequency in the grid by synchronizing to the other frequency setting components in the grid. In addition to this a model of the VSM was developed, where the VSM was the only energy source connected to the load. Because of the design of the virtual inertia the frequency of the virtual rotor was able to maintain the frequency without the need of external measurements.

The small signal models created have given the possibility to use linear analysis tools to evaluate stability and system response. The analysis has given further insight in the system response and the way that it is coupled. By comparing the linearized model with a corresponding model in Simulink, the models were validated such that

the system of equations was confirmed implying that the small signal model was confirmed. After validating the small signal models, linear analysis tools such as eigenvalues and participation factors have been used to study the system in steady state.

The control system of the SM managed to maintain a good response to a small disturbance. A power system stabilizer could be a good choice to implement in the control system of the SM to keep the electromechanical oscillations to a minimum. The oscillations of the rotor was shown to be within the desired range. Also, a more detailed model of the Exiter can give more degrees of freedom when tuning and better control of the SM rotor oscillations.

The VSM by itself have with the base case a very damped response, as a result from the tuning parameters of the virtual impedance and the swing equation parameters. When the VSM and SM is set together the damping of the VSM and the low damping of the SM results in a response between the two. By examining the eigenvalues of the systems with different components coupled, it could be seen how the eigenvalues is influenced by the different models. The SM was underdamped and the VSM was overdamped. The two put together resulted in accordance to the system response of the simulated models and the eigenvalues a system with a system with desirable response.

By iteratively changing the the inputs of the system and linearizing around each point the eigenvalue trajectory can be observed. This have shown that the system have a satisfactory stability margin within the tested area. The system is in no danger of becoming unstable by just changing the the input in delivered power or absorbed power. By observing the placement of the modes in the full system model it can be seen that the there are a variation of undamped and damped modes. It is not satisfactory that all states are damped. The inertia of a power grid will cause a low damping because of the nature of oscillations of systems with a high inertia. This means that it is desirable to have a variation of damped and undamped poles, in order to achieve a good stability margin.

Because the VSM can function connected to the load model both with and without the SM connected shows that this system is able to function with an all-electric operation, meaning the only source of energy is the VSM modeled as a battery storage system. This have not been tested by tripping the SM but should work in theory when the VSM is able to function in all operating modes. This shows the flexibility of the VSM design and shows some of the possibilities for hybrid operations for a marine power grid with a battery energy storage system.

It have been shown that this implementation of the VSM is able to handle a various different operating modes such as grid-connected which is relevant for a land based battery charging for the marine power grid, islanded operation where the VSM maintains the power grid on its own and in parallel with the SM showing how is can adapt to other frequencys in the grid.

10.1 Future work

A more detailed analysis can be done on this model. A parametric sensitivity analysis can be conducted in order to see how the different parameters influence the stability and if there are parameters with potentially more suitable values for the system, like the parameters for the VSM.

This implementation can be done different ways be using a different VSM topology. This would give insight in what the most suitable VSM implementation is, and with a stability analysis and make it possible to differentiate how the different control topologies influence the power grid.

The models can be tested in a more realistic way by implementing additional control on the load model. Here an DC-controller or active and reactive power control can be implemented. This will lead to more system states but will result in a more correct model. This will also have an impact on the system response leading to a more realistic operation of the grid.

Bibliography

[1] "Air Pollution http://www.imo.org/en/ourwork/environment/pollution prevention/airpollution/pages/air-pollution.aspx."

[2] H. Qian, J. Zhang, J. Lai, and W. Yu, "A high-efficiency grid-tie battery energy storage system," *IEEE Transactions on Power Electronics*, vol. 26, pp. 886–896, Mar. 2011.

[3] H. Jiayi, J. Chuanwen, and X. Rong, "A review on distributed energy resources and MicroGrid," *Renewable and Sustainable Energy Reviews*, vol. 12, pp. 2472–2483, Dec. 2008.

[4] Guan-Chyun Hsieh and J. C. Hung, "Phase-locked loop techniques. A survey," *IEEE Transactions on Industrial Electronics*, vol. 43, pp. 609–615, Dec. 1996.

[5] O. Mo, S. D'Arco, and J. A. Suul, "Evaluation of Virtual Synchronous Machines With Dynamic or Quasi-Stationary Machine Models," *IEEE Transactions on Industrial Electronics*, vol. 64, pp. 5952–5962, July 2017.

[6] Prabha Kundur, *Power System Stability and Control*. 2005.

[7] A. K. AAdnanes, "Maritime Electrical Installations And Diesel Electric Propulsion," Jan. 2003.

[8] E. Skjong, E. Rødskar, M. Molinas, T. A. Johansen, and J. Cunningham, "The Marine Vessel's Electrical Power System: From its Birth to Present Day," *Proceedings of the IEEE*, vol. 103, pp. 2410–2424, Dec. 2015.

[9] S. D'Arco and J. A. Suul, "Small-Signal analysis of an isolated power system controlled by a virtual synchronous machine," *2016 IEEE International Power Electronics and Motion Control Conference (PEMC)*, pp. 462–469, Sept. 2016.

[10] H. Beck and R. Hesse, "Virtual synchronous machine," *2007 9th International Conference on Electrical Power Quality and Utilisation*, pp. 1–6, Oct. 2007.

[11] Q. Zhong, "Virtual Synchronous Machines: A unified interface for grid integration," *IEEE Power Electronics Magazine*, vol. 3, pp. 18–27, Dec. 2016.

[12] H. Bevrani, T. Ise, and Y. Miura, "Virtual synchronous generators: A survey and new perspectives," *International Journal of Electrical Power & Energy Systems*, vol. 54, pp. 244–254, Jan. 2014.

[13] S. D'Arco and J. A. Suul, "Virtual synchronous machines — Classification of implementations and analysis of equivalence to droop controllers for microgrids," *2013 IEEE Grenoble Conference*, pp. 1–7, June 2013.

[14] V. Karapanos, "Testing a Virtual Synchronous Generator in a Real Time Simulated Power System," p. 7.

[15] Y. Hirase, K. Abe, K. Sugimoto, and Y. Shindo, "A grid-connected inverter with virtual synchronous generator model of algebraic type," *Electrical Engineering in Japan*, vol. 184, no. 4, pp. 10–21, 2013.

[16] M. P. N. v. Wesenbeeck, S. W. H. d. Haan, P. Varela, and K. Visscher, "Grid tied converter with virtual kinetic storage," *2009 IEEE Bucharest PowerTech*, pp. 1–7, June 2009.

[17] J. R. B. Jan Machowski, Janusz W. Bialek, *Power system dynamics: Stability and control.* 2012.

[18] E. Unamuno Ruiz, "Control and stability of Ac/Dc microgrids," 2017.

[19] Q. Zhong and G. Weiss, "Static synchronous generators for distributed generation and renewable energy," *2009 IEEE/PES Power Systems Conference and Exposition*, pp. 1–6, Mar. 2009.

[20] R. Aouini, B. Marinescu, K. B. Kilani, and M. Elleuch, "Synchronverter-Based Emulation and Control of HVDC Transmission," *IEEE Transactions on Power Systems*, vol. 31, pp. 278–286, Jan. 2016.

[21] V. Natarajan and G. Weiss, "Synchronverters With Better Stability Due to Virtual Inductors, Virtual Capacitors, and Anti-Windup," *IEEE Transactions on Industrial Electronics*, vol. 64, pp. 5994–6004, July 2017.

[22] K. Koyanagi, Y. Hida, Y. Ito, K. Yoshimi, R. Yokoyama, M. Inokuchi, T. Mouri, and J. Eguchi, "A Smart Photovoltaic Generation System Integrated with Lithium-ion Capacitor Storage," in *2011 46th International Universities' Power Engineering Conference (UPEC)*, pp. 1–6, Sept. 2011.

[23] S. D'Arco, J. A. Suul, and O. B. Fosso, "A Virtual Synchronous Machine implementation for distributed control of power converters in SmartGrids," *Electric Power Systems Research*, vol. 122, pp. 180–197, May 2015.

[24] B. Zhang, X. Yan, D. Li, X. Zhang, J. Han, and X. Xiao, "Stable Operation and Small-Signal Analysis of Multiple Parallel DG Inverters Based on a Virtual Synchronous Generator Scheme," *Energies*, vol. 11, p. 203, Jan. 2018.

[25] Olav Egeland and Jan Tommy Gravdahl, *Modeling and simulation for automatic control.* 2002.

[26] P. Kundur, J. Paserba, V. Ajjarapu, G. Andersson, A. Bose, C. Canizares, N. Hatziargyriou, D. Hill, A. Stankovic, C. Taylor, T. V. Cutsem, and V. Vittal, "Definition and classification of power system stability IEEE/CIGRE joint task

force on stability terms and definitions," *IEEE Transactions on Power Systems*, vol. 19, pp. 1387–1401, Aug. 2004.

[27] Jens G. Blachen, Trond Andresen, Bjarne A. Foss, *Reguleringsteknikk*. 2016.

[28] C. Bajracharya and M. Molinas, "Understanding of tuning techniques of converter controllers for VSC-HVDC," p. 8.

[29] O. Saborio Romano, "Small-signal modelling and stability analysis of a traditional generation unit and a virtual synchronous machine in grid-connected operation," *95*, 2015.

[30] N. Kroutikova, C. a. Hernandez-Aramburo, and T. C. Green, "State-space model of grid-connected inverters under current control mode," *IET Electric Power Applications*, vol. 1, pp. 329–338, May 2007.

Chapter 11

Appendix

11.1 Equation system

Here the equation system of the VSM connected to a grid, SM connected to a grid and the full system model can be found respectively.

VSM states:

$$\mathbf{x}_{vsm} = [v_{0,d,vsm} \; v_{0q,vsm} \; i_{cv,d,vsm} \; i_{cv,q,vsm} \; \gamma_{d,vsm} \; \gamma_{q,vsm} \; i_{0d,vsm} \; i_{0q,vsm}$$
$$\phi_{d,vsm} \; \phi_{q,vsm} \; \zeta_{vsm} \; is_{d,vsm} \; is_{q,vsm} \; q_{m,vsm} \; \omega_{vsm} \; \delta\theta_{vsm} \; \kappa_{vsm}] \qquad (11.1)$$
$$\mathbf{u}_{vsm} = [p_{vsm}^* \; q_{vsm}^* \; v_{g,d} \; v_{g,q} \; \hat{v}^* \; \omega_{vsm}^*]$$

11.1.1 VSM connected to a grid

$$\dot{v}_{0,d,vsm} = \omega_b \, \omega_{\text{vsm}} \, v_{0,q,\text{vsm}} - \frac{i_{0,d,\text{vsm}} \, \omega_b}{c_f} + \frac{\text{icv}_{d,\text{vsm}} \, \omega_b}{c_f}$$

$$\dot{v}_{0,q vsm} = \frac{\text{icv}_{q,\text{vsm}} \, \omega_b}{c_f} - \frac{i_{0,q,\text{vsm}} \, \omega_b}{c_f} - \omega_b \, \omega_{\text{vsm}} \, v_{0,d,\text{vsm}}$$

$$\dot{i}_{cv,d,vsm} = \frac{\gamma_{d,\text{vsm}} \, k_{\text{ic,vsm}} \, \omega_b}{l_f} - \frac{\text{icv}_{d,\text{vsm}} \, \omega_b \, (k_{\text{pc,vsm}} + r_f)}{l_f} + \frac{\text{is}_{d,\text{vsm}} \, k_{\text{pc,vsm}} \, \omega_b}{l_f} - \frac{k_{\text{ad,vsm}} \, \omega_b \, \varphi_{d,\text{vsm}}}{l_f}$$
$$- \frac{\omega_b \, v_{0,d,\text{vsm}} \, (k_{\text{ad,vsm}} - k_{\text{ffv}} + 1)}{l_f}$$

$$\dot{i}_{cv,q,vsm} = \frac{\gamma_{q,\text{vsm}} \, k_{\text{ic,vsm}} \, \omega_b}{l_f} - \frac{\text{icv}_{q,\text{vsm}} \, \omega_b \, (k_{\text{pc,vsm}} + r_f)}{l_f} + \frac{\text{is}_{q,\text{vsm}} \, k_{\text{pc,vsm}} \, \omega_b}{l_f} - \frac{k_{\text{ad,vsm}} \, \omega_b \, \varphi_{q,\text{vsm}}}{l_f}$$
$$- \frac{\omega_b \, v_{0,q,\text{vsm}} \, (k_{\text{ad,vsm}} - k_{\text{ffv}} + 1)}{l_f}$$

$$\dot{\gamma}_{d,vsm} = \text{is}_{d,\text{vsm}} - \text{icv}_{d,\text{vsm}}$$

$$\dot{\gamma}_{q,vsm} = \text{is}_{q,\text{vsm}} - \text{icv}_{q,\text{vsm}}$$

$$\dot{i}_{0,d,vsm} = \frac{\omega_b \, v_{0,d,\text{vsm}}}{l_g} + i_{0,q,\text{vsm}} \, \omega_b \, \omega_{\text{vsm}} -$$

$$\frac{i_{0,d,\text{vsm}} \, \omega_b \, r_g}{l_g} - \frac{\omega_b \, v_{\text{hat},g,d} \, \cos(\delta_{\theta,\text{vsm}})}{l_g} - \frac{\omega_b \, v_{\text{hat},g,q} \, \sin(\delta_{\theta,\text{vsm}})}{l_g}$$

$$\dot{i}_{0,q,vsm} = \frac{\omega_b \, v_{0,q,\text{vsm}}}{l_g} - i_{0,d,\text{vsm}} \, \omega_b \, \omega_{\text{vsm}} -$$

$$\frac{i_{0,q,\text{vsm}} \, \omega_b \, r_g}{l_g} - \frac{\omega_b \, v_{\text{hat},g,q} \, \cos(\delta_{\theta,\text{vsm}})}{l_g} + \frac{\omega_b \, v_{\text{hat},g,d} \, \sin(\delta_{\theta,\text{vsm}})}{l_g}$$

$$\dot{\phi}_{d,vsm} = -\omega_{\text{ad,vsm}} \, \varphi_{d,\text{vsm}} - \omega_{\text{ad,vsm}} \, v_{0,d,\text{vsm}}$$

$$\dot{\phi}_{q,vsm} = -\omega_{\text{ad,vsm}} \, \varphi_{q,\text{vsm}} - \omega_{\text{ad,vsm}} \, v_{0,q,\text{vsm}}$$

$$\dot{\zeta}_{vsm} = v_{\text{hat,star,vsm}} - k_{q,\text{vsm}} \, q_{m,\text{vsm}} + k_{q,\text{vsm}} \, q_{\text{star,vsm}} - \sqrt{v_{0,d,\text{vsm}}^2 + v_{0,q,\text{vsm}}^2}$$

$$\dot{i}_{s,d,vsm} = \text{is}_{q,\text{vsm}} \, \omega_b \, \omega_{\text{vsm}} - \frac{\omega_b \, v_{0,d,\text{vsm}}}{l_{s,\text{vsm}}} -$$

$$\frac{k_{\text{pv,vsm}} \, \omega_b \, \sqrt{v_{0,d,\text{vsm}}^2 + v_{0,q,\text{vsm}}^2}}{l_{s,\text{vsm}}} - \frac{\text{is}_{d,\text{vsm}} \, \omega_b \, r_{s,\text{vsm}}}{l_{s,\text{vsm}}} +$$

$$\frac{k_{\text{pv,vsm}} \, \omega_b \, v_{\text{hat,star,vsm}}}{l_{s,\text{vsm}}} + \frac{k_{\text{iv,vsm}} \, \omega_b \, \zeta_{\text{vsm}}}{l_{s,\text{vsm}}} - \frac{k_{\text{pv,vsm}} \, k_{q,\text{vsm}} \, \omega_b \, q_{m,\text{vsm}}}{l_{s,\text{vsm}}} + \frac{k_{\text{pv,vsm}} \, k_{q,\text{vsm}} \, \omega_b \, q_{\text{star,vsm}}}{l_{s,\text{vsm}}}$$

$$\dot{i}_{s,q,vsm} = -\frac{\omega_b \, v_{0,q,\text{vsm}}}{l_{s,\text{vsm}}} - \text{is}_{d,\text{vsm}} \, \omega_b \, \omega_{\text{vsm}} - \frac{\text{is}_{q,\text{vsm}} \, \omega_b \, r_{s,\text{vsm}}}{l_{s,\text{vsm}}}$$

$$q_{m,vsm} = i_{0,d,\text{vsm}} \, \omega_{\text{qf,vsm}} \, v_{0,q,\text{vsm}} - \omega_{\text{qf,vsm}} \, q_{m,\text{vsm}} - i_{0,q,\text{vsm}} \, \omega_{\text{qf,vsm}} \, v_{0,d,\text{vsm}}$$

$$\dot{\omega}_{vsm} = \frac{p_{\text{star,vsm}}}{T_a} - \frac{i_{0,d,\text{vsm}} \, v_{0,d,\text{vsm}} + i_{0,q,\text{vsm}} \, v_{0,q,\text{vsm}}}{T_a}$$

$$-\frac{\omega_{\text{vsm}} \, (k_{d,\text{vsm}} + k_{\omega,\text{vsm}})}{T_a} + \frac{k_{d,\text{vsm}} \, \kappa_{\text{vsm}}}{T_a} + \frac{k_{\omega,\text{vsm}} \, \omega_{\text{star,vsm}}}{T_a}$$

$$\dot{\delta\theta}_{vsm} = \omega_b \, \omega_{\text{vsm}} - \omega_b \, \omega_g$$

$$\dot{\kappa}_{vsm} = \omega_{\text{vsm}} \, \omega_{d,\text{vsm}} - \kappa_{\text{vsm}} \, \omega_{d,\text{vsm}}$$

11.1.2 SM connected to a grid

SM states:

$$\mathbf{x} = [v_{d,sm} \ v_{q,sm} \ i_{0,d,sm} \ i_{0,q,sm} \ i_{d,sm} \ i_{q,sm} \ i_{fd,sm} \ i_{1d,sm} \ i_{1q,sm} \ \omega_{sm} \ \delta\theta_{sm} \ p_{m,sm} \ ...$$

$$q_{m,sm} \ \zeta_{sm} \ v_{fd,sm}] \quad (11.2)$$

$$\mathbf{u} = [\hat{v}_{g,d} \ \hat{v}_{g,q} \ \omega_g \ p_{sm}^* \ q_{sm}^* \ \hat{v}^* \ \omega_{sm}^*]$$

$$\dot{v}_{sm,d} = \omega_b\,\omega_g\,v_{\mathrm{sm},q} - \frac{i_{0,\mathrm{sm},d}\,\omega_b}{c_{\mathrm{mg}}} + \frac{i_{\mathrm{sm},d}\,\omega_b}{c_{\mathrm{mg}}}$$

$$\dot{v}_{sm,q} = \frac{i_{\mathrm{sm},q}\,\omega_b}{c_{\mathrm{mg}}} - \frac{i_{0,\mathrm{sm},q}\,\omega_b}{c_{\mathrm{mg}}} - \omega_b\,\omega_g\,v_{\mathrm{sm},d}$$

$$\dot{i}_{0,sm,d} = \frac{\omega_b\,v_{\mathrm{sm},d}}{l_{\mathrm{mg}}} + i_{0,\mathrm{sm},q}\,\omega_b\,\omega_g - \frac{i_{0,\mathrm{sm},d}\,\omega_b\,r_{\mathrm{mg}}}{l_{\mathrm{mg}}} - \frac{\omega_b\,v_{\mathrm{hat},g,d}\,\cos\left(\delta_{\theta,\mathrm{sm}}\right)}{l_{\mathrm{mg}}}$$

$$\dot{i}_{0,sm,q} = \frac{\omega_b\,v_{\mathrm{sm},q}}{l_{\mathrm{mg}}} - i_{0,\mathrm{sm},d}\,\omega_b\,\omega_g - \frac{i_{0,\mathrm{sm},q}\,\omega_b\,r_{\mathrm{mg}}}{l_{\mathrm{mg}}} + \frac{\omega_b\,v_{\mathrm{hat},g,d}\,\sin\left(\delta_{\theta,\mathrm{sm}}\right)}{l_{\mathrm{mg}}}$$

$$\dot{i}_{sm,d} = \frac{\omega_b\,v_{\mathrm{sm},d}\left(l_{11,d}\,l_{\mathrm{ff},d} - l_{\mathrm{f1},d}{}^2\right)}{l_{11,d}\,l_{\mathrm{ad}}{}^2 + l_{\mathrm{ad}}\,l_{\mathrm{f1},d}{}^2 - 2\,l_{\mathrm{ad}}{}^2\,l_{\mathrm{f1},d} + l_{\mathrm{ad}}{}^2\,l_{\mathrm{ff},d} + l_{\mathrm{f1},d}{}^2\,l_l - l_{11,d}\,l_{\mathrm{ad}}\,l_{\mathrm{ff},d} - l_{11,d}\,l_{\mathrm{ff},d}\,l_l} -$$

$$\frac{l_{\mathrm{ad}}\,\omega_b\,v_{f,d}\left(l_{11,d} - l_{\mathrm{f1},d}\right)}{l_{11,d}\,l_{\mathrm{ad}}{}^2 + l_{\mathrm{ad}}\,l_{\mathrm{f1},d}{}^2 - 2\,l_{\mathrm{ad}}{}^2\,l_{\mathrm{f1},d} + l_{\mathrm{ad}}{}^2\,l_{\mathrm{ff},d} + l_{\mathrm{f1},d}{}^2\,l_l - l_{11,d}\,l_{\mathrm{ad}}\,l_{\mathrm{ff},d} - l_{11,d}\,l_{\mathrm{ff},d}\,l_l} +$$

$$\frac{i_{\mathrm{sm},d}\,\omega_b\,r_a\left(l_{11,d}\,l_{\mathrm{ff},d} - l_{\mathrm{f1},d}{}^2\right)}{l_{11,d}\,l_{\mathrm{ad}}{}^2 + l_{\mathrm{ad}}\,l_{\mathrm{f1},d}{}^2 - 2\,l_{\mathrm{ad}}{}^2\,l_{\mathrm{f1},d} + l_{\mathrm{ad}}{}^2\,l_{\mathrm{ff},d} + l_{\mathrm{f1},d}{}^2\,l_l - l_{11,d}\,l_{\mathrm{ad}}\,l_{\mathrm{ff},d} - l_{11,d}\,l_{\mathrm{ff},d}\,l_l} -$$

$$\frac{i_{\mathrm{sm},q}\,\omega_b\,\omega_{\mathrm{sm}}\left(l_{\mathrm{aq}} + l_l\right)\left(l_{11,d}\,l_{\mathrm{ff},d} - l_{\mathrm{f1},d}{}^2\right)}{l_{11,d}\,l_{\mathrm{ad}}{}^2 + l_{\mathrm{ad}}\,l_{\mathrm{f1},d}{}^2 - 2\,l_{\mathrm{ad}}{}^2\,l_{\mathrm{f1},d} + l_{\mathrm{ad}}{}^2\,l_{\mathrm{ff},d} + l_{\mathrm{f1},d}{}^2\,l_l - l_{11,d}\,l_{\mathrm{ad}}\,l_{\mathrm{ff},d} - l_{11,d}\,l_{\mathrm{ff},d}\,l_l} -$$

$$\frac{i_{1,d}\,l_{\mathrm{ad}}\,\omega_b\,r_{1,d}\left(l_{\mathrm{f1},d} - l_{\mathrm{ff},d}\right)}{l_{11,d}\,l_{\mathrm{ad}}{}^2 + l_{\mathrm{ad}}\,l_{\mathrm{f1},d}{}^2 - 2\,l_{\mathrm{ad}}{}^2\,l_{\mathrm{f1},d} + l_{\mathrm{ad}}{}^2\,l_{\mathrm{ff},d} + l_{\mathrm{f1},d}{}^2\,l_l - l_{11,d}\,l_{\mathrm{ad}}\,l_{\mathrm{ff},d} - l_{11,d}\,l_{\mathrm{ff},d}\,l_l} +$$

$$\frac{i_{f,d}\,l_{\mathrm{ad}}\,\omega_b\,r_{f,d}\left(l_{11,d} - l_{\mathrm{f1},d}\right)}{l_{11,d}\,l_{\mathrm{ad}}{}^2 + l_{\mathrm{ad}}\,l_{\mathrm{f1},d}{}^2 - 2\,l_{\mathrm{ad}}{}^2\,l_{\mathrm{f1},d} + l_{\mathrm{ad}}{}^2\,l_{\mathrm{ff},d} + l_{\mathrm{f1},d}{}^2\,l_l - l_{11,d}\,l_{\mathrm{ad}}\,l_{\mathrm{ff},d} - l_{11,d}\,l_{\mathrm{ff},d}\,l_l} +$$

$$\frac{i_{1,q}\,l_{\mathrm{aq}}\,\omega_b\,\omega_{\mathrm{sm}}\left(l_{11,d}\,l_{\mathrm{ff},d} - l_{\mathrm{f1},d}{}^2\right)}{l_{11,d}\,l_{\mathrm{ad}}{}^2 + l_{\mathrm{ad}}\,l_{\mathrm{f1},d}{}^2 - 2\,l_{\mathrm{ad}}{}^2\,l_{\mathrm{f1},d} + l_{\mathrm{ad}}{}^2\,l_{\mathrm{ff},d} + l_{\mathrm{f1},d}{}^2\,l_l - l_{11,d}\,l_{\mathrm{ad}}\,l_{\mathrm{ff},d} - l_{11,d}\,l_{\mathrm{ff},d}\,l_l}$$

$$\dot{i}_{sm,q} = \frac{\omega_b\,v_{\mathrm{sm},d}\left(l_{11,d}\,l_{\mathrm{ff},d} - l_{\mathrm{f1},d}{}^2\right)}{l_{11,d}\,l_{\mathrm{ad}}{}^2 + l_{\mathrm{ad}}\,l_{\mathrm{f1},d}{}^2 - 2\,l_{\mathrm{ad}}{}^2\,l_{\mathrm{f1},d} + l_{\mathrm{ad}}{}^2\,l_{\mathrm{ff},d} + l_{\mathrm{f1},d}{}^2\,l_l - l_{11,d}\,l_{\mathrm{ad}}\,l_{\mathrm{ff},d} - l_{11,d}\,l_{\mathrm{ff},d}\,l_l} -$$

$$\frac{l_{\mathrm{ad}}\,\omega_b\,v_{f,d}\left(l_{11,d} - l_{\mathrm{f1},d}\right)}{l_{11,d}\,l_{\mathrm{ad}}{}^2 + l_{\mathrm{ad}}\,l_{\mathrm{f1},d}{}^2 - 2\,l_{\mathrm{ad}}{}^2\,l_{\mathrm{f1},d} + l_{\mathrm{ad}}{}^2\,l_{\mathrm{ff},d} + l_{\mathrm{f1},d}{}^2\,l_l - l_{11,d}\,l_{\mathrm{ad}}\,l_{\mathrm{ff},d} - l_{11,d}\,l_{\mathrm{ff},d}\,l_l} +$$

$$\frac{i_{\mathrm{sm},d}\,\omega_b\,r_a\left(l_{11,d}\,l_{\mathrm{ff},d} - l_{\mathrm{f1},d}{}^2\right)}{l_{11,d}\,l_{\mathrm{ad}}{}^2 + l_{\mathrm{ad}}\,l_{\mathrm{f1},d}{}^2 - 2\,l_{\mathrm{ad}}{}^2\,l_{\mathrm{f1},d} + l_{\mathrm{ad}}{}^2\,l_{\mathrm{ff},d} + l_{\mathrm{f1},d}{}^2\,l_l - l_{11,d}\,l_{\mathrm{ad}}\,l_{\mathrm{ff},d} - l_{11,d}\,l_{\mathrm{ff},d}\,l_l} -$$

$$\frac{i_{\mathrm{sm},q}\,\omega_b\,\omega_{\mathrm{sm}}\left(l_{\mathrm{aq}} + l_l\right)\left(l_{11,d}\,l_{\mathrm{ff},d} - l_{\mathrm{f1},d}{}^2\right)}{l_{11,d}\,l_{\mathrm{ad}}{}^2 + l_{\mathrm{ad}}\,l_{\mathrm{f1},d}{}^2 - 2\,l_{\mathrm{ad}}{}^2\,l_{\mathrm{f1},d} + l_{\mathrm{ad}}{}^2\,l_{\mathrm{ff},d} + l_{\mathrm{f1},d}{}^2\,l_l - l_{11,d}\,l_{\mathrm{ad}}\,l_{\mathrm{ff},d} - l_{11,d}\,l_{\mathrm{ff},d}\,l_l} -$$

$$\frac{i_{1,d}\,l_{\mathrm{ad}}\,\omega_b\,r_{1,d}\left(l_{\mathrm{f1},d} - l_{\mathrm{ff},d}\right)}{l_{11,d}\,l_{\mathrm{ad}}{}^2 + l_{\mathrm{ad}}\,l_{\mathrm{f1},d}{}^2 - 2\,l_{\mathrm{ad}}{}^2\,l_{\mathrm{f1},d} + l_{\mathrm{ad}}{}^2\,l_{\mathrm{ff},d} + l_{\mathrm{f1},d}{}^2\,l_l - l_{11,d}\,l_{\mathrm{ad}}\,l_{\mathrm{ff},d} - l_{11,d}\,l_{\mathrm{ff},d}\,l_l} +$$

$$\frac{i_{f,d}\,l_{\mathrm{ad}}\,\omega_b\,r_{f,d}\left(l_{11,d} - l_{\mathrm{f1},d}\right)}{l_{11,d}\,l_{\mathrm{ad}}{}^2 + l_{\mathrm{ad}}\,l_{\mathrm{f1},d}{}^2 - 2\,l_{\mathrm{ad}}{}^2\,l_{\mathrm{f1},d} + l_{\mathrm{ad}}{}^2\,l_{\mathrm{ff},d} + l_{\mathrm{f1},d}{}^2\,l_l - l_{11,d}\,l_{\mathrm{ad}}\,l_{\mathrm{ff},d} - l_{11,d}\,l_{\mathrm{ff},d}\,l_l} +$$

$$\frac{i_{1,q}\,l_{\mathrm{aq}}\,\omega_b\,\omega_{\mathrm{sm}}\left(l_{11,d}\,l_{\mathrm{ff},d} - l_{\mathrm{f1},d}{}^2\right)}{l_{11,d}\,l_{\mathrm{ad}}{}^2 + l_{\mathrm{ad}}\,l_{\mathrm{f1},d}{}^2 - 2\,l_{\mathrm{ad}}{}^2\,l_{\mathrm{f1},d} + l_{\mathrm{ad}}{}^2\,l_{\mathrm{ff},d} + l_{\mathrm{f1},d}{}^2\,l_l - l_{11,d}\,l_{\mathrm{ad}}\,l_{\mathrm{ff},d} - l_{11,d}\,l_{\mathrm{ff},d}\,l_l}$$

$$\dot{i}_{f,d} = \frac{l_{\mathrm{ad}}\,\omega_b\,v_{\mathrm{sm},d}\,(l_{11,d} - l_{\mathrm{f1},d})}{l_{11,d}\,l_{\mathrm{ad}}{}^2 + l_{\mathrm{ad}}\,l_{\mathrm{f1},d}{}^2 - 2\,l_{\mathrm{ad}}{}^2\,l_{\mathrm{f1},d} + l_{\mathrm{ad}}{}^2\,l_{\mathrm{ff},d} + l_{\mathrm{f1},d}{}^2\,l_l - l_{11,d}\,l_{\mathrm{ad}}\,l_{\mathrm{ff},d} - l_{11,d}\,l_{\mathrm{ff},d}\,l_l} -$$

$$\frac{\omega_b\,v_{f,d}\,\left(-l_{\mathrm{ad}}{}^2 + l_{11,d}\,l_{\mathrm{ad}} + l_{11,d}\,l_l\right)}{l_{11,d}\,l_{\mathrm{ad}}{}^2 + l_{\mathrm{ad}}\,l_{\mathrm{f1},d}{}^2 - 2\,l_{\mathrm{ad}}{}^2\,l_{\mathrm{f1},d} + l_{\mathrm{ad}}{}^2\,l_{\mathrm{ff},d} + l_{\mathrm{f1},d}{}^2\,l_l - l_{11,d}\,l_{\mathrm{ad}}\,l_{\mathrm{ff},d} - l_{11,d}\,l_{\mathrm{ff},d}\,l_l} -$$

$$\frac{i_{1,d}\,\omega_b\,r_{1,d}\,\left(-l_{\mathrm{ad}}{}^2 + l_{\mathrm{f1},d}\,l_{\mathrm{ad}} + l_{\mathrm{f1},d}\,l_l\right)}{l_{11,d}\,l_{\mathrm{ad}}{}^2 + l_{\mathrm{ad}}\,l_{\mathrm{f1},d}{}^2 - 2\,l_{\mathrm{ad}}{}^2\,l_{\mathrm{f1},d} + l_{\mathrm{ad}}{}^2\,l_{\mathrm{ff},d} + l_{\mathrm{f1},d}{}^2\,l_l - l_{11,d}\,l_{\mathrm{ad}}\,l_{\mathrm{ff},d} - l_{11,d}\,l_{\mathrm{ff},d}\,l_l} +$$

$$\frac{i_{f,d}\,\omega_b\,r_{f,d}\,\left(-l_{\mathrm{ad}}{}^2 + l_{11,d}\,l_{\mathrm{ad}} + l_{11,d}\,l_l\right)}{l_{11,d}\,l_{\mathrm{ad}}{}^2 + l_{\mathrm{ad}}\,l_{\mathrm{f1},d}{}^2 - 2\,l_{\mathrm{ad}}{}^2\,l_{\mathrm{f1},d} + l_{\mathrm{ad}}{}^2\,l_{\mathrm{ff},d} + l_{\mathrm{f1},d}{}^2\,l_l - l_{11,d}\,l_{\mathrm{ad}}\,l_{\mathrm{ff},d} - l_{11,d}\,l_{\mathrm{ff},d}\,l_l} +$$

$$\frac{i_{\mathrm{sm},d}\,l_{\mathrm{ad}}\,\omega_b\,r_a\,(l_{11,d} - l_{\mathrm{f1},d})}{l_{11,d}\,l_{\mathrm{ad}}{}^2 + l_{\mathrm{ad}}\,l_{\mathrm{f1},d}{}^2 - 2\,l_{\mathrm{ad}}{}^2\,l_{\mathrm{f1},d} + l_{\mathrm{ad}}{}^2\,l_{\mathrm{ff},d} + l_{\mathrm{f1},d}{}^2\,l_l - l_{11,d}\,l_{\mathrm{ad}}\,l_{\mathrm{ff},d} - l_{11,d}\,l_{\mathrm{ff},d}\,l_l} +$$

$$\frac{i_{1,q}\,l_{\mathrm{ad}}\,l_{\mathrm{aq}}\,\omega_b\,\omega_{\mathrm{sm}}\,(l_{11,d} - l_{\mathrm{f1},d})}{l_{11,d}\,l_{\mathrm{ad}}{}^2 + l_{\mathrm{ad}}\,l_{\mathrm{f1},d}{}^2 - 2\,l_{\mathrm{ad}}{}^2\,l_{\mathrm{f1},d} + l_{\mathrm{ad}}{}^2\,l_{\mathrm{ff},d} + l_{\mathrm{f1},d}{}^2\,l_l - l_{11,d}\,l_{\mathrm{ad}}\,l_{\mathrm{ff},d} - l_{11,d}\,l_{\mathrm{ff},d}\,l_l} -$$

$$\frac{i_{\mathrm{sm},q}\,l_{\mathrm{ad}}\,\omega_b\,\omega_{\mathrm{sm}}\,(l_{\mathrm{aq}} + l_l)\,(l_{11,d} - l_{\mathrm{f1},d})}{l_{11,d}\,l_{\mathrm{ad}}{}^2 + l_{\mathrm{ad}}\,l_{\mathrm{f1},d}{}^2 - 2\,l_{\mathrm{ad}}{}^2\,l_{\mathrm{f1},d} + l_{\mathrm{ad}}{}^2\,l_{\mathrm{ff},d} + l_{\mathrm{f1},d}{}^2\,l_l - l_{11,d}\,l_{\mathrm{ad}}\,l_{\mathrm{ff},d} - l_{11,d}\,l_{\mathrm{ff},d}\,l_l}$$

$$\dot{i}_{1,d} = \frac{l_{\mathrm{ad}}\,\omega_b\,v_{\mathrm{sm},d}\,(l_{11,d} - l_{\mathrm{f1},d})}{l_{11,d}\,l_{\mathrm{ad}}{}^2 + l_{\mathrm{ad}}\,l_{\mathrm{f1},d}{}^2 - 2\,l_{\mathrm{ad}}{}^2\,l_{\mathrm{f1},d} + l_{\mathrm{ad}}{}^2\,l_{\mathrm{ff},d} + l_{\mathrm{f1},d}{}^2\,l_l - l_{11,d}\,l_{\mathrm{ad}}\,l_{\mathrm{ff},d} - l_{11,d}\,l_{\mathrm{ff},d}\,l_l} -$$

$$\frac{\omega_b\,v_{f,d}\,\left(-l_{\mathrm{ad}}{}^2 + l_{11,d}\,l_{\mathrm{ad}} + l_{11,d}\,l_l\right)}{l_{11,d}\,l_{\mathrm{ad}}{}^2 + l_{\mathrm{ad}}\,l_{\mathrm{f1},d}{}^2 - 2\,l_{\mathrm{ad}}{}^2\,l_{\mathrm{f1},d} + l_{\mathrm{ad}}{}^2\,l_{\mathrm{ff},d} + l_{\mathrm{f1},d}{}^2\,l_l - l_{11,d}\,l_{\mathrm{ad}}\,l_{\mathrm{ff},d} - l_{11,d}\,l_{\mathrm{ff},d}\,l_l} -$$

$$\frac{i_{1,d}\,\omega_b\,r_{1,d}\,\left(-l_{\mathrm{ad}}{}^2 + l_{\mathrm{f1},d}\,l_{\mathrm{ad}} + l_{\mathrm{f1},d}\,l_l\right)}{l_{11,d}\,l_{\mathrm{ad}}{}^2 + l_{\mathrm{ad}}\,l_{\mathrm{f1},d}{}^2 - 2\,l_{\mathrm{ad}}{}^2\,l_{\mathrm{f1},d} + l_{\mathrm{ad}}{}^2\,l_{\mathrm{ff},d} + l_{\mathrm{f1},d}{}^2\,l_l - l_{11,d}\,l_{\mathrm{ad}}\,l_{\mathrm{ff},d} - l_{11,d}\,l_{\mathrm{ff},d}\,l_l} +$$

$$\frac{i_{f,d}\,\omega_b\,r_{f,d}\,\left(-l_{\mathrm{ad}}{}^2 + l_{11,d}\,l_{\mathrm{ad}} + l_{11,d}\,l_l\right)}{l_{11,d}\,l_{\mathrm{ad}}{}^2 + l_{\mathrm{ad}}\,l_{\mathrm{f1},d}{}^2 - 2\,l_{\mathrm{ad}}{}^2\,l_{\mathrm{f1},d} + l_{\mathrm{ad}}{}^2\,l_{\mathrm{ff},d} + l_{\mathrm{f1},d}{}^2\,l_l - l_{11,d}\,l_{\mathrm{ad}}\,l_{\mathrm{ff},d} - l_{11,d}\,l_{\mathrm{ff},d}\,l_l} +$$

$$\frac{i_{\mathrm{sm},d}\,l_{\mathrm{ad}}\,\omega_b\,r_a\,(l_{11,d} - l_{\mathrm{f1},d})}{l_{11,d}\,l_{\mathrm{ad}}{}^2 + l_{\mathrm{ad}}\,l_{\mathrm{f1},d}{}^2 - 2\,l_{\mathrm{ad}}{}^2\,l_{\mathrm{f1},d} + l_{\mathrm{ad}}{}^2\,l_{\mathrm{ff},d} + l_{\mathrm{f1},d}{}^2\,l_l - l_{11,d}\,l_{\mathrm{ad}}\,l_{\mathrm{ff},d} - l_{11,d}\,l_{\mathrm{ff},d}\,l_l} +$$

$$\frac{i_{1,q}\,l_{\mathrm{ad}}\,l_{\mathrm{aq}}\,\omega_b\,\omega_{\mathrm{sm}}\,(l_{11,d} - l_{\mathrm{f1},d})}{l_{11,d}\,l_{\mathrm{ad}}{}^2 + l_{\mathrm{ad}}\,l_{\mathrm{f1},d}{}^2 - 2\,l_{\mathrm{ad}}{}^2\,l_{\mathrm{f1},d} + l_{\mathrm{ad}}{}^2\,l_{\mathrm{ff},d} + l_{\mathrm{f1},d}{}^2\,l_l - l_{11,d}\,l_{\mathrm{ad}}\,l_{\mathrm{ff},d} - l_{11,d}\,l_{\mathrm{ff},d}\,l_l} -$$

$$\frac{i_{\mathrm{sm},q}\,l_{\mathrm{ad}}\,\omega_b\,\omega_{\mathrm{sm}}\,(l_{\mathrm{aq}} + l_l)\,(l_{11,d} - l_{\mathrm{f1},d})}{l_{11,d}\,l_{\mathrm{ad}}{}^2 + l_{\mathrm{ad}}\,l_{\mathrm{f1},d}{}^2 - 2\,l_{\mathrm{ad}}{}^2\,l_{\mathrm{f1},d} + l_{\mathrm{ad}}{}^2\,l_{\mathrm{ff},d} + l_{\mathrm{f1},d}{}^2\,l_l - l_{11,d}\,l_{\mathrm{ad}}\,l_{\mathrm{ff},d} - l_{11,d}\,l_{\mathrm{ff},d}\,l_l}$$

$$\dot{i}_{1,q} = \frac{i_{1,d}\, l_{\mathrm{ad}}\, l_{\mathrm{aq}}\, \omega_b\, \omega_{\mathrm{sm}}}{-l_{\mathrm{aq}}{}^2 + l_{11,q}\, l_{\mathrm{aq}} + l_{11,q}\, l_l} - \frac{i_{1,q}\, \omega_b\, r_{1,q}\, (l_{\mathrm{aq}} + l_l)}{-l_{\mathrm{aq}}{}^2 + l_{11,q}\, l_{\mathrm{aq}} + l_{11,q}\, l_l} - \frac{i_{\mathrm{sm},q}\, l_{\mathrm{aq}}\, \omega_b\, r_a}{-l_{\mathrm{aq}}{}^2 + l_{11,q}\, l_{\mathrm{aq}} + l_{11,q}\, l_l} -$$

$$\frac{i_{\mathrm{sm},d}\, l_{\mathrm{aq}}\, \omega_b\, \omega_{\mathrm{sm}}\, (l_{\mathrm{ad}} + l_l)}{-l_{\mathrm{aq}}{}^2 + l_{11,q}\, l_{\mathrm{aq}} + l_{11,q}\, l_l} - \frac{l_{\mathrm{aq}}\, \omega_b\, v_{\mathrm{sm},q}}{-l_{\mathrm{aq}}{}^2 + l_{11,q}\, l_{\mathrm{aq}} + l_{11,q}\, l_l} + \frac{i_{f,d}\, l_{\mathrm{ad}}\, l_{\mathrm{aq}}\, \omega_b\, \omega_{\mathrm{sm}}}{-l_{\mathrm{aq}}{}^2 + l_{11,q}\, l_{\mathrm{aq}} + l_{11,q}\, l_l}$$

$$\dot{\omega}_{sm} = \frac{p_{m,\mathrm{sm}}}{T_{\mathrm{sm}}\, \omega_{\mathrm{sm}}} - \frac{i_{1,d}\, i_{\mathrm{sm},q}\, l_{\mathrm{ad}}}{T_{\mathrm{sm}}} + \frac{i_{1,q}\, i_{\mathrm{sm},d}\, l_{\mathrm{aq}}}{T_{\mathrm{sm}}} - \frac{i_{f,d}\, i_{\mathrm{sm},q}\, l_{\mathrm{ad}}}{T_{\mathrm{sm}}} + \frac{i_{\mathrm{sm},d}\, i_{\mathrm{sm},q}\, (l_{\mathrm{ad}} - l_{\mathrm{aq}})}{T_{\mathrm{sm}}}$$

$$\dot{\delta\theta}_{sm} = \omega_b\, \omega_{\mathrm{sm}} - \omega_b\, \omega_g$$

$$\dot{p}_{m,sm} = \frac{p_{\mathrm{sm,star}}}{T_{\mathrm{gt}}} - \frac{p_{m,\mathrm{sm}}}{T_{\mathrm{gt}}} - \frac{k_{\omega,\mathrm{sm}}\, \omega_{\mathrm{sm}}}{T_{\mathrm{gt}}} + \frac{k_{\omega,\mathrm{sm}}\, \omega_{\mathrm{sm,star}}}{T_{\mathrm{gt}}}$$

$$\dot{q}_{m,sm} = \omega_{f,\mathrm{sm}}\, (i_{\mathrm{sm},d}\, v_{\mathrm{sm},q} - i_{\mathrm{sm},q}\, v_{\mathrm{sm},d}) - \omega_{f,\mathrm{sm}}\, q_{m,\mathrm{sm}}$$

$$\dot{\zeta}_{sm} = v_{\mathrm{hat,sm,star}} - k_{q,\mathrm{sm}}\, q_{m,\mathrm{sm}} + k_{q,\mathrm{sm}}\, q_{m,\mathrm{sm,star}} - \sqrt{v_{\mathrm{sm},d}{}^2 + v_{\mathrm{sm},q}{}^2}$$

$$\dot{v}_{f,d} = \frac{k_{p,\mathrm{ex}}\, v_{\mathrm{hat,sm,star}}}{T_{\mathrm{ex}}} - \frac{k_{p,\mathrm{ex}}\, \sqrt{v_{\mathrm{sm},d}{}^2 + v_{\mathrm{sm},q}{}^2}}{T_{\mathrm{ex}}} - \frac{v_{f,d}}{T_{\mathrm{ex}}} +$$

$$\frac{k_{i,\mathrm{ex}}\, \zeta_{\mathrm{sm}}}{T_{\mathrm{ex}}} - \frac{k_{p,\mathrm{ex}}\, k_{q,\mathrm{sm}}\, q_{m,\mathrm{sm}}}{T_{\mathrm{ex}}} + \frac{k_{p,\mathrm{ex}}\, k_{q,\mathrm{sm}}\, q_{m,\mathrm{sm,star}}}{T_{\mathrm{ex}}}$$

11.1.3 Full system model

The states in the full system model

$$\begin{aligned}
\mathbf{x} = [&v_{0,d,vsm}\ v_{0q,vsm}\ i_{cv,d,vsm}\ i_{cv,q,vsm}\ \gamma_{d,vsm}\ \gamma_{q,vsm}\ i_{0d,vsm}\ i_{0q,vsm}\cdots \\
&\phi_{d,vsm}\ \phi_{q,vsm}\ \zeta_{vsm}\ is_{d,vsm}\ is_{q,vsm}\ q_{m,vsm}\ \omega_{vsm}\ \kappa_{vsm}v_{d,sm}\ v_{q,sm}\cdots \\
&i_{0,d,sm}\ i_{0,q,sm}\ i_{d,sm}\ i_{q,sm}\ i_{fd,sm}\ i_{1d,sm}\ i_{1q,sm}\ \omega_{sm}\ \delta\theta_{sm}\ p_{m,sm}\ \cdots \\
&q_{m,sm}\ \zeta_{sm}\ v_{fd,sm}v_{0d,l}\ v_{cvq,l}\ i_{cvd,l}\ \gamma_{d,l}\ \gamma_{q,l}i_{0d,l}\ i_{0d,l}\ \phi_{d,l}\cdots \\
&\phi_{q,l}\ v_{pll,d,l}\ v_{pll,d,l}\ \delta\theta_{pll,l}\ v_{g,d,l}\ v_{g,d,l}] \\
\mathbf{u} = [&p^*_{vsm}\ q^*_{vsm}\ \hat{v}^*\ \omega^*_{vsm}\ p^*_{sm}\ q^*_{sm}\ \hat{v}^*\ \omega^*_{sm}\ i^*_{cv,d}\ i^*_{cv,q}]
\end{aligned} \tag{11.3}$$

Some equations defined in order to simplify the equation set:

$$\omega_{pll,n} = 1$$

$$\omega_{pll} = (k_{p,pll}atan(v_{pll,q}/v_{pll,q}) + k_{i,pll}\epsilon + \omega_{pll,n}$$

$$v_{cv,load,d} = k_{pc,load}(i^*_{cv,d} - i_{cv,load}) + k_{ic,load}\gamma_{load}$$

$$-l_{f,load}i_{cv,d,load}\omega_{pll} - k_{ad,l}v_{0,d,load} + k_{ad,load}$$

$$\dot{v}_{0,d,vsm} = \omega_b \, \omega_{\text{vsm}} \, v_{0,q,\text{vsm}} - \frac{i_{0,d,\text{vsm}} \, \omega_b}{c_f} + \frac{\text{icv}_{d,\text{vsm}} \, \omega_b}{c_f}$$

$$\dot{v}_{0,q,vsm} = \frac{\text{icv}_{q,\text{vsm}} \, \omega_b}{c_f} - \frac{i_{0,q,\text{vsm}} \, \omega_b}{c_f} - \omega_b \, \omega_{\text{vsm}} \, v_{0,d,\text{vsm}}$$

$$\dot{i}_{cv,d,vsm} = \frac{\gamma_{d,\text{vsm}} \, k_{\text{ic,vsm}} \, \omega_b}{l_f} - \frac{\text{icv}_{d,\text{vsm}} \, \omega_b \, (k_{\text{pc,vsm}} + r_f)}{l_f} + \frac{\text{is}_{d,\text{vsm}} \, k_{\text{pc,vsm}} \, \omega_b}{l_f} - \frac{k_{\text{ad,vsm}} \, \omega_b \, \varphi_{d,\text{vsm}}}{l_f}$$

$$- \frac{\omega_b \, v_{0,d,\text{vsm}} \, (k_{\text{ad,vsm}} - k_{\text{ffv}} + 1)}{l_f}$$

$$\dot{i}_{cv,q,vsm} = \frac{\gamma_{q,\text{vsm}} \, k_{\text{ic,vsm}} \, \omega_b}{l_f} - \frac{\text{icv}_{q,\text{vsm}} \, \omega_b \, (k_{\text{pc,vsm}} + r_f)}{l_f} + \frac{\text{is}_{q,\text{vsm}} \, k_{\text{pc,vsm}} \, \omega_b}{l_f} - \frac{k_{\text{ad,vsm}} \, \omega_b \, \varphi_{q,\text{vsm}}}{l_f}$$

$$- \frac{\omega_b \, v_{0,q,\text{vsm}} \, (k_{\text{ad,vsm}} - k_{\text{ffv}} + 1)}{l_f}$$

$$\dot{\gamma}_{d,vsm} = \text{is}_{d,\text{vsm}} - \text{icv}_{d,\text{vsm}}$$

$$\dot{\gamma}_{q,vsm} = \text{is}_{q,\text{vsm}} - \text{icv}_{q,\text{vsm}}$$

$$\dot{i}_{0,d,vsm} = \frac{\omega_b \, v_{0,d,\text{vsm}}}{l_g} - \frac{\omega_b \, v_{g,d}}{l_g} + i_{0,q,\text{vsm}} \, \omega_b \, \omega_{\text{vsm}} - \frac{i_{0,d,\text{vsm}} \, \omega_b \, r_g}{l_g}$$

$$\dot{i}_{0,q,vsm} = \frac{\omega_b \, v_{0,q,\text{vsm}}}{l_g} - \frac{\omega_b \, v_{g,q}}{l_g} - i_{0,d,\text{vsm}} \, \omega_b \, \omega_{\text{vsm}} - \frac{i_{0,q,\text{vsm}} \, \omega_b \, r_g}{l_g}$$

$$\dot{\phi}_{d,vsm} = load - \omega_{\text{ad,vsm}} \, \varphi_{d,\text{vsm}} - \omega_{\text{ad,vsm}} \, v_{0,d,\text{vsm}}$$

$$\dot{\phi}_{q,vsm} = -\omega_{\text{ad,vsm}} \, \varphi_{q,\text{vsm}} - \omega_{\text{ad,vsm}} \, v_{0,q,\text{vsm}}$$

$$\dot{\zeta}_{vsm} = v_{\text{hat,star,vsm}} - k_{q,\text{vsm}} \, q_{m,\text{vsm}} + k_{q,\text{vsm}} \, q_{\text{star,vsm}} - \sqrt{v_{0,d,\text{vsm}}{}^2 + v_{0,q,\text{vsm}}{}^2}$$

$$\dot{i}_{s,d,vsm} = \text{is}_{q,\text{vsm}} \, \omega_b \, \omega_{\text{vsm}} - \frac{\omega_b \, v_{0,d,\text{vsm}}}{l_{s,\text{vsm}}} - \frac{k_{\text{pv,vsm}} \, \omega_b \, \sqrt{v_{0,d,\text{vsm}}{}^2 + v_{0,q,\text{vsm}}{}^2}}{l_{s,\text{vsm}}} -$$

$$\frac{\text{is}_{d,\text{vsm}} \, \omega_b \, r_{s,\text{vsm}}}{l_{s,\text{vsm}}} + \frac{k_{\text{pv,vsm}} \, \omega_b \, v_{\text{hat,star,vsm}}}{l_{s,\text{vsm}}} + \frac{k_{\text{iv,vsm}} \, \omega_b \, \zeta_{\text{vsm}}}{l_{s,\text{vsm}}} - \frac{k_{\text{pv,vsm}} \, k_{q,\text{vsm}} \, \omega_b \, q_{m,\text{vsm}}}{l_{s,\text{vsm}}}$$

$$+ \frac{k_{\text{pv,vsm}} \, k_{q,\text{vsm}} \, \omega_b \, q_{\text{star,vsm}}}{l_{s,\text{vsm}}}$$

$$\dot{i}_{s,q,vsm} = -\frac{\omega_b \, v_{0,q,\text{vsm}}}{l_{s,\text{vsm}}} - \text{is}_{d,\text{vsm}} \, \omega_b \, \omega_{\text{vsm}} - \frac{\text{is}_{q,\text{vsm}} \, \omega_b \, r_{s,\text{vsm}}}{l_{s,\text{vsm}}}$$

$$\dot{q}_{m,vsm} = i_{0,d,\text{vsm}} \, \omega_{\text{qf,vsm}} \, v_{0,q,\text{vsm}} - \omega_{\text{qf,vsm}} \, q_{m,\text{vsm}} - i_{0,q,\text{vsm}} \, \omega_{\text{qf,vsm}} \, v_{0,d,\text{vsm}}$$

$$\dot{\omega}_{vsm} = \frac{p_{\text{star,vsm}}}{T_a} - \frac{i_{0,d,\text{vsm}} \, v_{0,d,\text{vsm}} + i_{0,q,\text{vsm}} \, v_{0,q,\text{vsm}}}{T_a}$$

$$- \frac{\omega_{\text{vsm}} \, (k_{d,\text{vsm}} + k_{\omega,\text{vsm}})}{T_a} + \frac{k_{d,\text{vsm}} \, \kappa_{\text{vsm}}}{T_a} + \frac{k_{\omega,\text{vsm}} \, \omega_{\text{star,vsm}}}{T_a}$$

$$\dot{\kappa}_{vsm} = \omega_{\text{vsm}} \, \omega_{d,\text{vsm}} - \kappa_{\text{vsm}} \, \omega_{d,\text{vsm}}$$

$$\dot{v}_{0,d,load} = \omega_b\,\omega_{\text{vsm}}\,v_{0,q} - \frac{i_{0,d}\,\omega_b}{c_f} + \frac{\text{icv}_d\,\omega_b}{c_f}$$

$$\dot{v}_{0,q,load} = \frac{\text{icv}_q\,\omega_b}{c_f} - \frac{i_{0,q}\,\omega_b}{c_f} - \omega_b\,\omega_{\text{vsm}}\,v_{0,d}$$

$$\dot{i}_{cv,d,load} = \frac{\omega_b}{l_f}(v_{cv,d} - r_f i_{cv,d} - v_{0,d} + l_f i_{cv,q,load}\omega_{vsm}$$

$$\dot{i}_{cv,q,load} = \frac{\omega_b}{l_f}(v_{cv,q} - r_f i_{cv,q} - v_{0,q} - l_f i_{cv,d,load}\omega_{vsm}$$

$$\dot{\gamma}_{d,load} = \text{icv}_{d,\text{star}} - \text{icv}_d$$

$$\dot{\gamma}_{q,load} = \text{icv}_{q,\text{star}} - \text{icv}_q$$

$$\dot{i}_{0,d,load} = \frac{\omega_b\,v_{0,d}}{l_g} + i_{0,q}\,\omega_b\,\omega_{\text{vsm}} - \frac{i_{0,d}\,\omega_b\,r_g}{l_g} - \frac{\omega_b\,v_{g,d}\,\cos\left(\delta_{\theta,\text{pll}}\right)}{l_g} - \frac{\omega_b\,v_{g,q}\,\sin\left(\delta_{\theta,\text{pll}}\right)}{l_g}$$

$$\dot{i}_{0,q,load} = \frac{\omega_b\,v_{0,q}}{l_g} - i_{0,d}\,\omega_b\,\omega_{\text{vsm}} - \frac{i_{0,q}\,\omega_b\,r_g}{l_g} - \frac{\omega_b\,v_{g,q}\,\cos\left(\delta\theta,\text{pll}\right)}{l_g} + \frac{\omega_b\,v_{g,d}\,\sin\left(\delta_{\theta,\text{pll}}\right)}{l_g}$$

$$\dot{\phi}_{d,load} = \omega_{\text{ad}}\,v_{0,d} - \omega_{\text{ad}}\,\varphi_d$$

$$\dot{\phi}_{q,load} = \omega_{\text{ad}}\,v_{0,q} - \omega_{\text{ad}}\,\varphi_q$$

$$\dot{v}_{pll,d,load} = \omega_{\text{lp,pll}}\,v_{0,d} - \omega_{\text{lp,pll}}\,v_{\text{pll},d}$$

$$\dot{v}_{pll,q,load} = \omega_{\text{lp,pll}}\,v_{0,q} - \omega_{\text{lp,pll}}\,v_{\text{pll},q}$$

$$\dot{\epsilon}_{load} = \text{atan}\left(\frac{v_{\text{pll},q}}{v_{\text{pll},d}}\right)$$

$$\dot{\delta}\theta_{pll} = \omega_b\left(\text{epsi}\,k_{i,\text{pll}} + k_{p,\text{pll}}\,\text{atan}\left(\frac{v_{\text{pll},q}}{v_{\text{pll},d}}\right) + 1\right) - \omega_b\,\omega_{\text{vsm}}$$

$$\dot{v}_{g,d} = \omega_b\,\omega_{\text{vsm}}\,v_{g,q} + \frac{i_{0,d,\text{vsm}}\,\omega_b}{c_l} + \frac{i_{0,d}\,\omega_b\,\cos\left(\delta_{\theta,\text{pll}}\right)}{c_l} + \frac{i_{0,\text{sm},d}\,\omega_b\,\cos\left(\delta_{\theta,\text{sm}}\right)}{c_l} - \frac{i_{0,q}\,\omega_b\,\sin\left(\delta_{\theta,\text{pll}}\right)}{c_l}$$
$$- \frac{i_{0,\text{sm},q}\,\omega_b\,\sin\left(\delta_{\theta,\text{sm}}\right)}{c_l} - \frac{\omega_b\,v_{g,d}}{c_l\,r_l}$$

$$\dot{v}_{g,q} = \frac{i_{0,q,\text{vsm}}\,\omega_b}{c_l} - \omega_b\,\omega_{\text{vsm}}\,v_{g,d} + \frac{i_{0,q}\,\omega_b\,\cos\left(\delta_{\theta,\text{pll}}\right)}{c_l} + \frac{i_{0,\text{sm},q}\,\omega_b\,\cos\left(\delta_{\theta,\text{sm}}\right)}{c_l} + \frac{i_{0,d}\,\omega_b\,\sin\left(\delta_{\theta,\text{pll}}\right)}{c_l}$$
$$+ \frac{i_{0,\text{sm},d}\,\omega_b\,\sin\left(\delta_{\theta,\text{sm}}\right)}{c_l} - \frac{\omega_b\,v_{g,q}}{c_l\,r_l}$$

$$\dot{v}_{sm,d} = \omega_b\,\omega_{\text{vsm}}\,v_{sm,q} - \frac{i_{0,\text{sm},d}\,\omega_b}{c_{\text{mg}}} + \frac{i_{\text{sm},d}\,\omega_b}{c_{\text{mg}}}$$

$$\dot{v}_{sm,q} = \frac{i_{\text{sm},q}\,\omega_b}{c_{\text{mg}}} - \frac{i_{0,\text{sm},q}\,\omega_b}{c_{\text{mg}}} - \omega_b\,\omega_{\text{vsm}}\,v_{sm,d}$$

$$\dot{i}_{0,sm,d} = \frac{\omega_b\,v_{sm,d}}{l_{\text{mg}}} + i_{0,\text{sm},q}\,\omega_b\,\omega_{\text{vsm}} - \frac{i_{0,\text{sm},d}\,\omega_b\,r_{\text{mg}}}{l_{\text{mg}}} - \frac{\omega_b\,v_{g,d}\,\cos\left(\delta_{\theta,\text{sm}}\right)}{l_{\text{mg}}} - \frac{\omega_b\,v_{g,q}\,\sin\left(\delta_{\theta,\text{sm}}\right)}{l_{\text{mg}}}$$

$$\dot{i}_{0,sm,q} = \frac{\omega_b\,v_{sm,q}}{l_{\text{mg}}} - i_{0,\text{sm},d}\,\omega_b\,\omega_{\text{vsm}} - \frac{i_{0,\text{sm},q}\,\omega_b\,r_{\text{mg}}}{l_{\text{mg}}} - \frac{\omega_b\,v_{g,q}\,\cos\left(\delta_{\theta,\text{sm}}\right)}{l_{\text{mg}}} + \frac{\omega_b\,v_{g,d}\,\sin\left(\delta_{\theta,\text{sm}}\right)}{l_{\text{mg}}}$$

$$\dot{i}_{sm,d} = \frac{\omega_b\,v_{\mathrm{sm},d}\,\left(l_{11,d}\,l_{\mathrm{ff},d} - l_{\mathrm{f1},d}{}^2\right)}{l_{11,d}\,l_{\mathrm{ad}}{}^2 + l_{\mathrm{ad}}\,l_{\mathrm{f1},d}{}^2 - 2\,l_{\mathrm{ad}}{}^2\,l_{\mathrm{f1},d} + l_{\mathrm{ad}}{}^2\,l_{\mathrm{ff},d} + l_{\mathrm{f1},d}{}^2\,l_l - l_{11,d}\,l_{\mathrm{ad}}\,l_{\mathrm{ff},d} - l_{11,d}\,l_{\mathrm{ff},d}\,l_l} -$$

$$\frac{l_{\mathrm{ad}}\,\omega_b\,v_{f,d}\,\left(l_{11,d} - l_{\mathrm{f1},d}\right)}{l_{11,d}\,l_{\mathrm{ad}}{}^2 + l_{\mathrm{ad}}\,l_{\mathrm{f1},d}{}^2 - 2\,l_{\mathrm{ad}}{}^2\,l_{\mathrm{f1},d} + l_{\mathrm{ad}}{}^2\,l_{\mathrm{ff},d} + l_{\mathrm{f1},d}{}^2\,l_l - l_{11,d}\,l_{\mathrm{ad}}\,l_{\mathrm{ff},d} - l_{11,d}\,l_{\mathrm{ff},d}\,l_l} +$$

$$\frac{i_{\mathrm{sm},d}\,\omega_b\,r_a\,\left(l_{11,d}\,l_{\mathrm{ff},d} - l_{\mathrm{f1},d}{}^2\right)}{l_{11,d}\,l_{\mathrm{ad}}{}^2 + l_{\mathrm{ad}}\,l_{\mathrm{f1},d}{}^2 - 2\,l_{\mathrm{ad}}{}^2\,l_{\mathrm{f1},d} + l_{\mathrm{ad}}{}^2\,l_{\mathrm{ff},d} + l_{\mathrm{f1},d}{}^2\,l_l - l_{11,d}\,l_{\mathrm{ad}}\,l_{\mathrm{ff},d} - l_{11,d}\,l_{\mathrm{ff},d}\,l_l} -$$

$$\frac{i_{\mathrm{sm},q}\,\omega_b\,\omega_{\mathrm{sm}}\,\left(l_{\mathrm{aq}} + l_l\right)\,\left(l_{11,d}\,l_{\mathrm{ff},d} - l_{\mathrm{f1},d}{}^2\right)}{l_{11,d}\,l_{\mathrm{ad}}{}^2 + l_{\mathrm{ad}}\,l_{\mathrm{f1},d}{}^2 - 2\,l_{\mathrm{ad}}{}^2\,l_{\mathrm{f1},d} + l_{\mathrm{ad}}{}^2\,l_{\mathrm{ff},d} + l_{\mathrm{f1},d}{}^2\,l_l - l_{11,d}\,l_{\mathrm{ad}}\,l_{\mathrm{ff},d} - l_{11,d}\,l_{\mathrm{ff},d}\,l_l} -$$

$$\frac{i_{1,d}\,l_{\mathrm{ad}}\,\omega_b\,r_{1,d}\,\left(l_{\mathrm{f1},d} - l_{\mathrm{ff},d}\right)}{l_{11,d}\,l_{\mathrm{ad}}{}^2 + l_{\mathrm{ad}}\,l_{\mathrm{f1},d}{}^2 - 2\,l_{\mathrm{ad}}{}^2\,l_{\mathrm{f1},d} + l_{\mathrm{ad}}{}^2\,l_{\mathrm{ff},d} + l_{\mathrm{f1},d}{}^2\,l_l - l_{11,d}\,l_{\mathrm{ad}}\,l_{\mathrm{ff},d} - l_{11,d}\,l_{\mathrm{ff},d}\,l_l} +$$

$$\frac{i_{f,d}\,l_{\mathrm{ad}}\,\omega_b\,r_{f,d}\,\left(l_{11,d} - l_{\mathrm{f1},d}\right)}{l_{11,d}\,l_{\mathrm{ad}}{}^2 + l_{\mathrm{ad}}\,l_{\mathrm{f1},d}{}^2 - 2\,l_{\mathrm{ad}}{}^2\,l_{\mathrm{f1},d} + l_{\mathrm{ad}}{}^2\,l_{\mathrm{ff},d} + l_{\mathrm{f1},d}{}^2\,l_l - l_{11,d}\,l_{\mathrm{ad}}\,l_{\mathrm{ff},d} - l_{11,d}\,l_{\mathrm{ff},d}\,l_l} +$$

$$\frac{i_{1,q}\,l_{\mathrm{aq}}\,\omega_b\,\omega_{\mathrm{sm}}\,\left(l_{11,d}\,l_{\mathrm{ff},d} - l_{\mathrm{f1},d}{}^2\right)}{l_{11,d}\,l_{\mathrm{ad}}{}^2 + l_{\mathrm{ad}}\,l_{\mathrm{f1},d}{}^2 - 2\,l_{\mathrm{ad}}{}^2\,l_{\mathrm{f1},d} + l_{\mathrm{ad}}{}^2\,l_{\mathrm{ff},d} + l_{\mathrm{f1},d}{}^2\,l_l - l_{11,d}\,l_{\mathrm{ad}}\,l_{\mathrm{ff},d} - l_{11,d}\,l_{\mathrm{ff},d}\,l_l}$$

$$\dot{i}_{sm,q} = \frac{i_{1,d}\,l_{11,q}\,l_{\mathrm{ad}}\,\omega_b\,\omega_{\mathrm{sm}}}{-l_{\mathrm{aq}}{}^2 + l_{11,q}\,l_{\mathrm{aq}} + l_{11,q}\,l_l} - \frac{i_{1,q}\,l_{\mathrm{aq}}\,\omega_b\,r_{1,q}}{-l_{\mathrm{aq}}{}^2 + l_{11,q}\,l_{\mathrm{aq}} + l_{11,q}\,l_l} - \frac{i_{\mathrm{sm},q}\,l_{11,q}\,\omega_b\,r_a}{-l_{\mathrm{aq}}{}^2 + l_{11,q}\,l_{\mathrm{aq}} + l_{11,q}\,l_l} -$$

$$\frac{i_{\mathrm{sm},d}\,l_{11,q}\,\omega_b\,\omega_{\mathrm{sm}}\,\left(l_{\mathrm{ad}} + l_l\right)}{-l_{\mathrm{aq}}{}^2 + l_{11,q}\,l_{\mathrm{aq}} + l_{11,q}\,l_l} - \frac{l_{11,q}\,\omega_b\,v_{\mathrm{sm},q}}{-l_{\mathrm{aq}}{}^2 + l_{11,q}\,l_{\mathrm{aq}} + l_{11,q}\,l_l} + \frac{i_{f,d}\,l_{11,q}\,l_{\mathrm{ad}}\,\omega_b\,\omega_{\mathrm{sm}}}{-l_{\mathrm{aq}}{}^2 + l_{11,q}\,l_{\mathrm{aq}} + l_{11,q}\,l_l}$$

$$\dot{i}_{f,d} = \frac{l_{\mathrm{ad}}\,\omega_b\,v_{\mathrm{sm},d}\,\left(l_{11,d} - l_{\mathrm{f1},d}\right)}{l_{11,d}\,l_{\mathrm{ad}}{}^2 + l_{\mathrm{ad}}\,l_{\mathrm{f1},d}{}^2 - 2\,l_{\mathrm{ad}}{}^2\,l_{\mathrm{f1},d} + l_{\mathrm{ad}}{}^2\,l_{\mathrm{ff},d} + l_{\mathrm{f1},d}{}^2\,l_l - l_{11,d}\,l_{\mathrm{ad}}\,l_{\mathrm{ff},d} - l_{11,d}\,l_{\mathrm{ff},d}\,l_l} -$$

$$\frac{\omega_b\,v_{f,d}\,\left(-l_{\mathrm{ad}}{}^2 + l_{11,d}\,l_{\mathrm{ad}} + l_{11,d}\,l_l\right)}{l_{11,d}\,l_{\mathrm{ad}}{}^2 + l_{\mathrm{ad}}\,l_{\mathrm{f1},d}{}^2 - 2\,l_{\mathrm{ad}}{}^2\,l_{\mathrm{f1},d} + l_{\mathrm{ad}}{}^2\,l_{\mathrm{ff},d} + l_{\mathrm{f1},d}{}^2\,l_l - l_{11,d}\,l_{\mathrm{ad}}\,l_{\mathrm{ff},d} - l_{11,d}\,l_{\mathrm{ff},d}\,l_l} -$$

$$\frac{i_{1,d}\,\omega_b\,r_{1,d}\,\left(-l_{\mathrm{ad}}{}^2 + l_{\mathrm{f1},d}\,l_{\mathrm{ad}} + l_{\mathrm{f1},d}\,l_l\right)}{l_{11,d}\,l_{\mathrm{ad}}{}^2 + l_{\mathrm{ad}}\,l_{\mathrm{f1},d}{}^2 - 2\,l_{\mathrm{ad}}{}^2\,l_{\mathrm{f1},d} + l_{\mathrm{ad}}{}^2\,l_{\mathrm{ff},d} + l_{\mathrm{f1},d}{}^2\,l_l - l_{11,d}\,l_{\mathrm{ad}}\,l_{\mathrm{ff},d} - l_{11,d}\,l_{\mathrm{ff},d}\,l_l} +$$

$$\frac{i_{f,d}\,\omega_b\,r_{f,d}\,\left(-l_{\mathrm{ad}}{}^2 + l_{11,d}\,l_{\mathrm{ad}} + l_{11,d}\,l_l\right)}{l_{11,d}\,l_{\mathrm{ad}}{}^2 + l_{\mathrm{ad}}\,l_{\mathrm{f1},d}{}^2 - 2\,l_{\mathrm{ad}}{}^2\,l_{\mathrm{f1},d} + l_{\mathrm{ad}}{}^2\,l_{\mathrm{ff},d} + l_{\mathrm{f1},d}{}^2\,l_l - l_{11,d}\,l_{\mathrm{ad}}\,l_{\mathrm{ff},d} - l_{11,d}\,l_{\mathrm{ff},d}\,l_l} +$$

$$\frac{i_{\mathrm{sm},d}\,l_{\mathrm{ad}}\,\omega_b\,r_a\,\left(l_{11,d} - l_{\mathrm{f1},d}\right)}{l_{11,d}\,l_{\mathrm{ad}}{}^2 + l_{\mathrm{ad}}\,l_{\mathrm{f1},d}{}^2 - 2\,l_{\mathrm{ad}}{}^2\,l_{\mathrm{f1},d} + l_{\mathrm{ad}}{}^2\,l_{\mathrm{ff},d} + l_{\mathrm{f1},d}{}^2\,l_l - l_{11,d}\,l_{\mathrm{ad}}\,l_{\mathrm{ff},d} - l_{11,d}\,l_{\mathrm{ff},d}\,l_l} +$$

$$\frac{i_{1,q}\,l_{\mathrm{ad}}\,l_{\mathrm{aq}}\,\omega_b\,\omega_{\mathrm{sm}}\,\left(l_{11,d} - l_{\mathrm{f1},d}\right)}{l_{11,d}\,l_{\mathrm{ad}}{}^2 + l_{\mathrm{ad}}\,l_{\mathrm{f1},d}{}^2 - 2\,l_{\mathrm{ad}}{}^2\,l_{\mathrm{f1},d} + l_{\mathrm{ad}}{}^2\,l_{\mathrm{ff},d} + l_{\mathrm{f1},d}{}^2\,l_l - l_{11,d}\,l_{\mathrm{ad}}\,l_{\mathrm{ff},d} - l_{11,d}\,l_{\mathrm{ff},d}\,l_l} -$$

$$\frac{i_{\mathrm{sm},q}\,l_{\mathrm{ad}}\,\omega_b\,\omega_{\mathrm{sm}}\,\left(l_{\mathrm{aq}} + l_l\right)\,\left(l_{11,d} - l_{\mathrm{f1},d}\right)}{l_{11,d}\,l_{\mathrm{ad}}{}^2 + l_{\mathrm{ad}}\,l_{\mathrm{f1},d}{}^2 - 2\,l_{\mathrm{ad}}{}^2\,l_{\mathrm{f1},d} + l_{\mathrm{ad}}{}^2\,l_{\mathrm{ff},d} + l_{\mathrm{f1},d}{}^2\,l_l - l_{11,d}\,l_{\mathrm{ad}}\,l_{\mathrm{ff},d} - l_{11,d}\,l_{\mathrm{ff},d}\,l_l}$$

$$\dot{i}_{1,d} = \frac{\omega_b \, v_{f,d} \left(-l_{\mathrm{ad}}^2 + l_{\mathrm{f1},d} \, l_{\mathrm{ad}} + l_{\mathrm{f1},d} \, l_l\right)}{l_{11,d} \, l_{\mathrm{ad}}^2 + l_{\mathrm{ad}} \, l_{\mathrm{f1},d}^2 - 2 \, l_{\mathrm{ad}}^2 \, l_{\mathrm{f1},d} + l_{\mathrm{ad}}^2 \, l_{\mathrm{ff},d} + l_{\mathrm{f1},d}^2 \, l_l - l_{11,d} \, l_{\mathrm{ad}} \, l_{\mathrm{ff},d} - l_{11,d} \, l_{\mathrm{ff},d} \, l_l} -$$

$$\frac{l_{\mathrm{ad}} \, \omega_b \, v_{\mathrm{sm},d} \left(l_{\mathrm{f1},d} - l_{\mathrm{ff},d}\right)}{l_{11,d} \, l_{\mathrm{ad}}^2 + l_{\mathrm{ad}} \, l_{\mathrm{f1},d}^2 - 2 \, l_{\mathrm{ad}}^2 \, l_{\mathrm{f1},d} + l_{\mathrm{ad}}^2 \, l_{\mathrm{ff},d} + l_{\mathrm{f1},d}^2 \, l_l - l_{11,d} \, l_{\mathrm{ad}} \, l_{\mathrm{ff},d} - l_{11,d} \, l_{\mathrm{ff},d} \, l_l} +$$

$$\frac{i_{1,d} \, \omega_b \, r_{1,d} \left(-l_{\mathrm{ad}}^2 + l_{\mathrm{ff},d} \, l_{\mathrm{ad}} + l_{\mathrm{ff},d} \, l_l\right)}{l_{11,d} \, l_{\mathrm{ad}}^2 + l_{\mathrm{ad}} \, l_{\mathrm{f1},d}^2 - 2 \, l_{\mathrm{ad}}^2 \, l_{\mathrm{f1},d} + l_{\mathrm{ad}}^2 \, l_{\mathrm{ff},d} + l_{\mathrm{f1},d}^2 \, l_l - l_{11,d} \, l_{\mathrm{ad}} \, l_{\mathrm{ff},d} - l_{11,d} \, l_{\mathrm{ff},d} \, l_l} -$$

$$\frac{i_{f,d} \, \omega_b \, r_{f,d} \left(-l_{\mathrm{ad}}^2 + l_{\mathrm{f1},d} \, l_{\mathrm{ad}} + l_{\mathrm{f1},d} \, l_l\right)}{l_{11,d} \, l_{\mathrm{ad}}^2 + l_{\mathrm{ad}} \, l_{\mathrm{f1},d}^2 - 2 \, l_{\mathrm{ad}}^2 \, l_{\mathrm{f1},d} + l_{\mathrm{ad}}^2 \, l_{\mathrm{ff},d} + l_{\mathrm{f1},d}^2 \, l_l - l_{11,d} \, l_{\mathrm{ad}} \, l_{\mathrm{ff},d} - l_{11,d} \, l_{\mathrm{ff},d} \, l_l} -$$

$$\frac{i_{\mathrm{sm},d} \, l_{\mathrm{ad}} \, \omega_b \, r_a \left(l_{\mathrm{f1},d} - l_{\mathrm{ff},d}\right)}{l_{11,d} \, l_{\mathrm{ad}}^2 + l_{\mathrm{ad}} \, l_{\mathrm{f1},d}^2 - 2 \, l_{\mathrm{ad}}^2 \, l_{\mathrm{f1},d} + l_{\mathrm{ad}}^2 \, l_{\mathrm{ff},d} + l_{\mathrm{f1},d}^2 \, l_l - l_{11,d} \, l_{\mathrm{ad}} \, l_{\mathrm{ff},d} - l_{11,d} \, l_{\mathrm{ff},d} \, l_l} -$$

$$\frac{i_{1,q} \, l_{\mathrm{ad}} \, l_{\mathrm{aq}} \, \omega_b \, \omega_{\mathrm{sm}} \left(l_{\mathrm{f1},d} - l_{\mathrm{ff},d}\right)}{l_{11,d} \, l_{\mathrm{ad}}^2 + l_{\mathrm{ad}} \, l_{\mathrm{f1},d}^2 - 2 \, l_{\mathrm{ad}}^2 \, l_{\mathrm{f1},d} + l_{\mathrm{ad}}^2 \, l_{\mathrm{ff},d} + l_{\mathrm{f1},d}^2 \, l_l - l_{11,d} \, l_{\mathrm{ad}} \, l_{\mathrm{ff},d} - l_{11,d} \, l_{\mathrm{ff},d} \, l_l} +$$

$$\frac{i_{\mathrm{sm},q} \, l_{\mathrm{ad}} \, \omega_b \, \omega_{\mathrm{sm}} \left(l_{\mathrm{aq}} + l_l\right) \left(l_{\mathrm{f1},d} - l_{\mathrm{ff},d}\right)}{l_{11,d} \, l_{\mathrm{ad}}^2 + l_{\mathrm{ad}} \, l_{\mathrm{f1},d}^2 - 2 \, l_{\mathrm{ad}}^2 \, l_{\mathrm{f1},d} + l_{\mathrm{ad}}^2 \, l_{\mathrm{ff},d} + l_{\mathrm{f1},d}^2 \, l_l - l_{11,d} \, l_{\mathrm{ad}} \, l_{\mathrm{ff},d} - l_{11,d} \, l_{\mathrm{ff},d} \, l_l}$$

$$\dot{i}_{1,q} = \frac{i_{1,d} \, l_{\mathrm{ad}} \, l_{\mathrm{aq}} \, \omega_b \, \omega_{\mathrm{sm}}}{-l_{\mathrm{aq}}^2 + l_{11,q} \, l_{\mathrm{aq}} + l_{11,q} \, l_l} - \frac{i_{1,q} \, \omega_b \, r_{1,q} \left(l_{\mathrm{aq}} + l_l\right)}{-l_{\mathrm{aq}}^2 + l_{11,q} \, l_{\mathrm{aq}} + l_{11,q} \, l_l} - \frac{i_{\mathrm{sm},q} \, l_{\mathrm{aq}} \, \omega_b \, r_a}{-l_{\mathrm{aq}}^2 + l_{11,q} \, l_{\mathrm{aq}} + l_{11,q} \, l_l}$$

$$- \frac{i_{\mathrm{sm},d} \, l_{\mathrm{aq}} \, \omega_b \, \omega_{\mathrm{sm}} \left(l_{\mathrm{ad}} + l_l\right)}{-l_{\mathrm{aq}}^2 + l_{11,q} \, l_{\mathrm{aq}} + l_{11,q} \, l_l} - \frac{l_{\mathrm{aq}} \, \omega_b \, v_{\mathrm{sm},q}}{-l_{\mathrm{aq}}^2 + l_{11,q} \, l_{\mathrm{aq}} + l_{11,q} \, l_l} + \frac{i_{f,d} \, l_{\mathrm{ad}} \, l_{\mathrm{aq}} \, \omega_b \, \omega_{\mathrm{sm}}}{-l_{\mathrm{aq}}^2 + l_{11,q} \, l_{\mathrm{aq}} + l_{11,q} \, l_l}$$

$$\dot{\omega}_{sm} = \frac{p_{m,\mathrm{sm}}}{T_{\mathrm{sm}} \, \omega_{\mathrm{sm}}} - \frac{i_{1,d} \, i_{\mathrm{sm},q} \, l_{\mathrm{ad}}}{T_{\mathrm{sm}}} + \frac{i_{1,q} \, i_{\mathrm{sm},d} \, l_{\mathrm{aq}}}{T_{\mathrm{sm}}} - \frac{i_{f,d} \, i_{\mathrm{sm},q} \, l_{\mathrm{ad}}}{T_{\mathrm{sm}}} + \frac{i_{\mathrm{sm},d} \, i_{\mathrm{sm},q} \left(l_{\mathrm{ad}} - l_{\mathrm{aq}}\right)}{T_{\mathrm{sm}}}$$

$$\dot{\delta\theta}_{sm} = \omega_b \, \omega_{\mathrm{sm}} - \omega_b \, \omega_{\mathrm{vsm}}$$

$$\dot{p}_{m,sm} = \frac{p_{\mathrm{sm,star}}}{T_{\mathrm{gt}}} - \frac{p_{m,\mathrm{sm}}}{T_{\mathrm{gt}}} - \frac{k_{\omega,\mathrm{sm}} \, \omega_{\mathrm{sm}}}{T_{\mathrm{gt}}}$$

$$+ \frac{k_{\omega,\mathrm{sm}} \, \omega_{\mathrm{sm,star}}}{T_{\mathrm{gt}}}$$

$$\dot{q}_{m,sm} = \omega_{f,\mathrm{sm}} \left(i_{\mathrm{sm},d} \, v_{\mathrm{sm},q} - i_{\mathrm{sm},q} \, v_{\mathrm{sm},d}\right) - \omega_{f,\mathrm{sm}} \, q_{m,\mathrm{sm}}$$

$$\dot{\zeta}_{sm} = v_{\mathrm{hat,sm,star}} - k_{q,\mathrm{sm}} \, q_{m,\mathrm{sm}} + k_{q,\mathrm{sm}} \, q_{m,\mathrm{sm,star}} - \sqrt{v_{\mathrm{sm},d}^2 + v_{\mathrm{sm},q}^2}$$

$$\dot{v}_{f,d} = \frac{k_{p,\mathrm{ex}} \, v_{\mathrm{hat,sm,star}}}{T_{\mathrm{ex}}} - \frac{k_{p,\mathrm{ex}} \sqrt{v_{\mathrm{sm},d}^2 + v_{\mathrm{sm},q}^2}}{T_{\mathrm{ex}}} - \frac{v_{f,d}}{T_{\mathrm{ex}}} + \frac{k_{i,\mathrm{ex}} \, \zeta_{\mathrm{sm}}}{T_{\mathrm{ex}}}$$

$$- \frac{k_{p,\mathrm{ex}} \, k_{q,\mathrm{sm}} \, q_{m,\mathrm{sm}}}{T_{\mathrm{ex}}} + \frac{k_{p,\mathrm{ex}} \, k_{q,\mathrm{sm}} \, q_{m,\mathrm{sm,star}}}{T_{\mathrm{ex}}}$$

11.2   SM parameters

Table showing the parameters of the SM

Parameter	Value
$r_{1,d}$	0.050477
$l_{11,d}$	2.6734
$r_{1,q}$	0.010024
$l_{11,q}$	1.6117
r_f	0.0036817
l_{f1}	2.3955
r_a	0.013184
l_{ad}	2.3955
l_{aq}	1.3955
l_l	0.05450
l_{ff}	2.5504
T_{sm}	1.7
$k_{d,sm}$	0